Aus dem Institut für Neurophysiologie
der Medizinischen Fakultät Charité – Universitätsmedizin Berlin

DISSERTATION

Modulation of fast neuronal network oscillations in the hippocampal formation

zur Erlangung des akademischen Grades
Doctor of Philosophy in Medical Neurosciences
(PhD in Medical Neurosciences)

vorgelegt der Medizinischen Fakultät
Charité – Universitätsmedizin Berlin

von
Jan-Oliver Hollnagel
aus Winsen/Luhe

Datum der Promotion: 10.03.2017

Table of Contents

Zusammenfassung

Die vorliegende Dissertation basiert auf drei Artikeln, die vor ihrer Publikation einen peer-review Prozess durchlaufen haben. Die zugrundeliegenden Experimente wurden im Institut für Neurophysiologie der Charité-Universitätsmedizin Berlin geplant und durchgeführt.

Experimente an sich frei bewegenden Tieren haben gezeigt, dass zwei Arten von Netzwerkaktivität für die Gedächtnisbildung von Bedeutung sind. Während exploratives Verhalten und paradoxer (REM) Schlaf durch Gamma-Oszillationen gekennzeichnet sind, tritt eine als „sharp wave-ripple“ (SPW-R) bezeichnete Netzwerkaktivität vor allem während Ruhephasen, der Nahrungsaufnahme und orthodoxen (non-REM) Schlaf auf. Ich habe Mechanismen untersucht, die für die Aufrechterhaltung, das Entstehen sowie die Unterdrückung der SPW-R Aktivität verantwortlich sind. Der Metabolismus des Neurotransmitters Acetylcholin wurde ebenfalls untersucht, da er für den Wechsel zwischen den beiden Netzwerkaktivitäten von Bedeutung ist.

Ich konnte zeigen, dass induzierte SPW-R durch Gabe von Nikotin dosisabhängig in krampfähnliche Aktivitätsmuster (REDs) transformiert werden können. Die Ursache hierfür ist eine reduzierte Inhibition von Pyramidenzellen in der hippocampalen CA3 Region. Durch unspezifische Erregung (Erhöhung der extrazellulären Kaliumkonzentration von 3 auf 8.5 mM) konnte in unstimulierten Schnitten RED ausgelöst werden, was in Gegenwart von SPW-Rs aufgrund erhöhter Inhibition nicht möglich war.

In der nächsten Studie habe ich den Einfluss von $GABA_B$ Rezeptoren auf die Calcium-abhängige Transmitterfreisetzung untersucht. Die transiente Unterdrückung der SPW-R durch Aktivierung des $GABA_B$ Rezeptors mit Baclofen konnte durch Co-Applikation des Antagonisten CGP55846 verhindert werden. In Gegenwart von Baclofen war die Induktion der SPW-R dennoch möglich.

Schließlich habe ich den Acetylcholinmetabolismus untersucht. Durch Hemmung des Acetylcholinabbaus durch die Acetylcholinesterase konnte ich dosisabhängig unterschiedlich starke Formen von Gamma-Oszillationen auslösen, die durch Zugabe von Acetylcholin noch stärker ausgeprägt wurden. Der experimentelle Nachweis, einer Möglichkeit zur extrazellulären Bildung von Acetylcholin, konnte nicht erbracht werden.

Abstract

The present dissertation comprises three articles published in international peer-reviewed journals. The experiments were planned and conducted at the Institute of Neurophysiology (Charité-Universitätsmedizin Berlin).

Freely moving animals display two prominent states of network activity that are related to memory formation. Explorative behaviour and rapid-eye-movement (REM) sleep are characterised by short periods of gamma oscillations nested in theta oscillations, whereas sharp wave-ripple (SPW-R) activity is observed during immobility, consummatory behaviour and slow-wave sleep. I studied different aspects involved in maintenance and stabilisation of SPW-R activity, their emergence and suppression, and the acetylcholine metabolism which is involved in the switch from SPW-R activity to gamma oscillations.

I show that application of nicotine led to a dose-dependent shift from SPW-R activity to seizure like events (SLEs). The transition could be linked to a reduced inhibition of pyramidal cells in area CA3. We found that elevation of $[K^+]_o$ from 3 to 8.5 mM led to REDs in naïve slices whereas their generation was prevented during episodes of stimulus-induced SPW-R activity. Under this condition the inhibitory conductance was significantly increased.

In the next study I demonstrate the role of $GABA_B$ receptor mediated inhibition in presynaptic Ca^{2+} dependent transmitter release. Stimulus-induced SPW-Rs were transiently blocked by application of the $GABA_B$ receptor agonist baclofen, an effect that could be prevented by co-application with the antagonist CGP55846. However, CGP55846 itself had no effect on the incidence of SPW-Rs. Interestingly, the induction of SPW-Rs was still possible when baclofen was applied during tetanic stimulation.

Lastly, I investigated the acetylcholine metabolism and its implications for the generation of gamma oscillations. Blocking the acetylcholinesterase to inhibit the extracellular degradation of ACh induced gamma oscillations. Additional application of ACh dose dependently increased power and coherence of the oscillations. I further employed experiments to provide evidence for an extracellularly located choline-acetyltransferase that would allow synthesising ACh from ambient residual choline. However, taken together, the results did not support the idea of an extracellular source of ACh.

1 Introduction

“Men ought to know that from nothing else but the brain come joys, delights, […] and lamentations. […] And by the same organ we become mad and delirious, and fears and terrors assail us […].” (Hippocrates, ca 400 BC).

1.1 Hippocampus

The hippocampal formation is part of the brain’s limbic system and was first described by the Venetian anatomist Giulio Cesare Aranzi in 1587 (Bir *et al.*, 2015). In 1911 Santiago Ramón y Cajal published a detailed illustration of the rodent hippocampus which is often referred to when it comes to the complexity of neuronal networks, especially in the hippocampus (Ramón y Cajal, 1995).

The hippocampal formation can be divided into three distinct subregions: the dentate gyrus (DG), the hippocampus proper represented by the cornu ammonis (CA; with subregions CA3, CA2, and CA1), and the subiculum. The parahippocampal region serves as the in- and output structure of the hippocampus. It consists of pre- and parasubiculum, entorhinal cortex (EC), perirhinal, and postrhinal cortex. The hippocampus receives input from other brain regions, mainly from the EC and the fornix. The EC in turn receives input from frontal cortical areas, the amygdala, and the olfactory bulb and projects to the DG but also directly to areas CA1 and CA3 thus bypassing the trisynaptic loop. The fornix interconnects the hippocampus with septal areas and the hypothalamus (van Strien *et al.*, 2009).

Within the hippocampus, input to the DG is provided by the perforant path mostly originating from stellate cells. Grid cells project directly to the CA regions. Granule cells of the DG project onto proximal apical dendrites of pyramidal cells in area CA3 via the mossy fibres. The axons of the CA3 neurons form the Schaffer collaterals which make contact to pyramidal cells in area CA1. Besides this trisynaptic circuit, a dense associative network interconnects CA3 pyramidal cells with each other (Amaral & Lavenex, 2007; Neves *et al.*, 2008).

Together with the rich diversity of interneurons present in the hippocampal formation the described architecture provides the hardware for complex activity patterns and is well known for its ability to generate different network oscillations in a state-dependent manner (Buzsáki *et al.*, 1983). According to the environmental task, intrinsic network properties change to facilitate the emergence of different frequencies in the field potential which are related to higher brain functions; e.g. spatial navigation (O'Keefe &

Nadel, 1978; Buzsáki & Moser, 2013) and memory formation (Scolville & Milner, 1957; Squire, 1992).

In the course of my PhD studies, I investigated the mechanisms underlying the emergence of high frequency network oscillations within the hippocampal formation *in vitro*.

1.2 Network oscillations

Extracellular field potentials provide us with a rather systemic approach for the understanding of network oscillations. As in intracellular recordings, any current across the cellular membrane (neuronal and glial) leads to a voltage deflection which is small in the extracellular space and only detectable if it originates from many cells forming the local field potential (LFP). Therefore, the LFP can be interpreted as the integration of the overall ionic flux, ranging from fast action potentials to slow membrane potential fluctuations (Buzsáki *et al.*, 2012; Hales & Pockett, 2014). Network field potential oscillations represent the synchronous rhythmic activity of neuronal ensembles formed by many neurons. Nevertheless, there is growing evidence for the involvement of network oscillations in providing a temporal frame for neuronal firing due to synaptic interactions and occasionally also via ephaptic coupling (Lisman & Jensen, 2013; Watrous *et al.*, 2015).

Neuronal networks in the mammalian brain are capable of oscillating at frequencies ranging from very slow to ultra-fast (0.025 - 600 Hz), with the latter often seen in tissue of pathologies like epilepsy. Widespread slow oscillations are believed to modulate faster local events (Moreno *et al.*, 2016). In this context, higher frequencies emerge from smaller networks (e.g. the hippocampus), whereas slower frequencies interconnect larger networks (Buzsáki & Draguhn, 2004).

1.2.1 Sharp wave-ripple complexes

Intracranial EEGs recorded in freely moving animals revealed different states of complex rhythmical activity within the hippocampal network. Oscillations in the theta (4-12 Hz) range with embedded activity in the gamma (30-100 Hz) range were characteristic for explorative behaviour and rapid-eye-movement sleep. During consummatory behaviour, immobility and slow-wave sleep so-called sharp wave-ripple (SPW-R) complexes (Buzsáki, 1986; Roumis & Frank, 2015) are observed.

SPW-Rs in the hippocampus are self-organised patterns that emerge from the extensive recurrent excitatory collaterals of the CA3 region (Buzsáki *et al.*, 1983) which is controlled via inhibitory interneurons (Schlingloff *et al.*, 2014; Kohus *et al.*, 2016).

In vivo, such states of rhythmic activity of associated neurons can be observed in different contexts, like consummatory behaviour, immobility and slow-wave sleep. In mouse hippocampal slice preparations they emerge spontaneously (Maier *et al.*, 2003) while in rat hippocampal slices electrical stimulation of the network is required to generate SPW-Rs unless recordings are made in very ventral parts of the hippocampus (Behrens *et al.*, 2005).

The method of inducing SPW-Rs provided me with the ability to study mechanisms that are involved in the initiation and generation of SPW-R activity. I took advantage of the fact that naïve slices, characterised by random baseline activity, would only show SPW-Rs following a stimulation paradigm usually employed for induction of long term potentiation (see section 3.2 on page 6) when studying the effect of $GABA_B$ receptors on SPW-Rs (Hollnagel *et al.*, 2014).

Furthermore, I studied the impact of a well-balanced interplay between excitation and inhibition to prevent switching from physiological to hyper-excitable states (Liotta *et al.*, 2011).

1.2.2 Gamma oscillations

Apart from SPW-R activity, the hippocampal network exhibits oscillations in the gamma (γ) range (~ 30 - 100 Hz). *In vivo*, this type of oscillation is often nested within slower theta (~ 7 Hz) oscillations (Leung *et al.*, 1982) and can be observed during arousal, attention and rapid eye movement sleep. In these situations, the acetylcholine (ACh) concentrations have been shown to be increased (Metherate *et al.*, 1987; Steriade *et al.*, 1993). Gamma oscillations are thought to provide a temporal frame for activation of neuronal ensembles to process neuronal information (Hájos & Paulsen, 2009; Kann *et al.*, 2014). In sparsely active networks such activity is thought to permit storage of information by spike timing-dependent plasticity.

In vitro, persistent γ-oscillations can be induced in hippocampal slice preparations either via activation of ionotropic glutamate receptors (Whittington *et al.*, 1995; Gloveli *et al.*, 2005) or via activation of muscarinic-cholinergic receptors by application of acetylcholine or carbachol (Fisahn *et al.*, 1998; Wójtowicz *et al.*, 2009). Moreover, similar

pharmacology has been used to reliably induce γ-oscillations in hippocampal slice cultures (Schneider *et al.*, 2015).

To investigate the role of a putative extracellular source of acetylcholine, as reported recently (Vijayaraghavan *et al.*, 2013), I studied the ACh metabolism and its impact on the generation of γ-oscillations (Hollnagel *et al.*, 2015).

1.3 Excitation versus Inhibition

Network oscillations, in general, rely on a well-balanced interplay between excitation and inhibition to maintain a steady state of activity among the contributing neurons. The complexity of the hippocampal formation's network architecture is ideally suited to provide the framework for generating slow and fast oscillations, which themselves provide the temporal frame for activation of single neurons as well as neuronal ensembles (Traub *et al.*, 2004; Klausberger & Somogyi, 2008).

The studies performed during my PhD thesis work show the impact of an equilibrated excitatory and inhibitory controlled input for maintaining specific oscillations in physiological orders (Liotta *et al.*, 2011), for recruiting neuronal ensembles to contribute to the generation of network oscillations (Hollnagel *et al.*, 2014), and how neurotransmitters like ACh can interact with oscillating networks to modulate ongoing activity (Hollnagel *et al.*, 2015) and to switch between oscillatory states (ul Haq *et al.*; submitted to Cerebral Cortex).

2 Aims

The main objective of the experimental work for my PhD thesis was to study the mechanisms underlying the generation of fast network oscillations. The generation of such oscillations strongly depends on an orchestrated activation of (at least transiently) interconnected neurons forming functional neuronal ensembles acting as microcircuits. Although this concept has been introduced more than 60 years ago (Hebb, 1949), the underlying mechanisms are still being extensively studied.

The publications derived from my own studies using electrophysiological methods focus on stimulus-induced sharp wave-ripple (SPW-Rs) complexes and γ-oscillations in rat hippocampal slices. The specific aims of each study will be described in more detail in the next subsections.

2.1 Publication I: (Liotta *et al.*, 2011)

The method of inducing SPW-Rs with repetitive stimulation has been criticised by reviewers and parts of the scientific community. It was linked to network states of hyper-excitability typical for recurrent epileptiform discharges (REDs) (Staley & Dudek, 2006). It was the aim of the study to show that indeed SPW-Rs and REDs are two distinct network states. I was able to convert SPW-Rs into REDs by partial removal of inhibition. My contribution focused on the impact of a reduced GABAergic conductance showing the importance of a well-balanced inhibitory component in the formation of this particular network activity.

2.2 Publication II: (Hollnagel *et al.*, 2014)

The model of inducing SPW-Rs stimulus-dependently provides us with the ability to investigate the mechanisms involved in the generation and expression of stimulus-induced SPW-Rs. It was the aim of the study to show the impact of $GABA_B$ receptor-mediated inhibition and its localisation at the pre- or postsynaptic site.

2.3 Publication III: (Hollnagel *et al.*, 2015)

It was the aim of the study to gain insight into the generation of γ-oscillations by modulation of the acetylcholine metabolism and to provide evidence for an extracellulary located source of ACh. The findings support currently unpublished work regarding the switch between SPW-R activity and γ-oscillations (ul Haq *et al.*; submitted to Cerebral Cortex).

3 Methodology

3.1 Animal preparation

All animal procedures were performed in accordance with the guidelines of the European Communities Council and were approved by the regional *Landesamt für Gesundheit und Soziales (LAGeSo), Berlin* (T0096/02, T0068/02).

Adult Wistar rats (aged 6 - 8 weeks, ~ 200 g) were used for all experiments. For the first publication (Liotta *et al.*, 2011), animals were decapitated under deep ether anaesthesia. Due to changes in the legislation, I switched to isoflurane anaesthesia. To prevent temporary blood-brain barrier opening (Tétrault *et al.*, 2008), I reduced the amount of and exposure to isoflurane by dissolving 1.5 vol% of the narcotic in a gas mixture comprising of 70% N_2O and 30% O_2. Following decapitation, brains were transferred into ice-cold artificial cerebrospinal fluid (aCSF, ~ 4°C) saturated with 95% O_2 and 5% CO_2. Horizontal hippocampal slices (400 µm) were prepared at an angle of about 12.5° in the fronto-occipital direction (with the frontal portion up) using a Leica VT1200 Vibratome (Wetzlar, Germany). This orientation preserves the connectivity within hippocampal subregions as well as to the entorhinal cortex (Boulton *et al.*, 1992). Slices were immediately transferred in an interface type recording chamber, perfused with aCSF (saturated with 95% O_2 and 5% CO_2) at a flow rate of ~ 1.8 ml/min and maintained at 36°C. aCSF contained (in mM): 129 NaCl, 21 $NaHCO_3$, 1.25 NaH_2PO_4, 1.8 $MgSO_4$, 1.6, $CaCl_2$, 3 KCl, 10 glucose. The osmolarity was 300 ± 5 mOsmol/l and pH was 7.4 at 34 - 36°C. Recordings were started 2 - 3 h after preparation.

To facilitate the induction of sharp wave-ripple activity (and thus reducing the number of animals), the concentration of $MgSO_4$ was lowered to 1.2 mM 1 h before starting the experiments (Windmüller *et al.*, 2005). For each experimental condition, up to two slices per animal were used. However, different protocols were often employed in slices from the same animal, in order to further minimize the overall number of individual animals sacrificed.

3.2 Electrophysiology

Extracellular field potentials (FP) were recorded in AC mode under interface conditions with carbon-fibre (0.4 - 1.2 MΩ) and glass electrodes (filled with 154 mM NaCl, 5 - 10 MΩ). For intracellular recordings, sharp microelectrodes (70 - 90 MΩ) were pulled from borosilicate glass (outer diameter of 1.2 mm) and filled with 2.5 M K^+-acetate. Ion-sensitive signals were obtained by using double barrelled K^+- or Ca^{2+}-selective

microelectrodes and sampled in DC mode. Intracellular signals were amplified by a SEC 05L amplifier (NPI Electronic Instruments, Tamm, Germany). Field potentials were amplified using a custom-made amplifier equipped with capacitance and offset potential compensation, filtered at 3 KHz, digitised on-line (CED-1401, Cambridge, United Kingdom) and stored on a computer disk for off-line analysis.

Induction of SPW-R complexes was achieved by a high frequency stimulation (HFS) protocol where 3 tetani (100 Hz, 0.4 s) with an interval of 40 s were applied and repeated up to 6 times every 5 minutes (Behrens *et al.*, 2005). The stimulus intensity was adjusted to a supramaximal level of about 60 - 70% of the maximal response determined by input-output curves.

3.3 Data analysis

While the analysis initially included quite a lot of manual data handling, I introduced custom written routines in MATLAB (The MathWorks, Natick, MA, USA) to facilitate the analysis. This optimised not only the time requirements but also the objectivity of data analysis. Furthermore, I adapted the routines for general lab use (Çalışkan *et al.*, 2015; Grosser *et al.*, 2015; Çalışkan *et al.*, 2016; Salar *et al.*, 2016). The procedures described below refer to the most recent progress in the analysis.

To analyse SPW-Rs I first separated the signal into its slow (wave) and fast components (ripples). The slow component is obtained by low-pass filtering (Butterworth, cut frequency: 45 Hz, 8^{th} order) and used for event detection and calculation of amplitude and duration. The area under the curve of the slow component reflecting the inhibitory ionic charge (Schönberger *et al.*, 2014) is determined via trapezoidal numerical integration. The ripple component is isolated by a band-pass filter (Butterworth, passband: 120 - 400 Hz, 8^{th} order). To assign the ripple frequency only subsequent ripples crossing a threshold of 3 times the standard deviation (SD) of the band-pass filtered signal. Ripple amplitudes were calculated using the triplepoint-minimax approach.

The amplitudes of population spikes (evoked by single or paired pulse) were measured similarly. The ratio between second and first orthodromic activation was used to determine the paired pulse ratio (PPR). For comparison of the PPR before and after drug application, I averaged 10 values for each condition.

Additionally, intracellular recordings were used to analyse the coefficient of variance (CV) as described by Faber & Korn (Faber & Korn, 1991). The resulting

distribution is used to locate a pharmacological effect at the pre- or postsynaptic site, by taking into account changes in stochastic quantal release of neurotransmitters.

Together with the latter two methods a third approach was taken to distinguish between pre- and postsynapse. To prove the effect of baclofen ($GABA_B$ receptor agonist) on presynaptic calcium signalling, I performed a set of experiments with Ca^{2+}-sensitive electrodes placed in stratum radiatum of hippocampal area CA1. Short trains of repetitive stimulation (20 Hz, 2s) were applied in absence of excitatory (glutamatergic) synaptic transmission which was blocked by CNQX (competitive AMPA/kainate receptor antagonist) and DL-2-APV (NMDA receptor antagonist). A decrease in the extracellular calcium concentration has been linked to presynaptic Ca^{2+} uptake (Alici *et al.*, 1997).

In those experiments where I aimed to get insight into the mechanism involved in the generation of γ-oscillations, power spectra of 1-min data epochs collected during the last 5 min were analysed. Values for peak power, peak frequency and power between 30 and 90 Hz could be directly derived from the power spectra. In addition, I analysed the 40-10 Hz quotient in a given treatment and termed it γ-θ ratio. Autocorrelation analysis of 5 min of data and further fitting of an exponential to the peaks in the autocorrelation function provided me with a measure for the inner coherence of the evoked γ-oscillations (Stenkamp *et al.*, 2001).

3.4 Statistical evaluation

All numerical data are expressed as mean ± standard error of the mean. If data were normally distributed, statistical evaluation was performed by a one-way analysis of variance (ANOVA) with Bonferroni's correction for multiple comparisons to identify significant differences between conditions. Non-parametric tests (Kruskal-Wallis as well as Friedman) were used and followed by Dunn's multiple comparisons, when data were not normally distributed. *p*-Values less than 0.05 were considered to indicate a significant difference between means.

4 Results

My thesis combines studies I contributed to (Publication I) as well as others that I primarily conducted and designed largely by myself (Publication II & Publication III; see section 7.1 on page 24). I avoided mentioning real values for description of the results to ease readability, and refer to main text and figures of the original publications.

4.1 Publication I: (Liotta *et al.*, 2011)

In this study, we compared stimulus-induced SPW-Rs to recurrent epileptiform discharges (REDs). Our main goal was to expose differences between both types of network activity. We could show that a partial removal of inhibition is sufficient to transform SPW-R activity into epileptiform activity.

To modulate efficacy of inhibition, we first exposed hippocampal slices to the nACh receptor agonist nicotine. Nicotine dose-dependently increased the synaptic response within the associational CA3 network stimulated via the Schaffer collaterals in area CA1. In presence of high concentrations (500 µM) of nicotine, multiple (recurrent) population spikes could be observed (Fig. 1C, Publication I, page 28), indicating a loss of inhibition. By contrast, application of nicotine had no effect on spontaneous activity recorded in naïve (unstimulated) slices.

As shown before, nicotine facilitates the induction of LTP (Fujii *et al.*, 2000; Nashmi & Lester, 2006). Accordingly, we found evidence that induction of SPW-R activity was facilitated in presence of nicotine. The enhanced inducibility of SPW-Rs was reverted to normal by applying the α7-nACh receptor antagonist methyllycaconitine (MLA, 10 nM) prior to wash in of nicotine (data not shown).

To determine whether nicotine modulates ongoing SPW-R activity, the agent was washed in after we had established stable SPW-Rs. While concentrations of 10 µM and 50 µM had no effect at all, significantly higher amplitudes were noted in presence of 100 µM nicotine. Bath application of 500 µM nicotine transformed SPW-Rs into REDs. Parallel monitoring of the overall network activity via extracellular potassium concentration ($[K^+]_o$) revealed pronounced increases of more than 4 mM $[K^+]_o$ under these conditions (Fig. 2, Publication I, page 29).

Simultaneous extra- and intracellular recordings revealed a significant increase of action potentials (APs) generated by cells showing excitatory postsynaptic potentials (EPSPs) in presence of nicotine. Remarkably, cells showing inhibitory postsynaptic potentials (IPSPs) during SPW-Rs events presented EPSPs and successive APs upon wash

in of 500 µM nicotine (Fig. 3, Publication I, page 31). Additionally, we found a significantly reduced jitter in AP firing relative to trough of ripples from sharp waves at concentrations of 100 µM nicotine whereas it significantly increased when nicotine levels were raised to 500 µM (Fig. 4, Publication I, page 31).

In another set of intracellular recordings, we first blocked glutamatergic transmission by co-application of DL-APV (50 µM) and CNQX (25 µM), and evoked IPSPs during depolarizing and hyperpolarizing current injections. In presence of nicotine (100 and 500 µM), the amplitudes of IPSPs were dose-dependently reduced (Fig. 5A, Publication I, page 32) and completely absent following the wash in of bicuculline (not shown). Wash in of MLA (10 nM) antagonised the effect of 100 µM nicotine, whereas concentrations of 500 µM nicotine still led to significant decreases of the evoked IPSP amplitude (Fig. 5C, Publication I, page 32). Accordingly, the inhibitory conductance was dose-dependently reduced and partially recovered in presence of MLA. A similar effect on the inhibitory conductance is shown for increasing concentrations of bicuculline (Fig. 7, Publication I, page 34).

I exposed naïve hippocampal slices to different concentrations of bicuculline to determine the concentration that would induce REDs. At low concentrations (1 µM) induction of REDs failed. In presence of 2 µM bicuculline, every second slice generated REDs. Application of 3 µM bicuculline led to REDs in all slices. With ongoing SPW-Rs activity, lower doses of bicuculline were needed for transition to REDs (1 µM: 64%, 2 µM: 100%, 3 µM: 100%). REDs induced under different conditions and with different concentrations showed similar properties (e.g. amplitude, duration and incidence). See figure 6 for comparison of nicotine- and bicuculline-mediated effect of disinhibition on SPW-Rs.

To finally prove that indeed the disinhibition leads to transformation of SPW-Rs into REDs we washed in a relatively high concentration of potassium (8.5 mM) that exceeded the concentrations recorded in presence of 500 µM nicotine. Although standard parameters describing SPW-Rs were elevated their transition to REDs was never observed, indicating that increased (overall) excitability is not involved in the transition (Fig. 9, Publication I, page 35).

4.2 Publication II: (Hollnagel *et al.*, 2014)

After having shown the impact of a well-balanced interplay between excitation and inhibition for the emergence of SPW-R activity, I examined the role of $GABA_B$ receptor mediated inhibition.

The application of the $GABA_B$ receptor agonist baclofen (0.5 µM) reversibly suppressed SPW-R activity. This suppression was accompanied by an overall reduction of baseline activity (Fig.1A, Publication II, page 44). Comparison of SPW-Rs before and after wash in of baclofen revealed no significant differences among parameters describing SPW-Rs (e.g.: amplitude, duration and frequency). Nevertheless, a significant reduction of the incidence of SPW-R events was noted. I next applied the induction protocol (see: Methodology 3.2 on page 6) in presence of baclofen. Under these conditions, lasting LTP, which is crucial for the induction of SPW-Rs (Behrens *et al.*, 2005; Behrens *et al.*, 2007), could only be induced in a subset of experiments (3 out of 10). Notably, about 25 min after washout of baclofen SPW-R activity could be observed in those experiments (Fig.1B, Publication II, page 44). Co-application of the $GABA_B$ antagonist CGP55846 with baclofen prevented the suppression of SPW-R activity, while application of sole CGP55846 had no major effects (data not shown).

$GABA_B$ receptors can be found both pre- and postsynaptically. I therefore performed a series of experiments to further characterize and locate the effect of baclofen. Intracellular recordings were obtained from CA1 pyramidal cells and paired pulse stimulation (interval: 50 ms) was applied to Schaffer collaterals with intensities subthreshold for induction of action potentials.

Related paired pulse ratios were calculated from naïve slices, as well as following drug application (baclofen: 0.5 µM, bicuculline: 5 µM). We found a significant increase in paired pulse ratio in presence of baclofen, which might indicate a presynaptic modulation possibly due to an altered probability of quantal transmitter release.

To further prove this hypothesis, we performed a coefficient of variation analysis which relates the amplitudes of the obtained EPSPs to the standard deviation of the amplitudes under different conditions. Here, an increase in the variability of cellular responses to an electrical stimulation corresponds to an altered transmitter release. The obtained plot (Fig.2B, Publication II, page 45) clearly points towards presynaptic depressive modulation and is in line with the finding that the paired pulse ratio was increased in presence of baclofen. Experiments monitoring the Ca^{2+} concentration in stratum radiatum during repetitive stimulation trains (20 Hz, 2s) additionally revealed a significant decrease in Ca^{2+} influx upon wash in of baclofen (Fig. 3, Publication II, page 45). Altogether, one can conclude that baclofen leads to a reduction of Ca^{2+} influx which accounts for the depression of evoked EPSPs recorded intra- and extracellularly via reduced transmitter release probability.

4.3 Publication III: (Hollnagel *et al.*, 2015)

The hippocampal formation is well known to generate network oscillations according to the environmental task, thus reflecting a state dependency for different types of frequencies. Elevated levels of acetylcholine (ACh) are observed during states of arousal and explorative behaviour characterised by network oscillations in the theta (θ) and gamma (γ) range (Klinkenberg *et al.*, 2011; Picciotto *et al.*, 2012) as well as during rapid eye movement (REM) sleep (Steriade *et al.*, 1993). We could recently show a transient ACh-dependent switch from SPW-R activity to γ-oscillations (ul Haq *et al.*; submitted to Cerebral Cortex). Additionally, it was reported that there might be evidence for an extracellularly located source of ACh (Vijayaraghavan *et al.*, 2013). I therefore became interested in the underlying ACh metabolism.

In a subset of experiments, I first determined the effect of increasing concentrations of physostigmine, which inhibits the enzyme acetylcholinesterase (AChE), which in turn is responsible for the degradation of ACh. It was not surprising to find a dose-dependent correlation for parameters describing the power and coherence of physostigmine-induced γ-oscillations (Fig. 3, Publication III, page 52). The main finding was that a concentration of 2 µM physostigmine can already and reliably induce γ-oscillations and that these oscillations can be further augmented or modulated by other agents.

Like physostigmine, increasing concentrations of acetylcholine applied with 2, 5 and 10 µM co-applied with 2 µM physostigmine led dose-dependently to more pronounced γ-oscillations. However, we found that peak power saturated between 5 and 10 µM ACh while the inner coherence still increased (Fig. 1 and 2, Publication III, pages 50 and 51). In general, I found peak frequencies slightly decreasing with increasing power of γ-oscillations.

Blockade of choline reuptake by hemicholinium-3 (HC-3, 100 µM) was not sufficient to induce γ-oscillations in naïve slices. Surprisingly, co-application of HC-3 with 2 µM physostigmine resulted in increased peak power of the leading frequency when compared to sole application of physostigmine or HC-3. I found the attenuation of γ-oscillations accelerated when application of HC-3 followed the washout of physostigmine (Fig. 4, Publication III, page 53). The same effect was observed when additional ACh (10 µM) was used for induction of γ-oscillations. These findings indicate that the reuptake of choline is crucial for maintenance of acetylcholine synthesis required for persistent γ-oscillations.

To prove evidence for an extracellularly located source of acetylcholine, we first tested for effects of BETA (100 µM), which limits the efficacy of acetylcholine synthesis by inhibition of the choline-acetyltransferase (ChAT). Due to its lipophilic nature, it is not possible to discriminate between extra- and intracellular effects per se. Hence, we pursued the experiments in presence of HC-3 (to limit reuptake of choline) and physostigmine (to establish persistent γ-oscillations). In summary, we found a general reduction of ongoing oscillatory activity (data not shown).

A putative extracellularly located ChAT provided with one of its substrates (acetyl-CoA) should lead to more pronounced γ-oscillations. I hypothesised that application of acetyl-CoA would positively modulate γ-oscillations. In the related experiments, acetyl-CoA (10 and 50 µM) was co-applied with 2 µM physostigmine. As shown before, in this concentration physostigmine would not fully block ACh degradation (Fig. 3, Publication III, page 52) and, therefore, permit for an acetyl-CoA-dependent increase of activity. This was not the case as we found a decrease in oscillatory activity, which depended on the dose of acetyl-CoA (Fig. 4, Publication III, page 53).

In another set of experiments, we preincubated the slices with 100 µM HC-3 followed by the application 10 µM acetyl-CoA to test whether accumulating choline together with the added acetyl-CoA would lead to extracellular synthesis of ACh and thus induce γ-oscillations. Under these conditions all parameters remained at baseline levels (data not shown).

In summary, we could connect the amount of ACh available with the strength of γ-oscillations observed under different conditions but had to reject the hypothesis that an extracellularly located ChAT can positively modulate ongoing activity in the γ-band.

5 Discussion

Within the hippocampal formation several mechanism provide the emergence of network oscillations that can be tuned dynamically (Draguhn *et al.*, 2014). The network architecture and its connectivity as well as a well-balanced interplay between excitation and inhibition are crucial for proper rhythmogenesis. *In vivo*, different states of brain activity can be observed in the EEG or by intracranial recordings (Buzsáki *et al.*, 2003). Among other mechanisms, fine tuning of excitation and inhibition might be involved in the generation and/or maintenance of such different oscillatory states (Bartos *et al.*, 2007; Schlingloff *et al.*, 2014). Additionally, the presence and availability of specific transmitters and their release probability provide another mechanism of how different network states can be stabilised (Dannenberg *et al.*, 2015).

My studies have addressed the aspects of the generation and modulation of rhythmic activity by pharmacological manipulations of hippocampal networks. I focussed my research on γ-oscillations and sharp wave-ripple (SPW-R) activity, which are involved in memory formation and consolidation.

Under experimental conditions, both types of oscillations can be studied either *in vivo* or *in vitro*. While *in vivo* studies offer a more intact neuronal network that can be accessed via chronically implanted electrodes a direct pharmacological intervention is rather difficult. Modulation of cellular network activity focusses on optogenetic approaches, which permit direct activation of genetically modified channels (Butler *et al.*, 2016). On the other hand, *in vitro* conditions as realised by slice preparations of hippocampal tissue enable research on pharmacological processes involved in higher brain functions. However, the advantage of a direct and relatively fast opportunity to modulate network activity pharmacologically is restricted to an isolated network, lacking input from regions further away and cut apart during slice preparation.

Nevertheless, hippocampal slice preparations from mice and rats are still successfully used to study network dynamics and their pharmacology (Colgin & Moser, 2010; Buzsáki & Wang, 2012; Buzsáki, 2015). It has to be kept in mind however, that slice preparations of similar thickness from the two species preserve different amounts of the hippocampal network due to different brain sizes. Slice preparations from mice are supposed to include a slightly more intact architecture (Routh *et al.*, 2009). In mouse hippocampal slices, SPW-Rs occur spontaneously and might therefore be well suited to study this type of oscillation directly (Maier *et al.*, 2003; Both *et al.*, 2008; Viereckel *et al.*, 2013). Rat hippocampal slices, however, are characterised by spontaneous network

activity in the theta range. Here, repetitive electric stimulation of the associational network in area CA3 leads to the emergence SPW-Rs similar to those observed in freely moving animals (Behrens *et al.*, 2005). The reduced network size facilitates the formation of neuronal ensembles whose participating individual neurons are sequentially activated thereby forming a synfire chain characteristic for individual SPW-R events (Tanaka *et al.*, 2009; Humble *et al.*, 2012; Le Duigou *et al.*, 2014). The stimulation protocol leads to a long-lasting form of LTP and allowed me to study epochs of spontaneous activity before application of the stimulation paradigm and its following SPW-R activity in the same slice. It was already shown that the reduced network size does not compromise the balance between excitation and inhibition. Instead, the augmentation of excitation was counterbalanced by increased inhibition (Maier *et al.*, 2003; Behrens *et al.*, 2007).

In the first project I aimed to study the role of inhibition in the maintenance and stabilisation of induced SPW-R activity and to differentiate between this type of oscillation and recurrent epileptiform discharges (REDs) characteristic for hyper-excitable network states. In this study, we could link the transition from SPW-Rs to REDs to a lack of inhibition (Liotta *et al.*, 2011).

We found that application of the nACh receptor agonist nicotine would initially lead to increased amplitudes of both, evoked population spikes and SPW-Rs. This effect could be antagonised by application of MLA which itself antagonises α7-nACh receptors (Alkondon *et al.*, 1992) highly expressed in cholecystokinin (CCK) expressing GABAergic basket cells (Freedman *et al.*, 1993; Frazier *et al.*, 1998). CCK-positive basket cells control the generation of action potentials of connected parvalbumin (PV) expressing interneurons, which themselves modulate the firing properties of hippocampal pyramidal cells (Karson *et al.*, 2009). We observed a switch to hyper-excitable recurrent activation when further increasing the concentration of nicotine. The conversion was accompanied by large increases in $[K^+]_o$ characteristic for REDs (Heinemann *et al.*, 1977). Interestingly, stimulus-induced SPW-Rs could not be converted to REDs by elevation of potassium to 8.5 mM, whereas unstimulated slices generated recurrent bursting activity in response to increased potassium. Under these conditions, rises of $[K^+]_o$ evoked by single SPW-Rs were smaller than those recorded in presence of bicuculline- or nicotine-induced REDs, suggesting that inhibition was still preserved. Intracellular recordings revealed that nicotine reduced the inhibitory conductance via α7-nACh receptors thereby modulating the $GABA_A$-mediated inhibition onto CA3 pyramidal cells.

In the next study, I targeted the role of inhibition in the generation of SPW-Rs and their maintenance focussing on slow metabotropic inhibition as mediated by $GABA_B$ receptors (Hollnagel *et al.*, 2014).

We found that application of the $GABA_B$ receptor antagonist reversibly blocked stimulus-induced SPW-R activity. This might be important during episodes of elevated GABA concentrations in which the transmitter diffuses to more distant, extrasynaptically located, $GABA_B$ receptors and thus regulates the incidence of SPW-R complexes or even supports the switch from one type of oscillation to another. We could locate the effect of $GABA_B$ to the presynaptic terminal by recording intracellular potentials and extracellular calcium concentrations. Applying the stimulation protocol in presence of baclofen on naïve slices did not generally prevent induction of LTP. Interestingly, SPW-R activity emerged once baclofen had been washed out indicating that the formation of neuronal ensembles during induction was still possible. We therefore concluded that the appearance of SPW-Rs is regulated via presynaptic transmitter release whereas the formation of neuronal ensembles participating in individual SPW-Rs depends on postsynaptic mechanisms responsible for synaptic strengthening.

Another mechanism, however, can regulate the firing behaviour of neurons as well. It was shown, that cholinergic activation of the network enhances spike timing dependent plasticity required to build initially labile engrams of the outer world which then have to be transformed into a more stable representation to become long lasting (Gais & Born, 2004; Thurley *et al.*, 2008). *In vivo* γ-oscillations are associated with the formation of (labile) memory traces while SPW-R activity is essential for the consolidation process and the switches between those two oscillation patterns are accompanied by changes of the acetylcholine (ACh) level (Hasselmo & McGaughy, 2004; Sullivan *et al.*, 2011). *In vivo*, episodes of γ-oscillations are nested within theta oscillations and last only for several hundreds of milliseconds (Klinkenberg *et al.*, 2011; Picciotto *et al.*, 2012) while our *in vitro* model provides a persistent type of γ-oscillations. Nevertheless, this model still enables us to study the role of ACh metabolism in initiating and maintaining γ-oscillations in more detail.

We found that blocking the extracellular degradation of ACh with increasing concentrations of physostigmine was already sufficient to establish persistent γ-oscillations in a dose dependent manner. We could not confirm that an extracellularly located choline-acetyltransferase would positively modulate ongoing γ-oscillations. When limiting the intracellular ACh recycling by block of choline reuptake we observed

faster washout kinetics of γ-oscillations. Thus, we conclude that emergence of γ-oscillations requires very low levels of acetylcholine.

Taken together, my work comprises experiments to investigate the mechanisms that modulate high frequency network oscillations within the hippocampal formation *in vitro*. This is of importance for a better understanding of higher cognitive functions as well as the pathophysiology of neurological disorders such as epilepsy or Alzheimer's disease.

6 References

Alici K, Gloveli T, Schmitz D, Heinemann U (1997). Effects of glutamate receptor agonists and antagonists on Ca^{2+} uptake in rat hippocampal slices lesioned by glucose deprivation or by kainate. Neuroscience 77 (1): 97–109.

Alkondon M, Pereira EF, Wonnacott S, Albuquerque EX (1992). Blockade of nicotinic currents in hippocampal neurons defines methyllycaconitine as a potent and specific receptor antagonist. Mol Pharmacol 41 (4): 802–808.

Amaral D & Lavenex P (2007). The hippocampus book. Chapter 3: Hippocampal Neuroanatomy. Oxford University Press, Oxford.

Bartos M, Vida I, Jonas P (2007). Synaptic mechanisms of synchronized gamma oscillations in inhibitory interneuron networks. Nat Rev Neurosci 8 (1): 45–56.

Behrens CJ, van den Boom LP, de Hoz L, Friedman A, Heinemann U (2005). Induction of sharp wave-ripple complexes in vitro and reorganization of hippocampal networks. Nat Neurosci 8 (11): 1560–1567.

Behrens CJ, van den Boom, L P, Heinemann U (2007). Effects of the GABA(A) receptor antagonists bicuculline and gabazine on stimulus-induced sharp wave-ripple complexes in adult rat hippocampus in vitro. Eur J Neurosci 25 (7): 2170–2181.

Bir SC, Ambekar S, Kukreja S, Nanda A (2015). Julius Caesar Arantius (Giulio Cesare Aranzi, 1530–1589) and the hippocampus of the human brain. History behind the discovery. J Neurosurg 122 (4): 971–975.

Both M, Bähner F, von Bohlen und Halbach, Oliver, Draguhn A (2008). Propagation of specific network patterns through the mouse hippocampus. Hippocampus 18 (9): 899–908.

Boulton CL, von Haebler D, Heinemann U (1992). Tracing of axonal connections by rhodamine-dextran-amine in the rat hippocampal-entorhinal cortex slice preparation. Hippocampus 2 (2): 99–106.

Butler JL, Mendonça PR, Robinson HP, Paulsen O (2016). Intrinsic Cornu Ammonis Area 1 Theta-Nested Gamma Oscillations Induced by Optogenetic Theta Frequency Stimulation. J Neurosci 36 (15): 4155–4169.

Buzsáki G (1986). Hippocampal sharp waves: their origin and significance. Brain Res 398 (2): 242–252.

Buzsáki G (2015). Hippocampal sharp wave-ripple. A cognitive biomarker for episodic memory and planning. Hippocampus 25 (10): 1073–1188.

Buzsáki G, Anastassiou CA, Koch C (2012). The origin of extracellular fields and currents — EEG, ECoG, LFP and spikes. Nat Rev Neurosci 13 (6): 407–420.

Buzsáki G, Buhl DL, Harris KD, Csicsvari J, Czéh B, Morozov A (2003). Hippocampal network patterns of activity in the mouse. Neuroscience 116 (1): 201–211.

Buzsáki G & Draguhn A (2004). Neuronal oscillations in cortical networks. Science 304 (5679): 1926–1929.

Buzsáki G, Leung LW, Vanderwolf CH (1983). Cellular bases of hippocampal EEG in the behaving rat. Brain Res 287 (2): 139–171.

Buzsáki G & Moser EI (2013). Memory, navigation and theta rhythm in the hippocampal-entorhinal system. Nat Neurosci 16 (2): 130–138.

Buzsáki G & Wang X-J (2012). Mechanisms of gamma oscillations. Annu Rev Neurosci 35: 203–225.

Çalışkan G, Albrecht A, Hollnagel JO, Rösler A, Richter-Levin G, Heinemann U, Stork O (2015). Long-term changes in the CA3 associative network of fear-conditioned mice. Stress 18 (2): 1–10.

Çalışkan G, Müller I, Semtner M, Winkelmann A, Raza AS, Hollnagel JO, Rösler A, Heinemann U, Stork O, Meier JC (2016). Identification of Parvalbumin Interneurons as Cellular Substrate of Fear Memory Persistence. Cereb Cortex 26 (5): 2325–2340.

Colgin LL & Moser EI (2010). Gamma Oscillations in the Hippocampus. Physiology 25 (5): 319–329.

Dannenberg H, Pabst M, Braganza O, Schoch S, Niediek J, Bayraktar M, Mormann F, Beck H (2015). Synergy of Direct and Indirect Cholinergic Septo-Hippocampal Pathways Coordinates Firing in Hippocampal Networks. J Neurosci 35 (22): 8394–8410.

Draguhn A, Keller M, Reichinnek S (2014). Coordinated network activity in the hippocampus. Front Neurol Neurosci 34: 26–35.

Faber DS & Korn H (1991). Applicability of the coefficient of variation method for analyzing synaptic plasticity. Biophys J 60 (5): 1288–1294.

Fisahn A, Pike FG, Buhl EH, Paulsen O (1998). Cholinergic induction of network oscillations at 40 Hz in the hippocampus in vitro. Nature 394 (6689): 186–189.

Frazier CJ, Rollins YD, Breese CR, Leonard S, Freedman R, Dunwiddie TV (1998). Acetylcholine activates an alpha-bungarotoxin-sensitive nicotinic current in rat hippocampal interneurons, but not pyramidal cells. J Neurosci 18 (4): 1187–1195.

Freedman R, Wetmore C, Strömberg I, Leonard S, Olson L (1993). Alpha-bungarotoxin binding to hippocampal interneurons: immunocytochemical characterization and effects on growth factor expression. J Neurosci 13 (5): 1965–1975.

Fujii S, Jia Y, Yang A, Sumikawa K (2000). Nicotine reverses GABAergic inhibition of long-term potentiation induction in the hippocampal CA1 region. Brain Res 863 (1-2): 259–265.

Gais S & Born J (2004). Low acetylcholine during slow-wave sleep is critical for declarative memory consolidation. Proc Natl Acad Sci U S A 101 (7): 2140–2144.

Gloveli T, Dugladze T, Rotstein HG, Traub RD, Monyer H, Heinemann U, Whittington MA, Kopell NJ (2005). Orthogonal arrangement of rhythm-generating microcircuits in the hippocampus. Proc Natl Acad Sci U S A 102 (37): 13295–13300.

Grosser S, Hollnagel JO, Gilling KE, Bartsch JC, Heinemann U, Behr J (2015). Gating of hippocampal output by β-adrenergic receptor activation in the pilocarpine model of epilepsy. Neuroscience 286: 325–337.

Hájos N & Paulsen O (2009). Network mechanisms of gamma oscillations in the CA3 region of the hippocampus. Neural Netw 22 (8): 1113–1119.

Hales CG & Pockett S (2014). The relationship between local field potentials (LFPs) and the electromagnetic fields that give rise to them. Front Syst Neurosci 8: 217.

Hasselmo ME & McGaughy J (2004). High acetylcholine levels set circuit dynamics for attention and encoding and low acetylcholine levels set dynamics for consolidation. Prog Brain Res 145: 207–231.

Hebb DO (1949). The organization of behavior. A neuropsychological theory. Wiley, New York.

Heinemann U, Lux HD, Gutnick MJ (1977). Extracellular free calcium and potassium during paroxsmal activity in the cerebral cortex of the cat. Exp Brain Res 27 (3-4): 237–243.

Hollnagel JO, Maslarova A, ul Haq R, Heinemann U (2014). $GABA_B$ receptor dependent modulation of sharp wave-ripple complexes in the rat hippocampus in vitro. Neurosci Lett 574: 15–20.

Hollnagel JO, ul Haq R, Behrens CJ, Maslarova A, Mody I, Heinemann U (2015). No evidence for role of extracellular choline-acetyltransferase in generation of gamma oscillations in rat hippocampal slices in vitro. Neuroscience 284: 459–469.

Humble J, Denham S, Wennekers T (2012). Spatio-temporal pattern recognizers using spiking neurons and spike-timing-dependent plasticity. Front Comput Neurosci 6.

Kann O, Papageorgiou IE, Draguhn A (2014). Highly energized inhibitory interneurons are a central element for information processing in cortical networks. J Cereb Blood Flow Metab 34 (8): 1270–1282.

Karson MA, Tang A-H, Milner TA, Alger BE (2009). Synaptic cross talk between perisomatic-targeting interneuron classes expressing cholecystokinin and parvalbumin in hippocampus. J Neurosci 29 (13): 4140–4154.

Klausberger T & Somogyi P (2008). Neuronal diversity and temporal dynamics: the unity of hippocampal circuit operations. Science 321 (5885): 53–57.

Klinkenberg I, Sambeth A, Blokland A (2011). Acetylcholine and attention. Behav Brain Res 221 (2): 430–442.

Kohus Z, Káli S, Rovira L, Schlingloff D, Papp O, Freund TF, Hájos N, Gulyás AI, Freund TF (2016). Properties and dynamics of inhibitory synaptic communication within the CA3 microcircuits of pyramidal cells and interneurons expressing parvalbumin or cholecystokinin. J Physiol.

Le Duigou C, Simonnet J, Teleñczuk MT, Fricker D, Miles R (2014). Recurrent synapses and circuits in the CA3 region of the hippocampus. An associative network. Front Cell Neurosci (Frontiers in Cellular Neuroscience) 7.

Leung LW, Lopes da Silva, F H, Wadman WJ (1982). Spectral characteristics of the hippocampal EEG in the freely moving rat. Electroencephalogr Clin Neurophysiol 54 (2): 203–219.

Liotta A, Çalışkan G, ul Haq R, Hollnagel JO, Rösler A, Heinemann U, Behrens CJ (2011). Partial disinhibition is required for transition of stimulus-induced sharp wave-ripple complexes into recurrent epileptiform discharges in rat hippocampal slices. J Neurophysiol 105 (1): 172–187.

Lisman JE & Jensen O (2013). The θ-γ neural code. Neuron 77 (6): 1002–1016.

Maier N, Nimmrich V, Draguhn A (2003). Cellular and network mechanisms underlying spontaneous sharp wave-ripple complexes in mouse hippocampal slices. J Physiol 550 (3): 873–887.

Metherate R, Tremblay N, Dykes RW (1987). Acetylcholine permits long-term enhancement of neuronal responsiveness in cat primary somatosensory cortex. Neuroscience 22 (1): 75–81.

Moreno A, Morris RG, Canals S (2016). Frequency-Dependent Gating of Hippocampal–Neocortical Interactions. Cereb Cortex 26 (5): 2105–2114.

Nashmi R & Lester HA (2006). CNS localization of neuronal nicotinic receptors. J Mol Neurosci 30 (1-2): 181–184.

Neves G, Cooke SF, Bliss TV (2008). Synaptic plasticity, memory and the hippocampus: a neural network approach to causality. Nat Rev Neurosci 9 (1): 65–75.

O'Keefe J & Nadel L (1978). The hippocampus as a cognitive map. Clarendon Press, Oxford.

Picciotto MR, Higley MJ, Mineur YS (2012). Acetylcholine as a neuromodulator: cholinergic signaling shapes nervous system function and behavior. Neuron 76 (1): 116–129.

Ramón y Cajal S (1995). Histology of the nervous system of man and vertebrates. Oxford University Press, New York.

Roumis DK & Frank LM (2015). Hippocampal sharp-wave ripples in waking and sleeping states. Curr Opin Neurobiol 35: 6–12.

Routh BN, Johnston D, Harris K, Chitwood RA (2009). Anatomical and electrophysiological comparison of CA1 pyramidal neurons of the rat and mouse. J Neurophysiol 102 (4): 2288–2302.

Salar S, Lapilover E, Müller J, Hollnagel JO, Lippmann K, Friedman A, Heinemann U (2016). Synaptic plasticity in area CA1 of rat hippocampal slices following intraventricular application of albumin. Neurobiol Dis 91: 155–165.

Schlingloff D, Káli S, Freund TF, Hájos N, Gulyás AI (2014). Mechanisms of sharp wave initiation and ripple generation. J Neurosci 34 (34): 11385–11398.

Schneider J, Lewen A, Ta T-T, Galow LV, Isola R, Papageorgiou IE, Kann O (2015). A reliable model for gamma oscillations in hippocampal tissue. J Neurosci Res 93 (7): 1067–1078.

Schönberger J, Draguhn A, Both M (2014). Lamina-specific contribution of glutamatergic and GABAergic potentials to hippocampal sharp wave-ripple complexes. Front Neural Circuits 8: 103.

Scolville WB & Milner B (1957). Loss of recent memory after bilateral hippocampal lesions. J Neurol Neurosurg Psychiatr 20 (1): 11–21.

Squire LR (1992). Declarative and nondeclarative memory: multiple brain systems supporting learning and memory. J Cogn Neurosci 4 (3): 232–243.

Staley KJ & Dudek FE (2006). Interictal spikes and epileptogenesis. Epilepsy Curr 6 (6): 199–202.

Stenkamp K, Palva JM, Uusisaari M, Schuchmann S, Schmitz D, Heinemann U, Kaila K (2001). Enhanced temporal stability of cholinergic hippocampal gamma oscillations following respiratory alkalosis in vitro. J Neurophysiol 85 (5): 2063–2069.

Steriade M, McCormick DA, Sejnowski TJ (1993). Thalamocortical oscillations in the sleeping and aroused brain. Science 262 (5134): 679–685.

Sullivan D, Csicsvari J, Mizuseki K, Montgomery S, Diba K, Buzsáki G (2011). Relationships between hippocampal sharp waves, ripples, and fast gamma oscillation: influence of dentate and entorhinal cortical activity. J Neurosci 31 (23): 8605–8616.

Tanaka T, Kaneko T, Aoyagi T (2009). Recurrent Infomax Generates Cell Assemblies, Neuronal Avalanches, and Simple Cell-Like Selectivity. Neural Comput 21 (4): 1038–1067.

Tétrault S, Chever O, Sik A, Amzica F (2008). Opening of the blood-brain barrier during isoflurane anaesthesia. Eur J Neurosci 28 (7): 1330–1341.

Thurley K, Leibold C, Gundlfinger A, Schmitz D, Kempter R (2008). Phase precession through synaptic facilitation. Neural Comput 20 (5): 1285–1324.

Traub RD, Bibbig A, LeBeau FE, Buhl EH, Whittington MA (2004). Cellular mechanisms of neuronal population oscillations in the hippocampus in vitro. Annu Rev Neurosci 27: 247–278.

van Strien NM, Cappaert NL, Witter MP (2009). The anatomy of memory. An interactive overview of the parahippocampal–hippocampal network. Nat Rev Neurosci 10 (4): 272–282.

Viereckel T, Kostic M, Bähner F, Draguhn A, Both M (2013). Effects of the GABA-uptake blocker NNC-711 on spontaneous sharp wave-ripple complexes in mouse hippocampal slices. Hippocampus 23 (5): 323–329.

Vijayaraghavan S, Karami A, Aeinehband S, Behbahani H, Grandien A, Nilsson B, Ekdahl KN, Lindblom RP, Piehl F, Darreh-Shori T (2013). Regulated Extracellular Choline Acetyltransferase Activity- The Plausible Missing Link of the Distant Action of

Acetylcholine in the Cholinergic Anti-Inflammatory Pathway. PLoS ONE 8 (6): e65936.

Watrous AJ, Fell J, Ekstrom AD, Axmacher N (2015). More than spikes: common oscillatory mechanisms for content specific neural representations during perception and memory. Curr Opin Neurobiol 31: 33–39.

Whittington MA, Traub RD, Jefferys JG (1995). Synchronized oscillations in interneuron networks driven by metabotropic glutamate receptor activation. Nature 373 (6515): 612–615.

Windmüller O, Lindauer U, Foddis M, Einhäupl KM, Dirnagl U, Heinemann U, Dreier JP (2005). Ion changes in spreading ischaemia induce rat middle cerebral artery constriction in the absence of NO. Brain 128 (9): 2042–2051.

Wójtowicz AM, van den Boom LP, Chakrabarty A, Maggio N, ul Haq R, Behrens CJ, Heinemann U (2009). Monoamines block kainate- and carbachol-induced gamma-oscillations but augment stimulus-induced gamma-oscillations in rat hippocampus in vitro. Hippocampus 19 (3): 273–288.

7 Affidavit

I, Jan-Oliver Hollnagel, certify under penalty of perjury by my own signature that I have submitted the thesis on the topic of "Modulation of fast neuronal network oscillations in the hippocampal formation". I wrote this thesis independently and without assistance from third parties, I used no other aids than the listed sources and resources.

All points based literally or in spirit on publications or presentations of other authors are, as such, in proper citations (see "uniform requirements for manuscripts (URM)" the ICMJE www.icmje.org) indicated. The sections on methodology (in particular practical work, laboratory requirements, statistical processing) and results (in particular images, graphics and tables) correspond to the URM (see above) and are answered by me. My contributions in the selected publications for this dissertation correspond to those that are specified in the following joint declaration with the responsible person and supervisor. All publications resulting from this thesis and which I am author of correspond to the URM (see above) and I am solely responsible.

The importance of this affidavit and the criminal consequences of a false affidavit (section 156,161 of the Criminal Code) are known to me and I understand the rights and responsibilities stated therein.

.....	.....
Date	Jan-Oliver Hollnagel

7.1 Declaration of contribution to the selected publications

I, Jan-Oliver Hollnagel, had the following share in the selected publications:

7.1.1 Publication I: (Liotta *et al.*, 2011)

Liotta A, Çalışkan G, ul Haq R, **Hollnagel JO**, Rösler A, Heinemann U, Behrens CJ (2011) Partial disinhibition is required for transition of stimulus-induced sharp wave-ripple complexes into recurrent epileptiform discharges in rat hippocampal slices. J. Neurophysiol. 105 (1): 172–187.

Impact Factor (2011): 3.316

Contribution: 15%

Contribution in detail: Participation in planning and conducting the experiments regarding the effect of bicuculline, associated data analysis, preparation of related figures and proof reading of the manuscript.

7.1.2 Publication II: (Hollnagel *et al.*, 2014)

Hollnagel JO, Maslarova A, ul Haq R, Heinemann U (2014) $GABA_B$ receptor dependent modulation of sharp wave-ripple complexes in the rat hippocampus in vitro. Neurosci. Lett. 574: 15–20.

Impact Factor (2013/2014): 2.055

Contribution: 70%

Contribution in detail: Planning and conducting the majority of the experiments, complete data analysis, preparation of figures, contribution to writing the manuscript and managing the peer review process.

7.1.3 Publication III: (Hollnagel *et al.*, 2015)

Hollnagel JO, ul Haq R, Behrens CJ, Maslarova A, Mody I, Heinemann U (2015) No evidence for role of extracellular choline-acetyltransferase in generation of gamma oscillations in rat hippocampal slices in vitro. Neuroscience 284: 459–469.

Impact Factor (2014/2015): 3.357

Contribution: 80%

Contribution in detail: Planning and conducting the majority of the experiments, complete data analysis, preparation of figures, contribution to writing the manuscript and managing the peer review process.

.....	.....
Prof. Dr. Uwe Heinemann	Dipl. Biol. Jan-Oliver Hollnagel

Publication I

J Neurophysiol 105: 172–187, 2011.
First published September 29, 2010; doi:10.1152/jn.00186.2010.

Partial Disinhibition Is Required for Transition of Stimulus-Induced Sharp Wave–Ripple Complexes Into Recurrent Epileptiform Discharges in Rat Hippocampal Slices

Agustin Liotta,[1]* Gürsel Çalışkan,[1]* Rizwan ul Haq,[1] Jan O. Hollnagel,[1] Anton Rösler,[1] Uwe Heinemann,[1,2] and Christoph J. Behrens[1]

[1]*Institute of Neurophysiology, Institute for Physiology and* [2]*NeuroCure Research Center, Charité–Universitätsmedizin Berlin, Berlin, Germany*

Submitted 16 February 2010; accepted in final form 16 September 2010

Liotta A, Çalışkan G, ul Haq R, Hollnagel JO, Rösler A, Heinemann U, Behrens CJ. Partial disinhibition is required for transition of stimulus-induced sharp wave–ripple complexes into recurrent epileptiform discharges in rat hippocampal slices. *J Neurophysiol* 105: 172–187, 2011. First published September 29, 2010; doi:10.1152/jn.00186.2010. Sharp wave–ripple complexes (SPW-Rs) in the intact rodent hippocampus are characterized by slow field potential transients superimposed by close to 200-Hz ripple oscillations. Similar events have been recorded in hippocampal slices where SPW-Rs occur spontaneously or can be induced by repeated application of high-frequency stimulation, a standard protocol for induction of long-lasting long-term potentiation. Such stimulation is reminiscent of protocols used to induce kindling epilepsy and ripple oscillations may be predictive of the epileptogenic zone in temporal lobe epilepsy. In the present study, we investigated the relation between recurrent epileptiform discharges (REDs) and SPW-Rs by studying effects of partial removal of inhibition. In particular, we compared the effects of nicotine, low-dose bicuculline methiodide (BMI), and elevated extracellular potassium concentration ($[K^+]_o$) on induced SPW-Rs. We show that nicotine dose-dependently transformed SPW-Rs into REDs. This transition was associated with reduced inhibitory conductance in CA3 pyramidal cells. Similar results were obtained from slices where the GABAergic conductance was reduced by application of low concentrations of BMI (1–2 μM). In contrast, sharp waves were diminished by phenobarbital. Elevating $[K^+]_o$ from 3 to 8.5 mM did not transform SPW-Rs into REDs but significantly increased their incidence and amplitude. Under these conditions, the equilibrium potential for inhibition was shifted in depolarizing direction, whereas inhibitory conductance was significantly increased. Interestingly, the propensity of elevated $[K^+]_o$ to induce seizure-like events was reduced in slices where SPW-Rs had been induced. In conclusion, recruitment of inhibitory cells during SPW-Rs may serve as a mechanism by which hyperexcitation and eventually seizure generation might be prevented.

INTRODUCTION

Hippocampal sharp waves consist of slow field potential transients that are superimposed by approximately 200-Hz network oscillations, termed "ripples" (Chrobak et al. 2000), and are predominantly observed in vivo during consummatory behavior and slow-wave sleep (Buzsáki 1986, 1998). Similar network activity has been observed in vitro where spontaneous sharp wave–ripple complexes (SPW-Rs) have been recorded in rodent hippocampal slices (Behrens et al. 2005; Both et al. 2008; Maier et al. 2003; Nimmrich et al. 2005). We have previously shown that in rat hippocampal slices SPW-Rs can be induced by standard protocols for induction of late or long-lasting long-term potentiation (LTP) (Behrens et al. 2005; Frey and Morris 1997). This is reminiscent of kindling-induced epileptiform activity. Interestingly, SPW-R-like activity has also been observed in epileptic rodents and in humans, suggesting that these events may serve as a biomarker for an epileptogenic zone (Staba et al. 2004). Indeed, it was suggested that stimulus-induced SPW-Rs are a model of epilepsy (Staley and Dudek 2006). We therefore decided to compare the properties of SPW-Rs and epileptiform activity induced by partial removal of inhibition and furthermore studied conditions under which SPW-Rs were converted into recurrent epileptiform discharges. In the present study, we investigated the effects of high concentrations of nicotine (100 and 500 μM) and low concentrations of bicuculline methiodide (BMI, 1–2 μM) on induced SPW-R activity and compared these with the effects of increased extracellular potassium concentration ($[K^+]_o$, 8.5 mM).

The hippocampus is densely packed with a variety of nicotinic acetylcholine receptors (nAChRs) localized on both principal cells and interneurons (Albuquerque et al. 1995; Freund and Katona 2007; Ji et al. 2001). Nicotine influences synaptic transmission in hippocampal slices (Giocomo and Hasselmo 2005; Radcliffe et al. 1999) and an α7-nAChR-dependent reduction of the GABAergic inhibition has been shown in area CA1 (Zhang and Berg 2007). We show that nicotine, which in contrast to recent observations in cerebellar slices, did not induce synchronized network discharges in area CA3 of naïve slices, but dose-dependently transformed SPW-Rs into prolonged network discharges reminiscent of REDs. This was associated with a partial reduction in the inhibitory conductance in CA3 pyramidal cells. Similarly, a dose-dependent transition of SPW-Rs into REDs resulted from application of BMI, whereas positive modulation of γ-aminobutyric acid type A ($GABA_A$)–mediated inhibition by phenobarbital significantly diminished SPW-R activity. Elevating $[K^+]_o$ has been shown to induce burst-like discharges in hippocampal pyramidal cells (Jensen et al. 1994; Korn et al. 1987; Rutecki et al. 1985) and to augment spontaneous and action potential (AP)–dependent transmitter release (Hablitz and Lundervold 1981), in part, by slowing repolarization of APs (for review see Lux

* These authors contributed equally to this work.
Address for reprint requests and other correspondence: C. J. Behrens, Institute for Neurophysiology, Johannes Müller-Center for Physiology, Charité–Universitätsmedizin Berlin, Oudenarder Strasse 16, 13347 Berlin, Germany (E-mail: christoph.behrens@charite.de).

et al. 1986). Elevation of $[K^+]_o$ also causes a depolarizing shift of the equilibrium potential E_{IPSP} (Jensen et al. 1993; Korn et al. 1987) due to reduced efficacy of the KCC2 transporter (Jarolimek et al. 1999; Staley and Proctor 1999). Our data show that during 8.5 mM $[K^+]_o$, the incidence and amplitude of stimulus-induced SPW-Rs were increased, whereas notably, any transition of SPW-Rs into REDs was prevented. In the absence of glutamatergic transmission, inhibitory conductance was increased in CA3 pyramidal cells. Furthermore, the propensity of elevated $[K^+]_o$ to induce seizure-like events (SLEs) was higher in naïve slices compared with stimulated slices, which expressed SPW-Rs. Together, our in vitro findings indicate that reduced $GABA_A$-mediated inhibition is one key prerequisite needed to transform SPW-Rs into recurrent epileptiform discharges.

METHODS

Slice preparation

Animal procedures were performed in accordance with the guidelines of the European Communities Council and approved by the regional authority (LaGeSO Berlin: T0068/02). Wistar rats (aged 6–8 wk, ~200 g) of either sex were decapitated under deep ether anesthesia. Horizontal hippocampal slices (400 μm/at bregma −4.7 to −7.3 mm) were prepared at an angle of about 12° in the frontooccipital direction (with the frontal portion up) using a vibratome (752 M Vibroslice; Campden Instruments, Loughborough, UK). Preparation of slices was done in ice-cold artificial cerebrospinal fluid (aCSF) containing (in mM): NaCl 129, $NaHCO_3$ 21, KCl 3, $CaCl_2$ 1.6, $MgSO_4$ 1.8, NaH_2PO_4 1.25, and glucose 10, saturated with 95% O_2-5% CO_2. Slices were immediately transferred to an interface chamber perfused with aCSF at 36 ± 0.5°C (flow rate: ~1.6 ml/min, pH 7.4, osmolarity: 295–300 mosmol/kg). Recordings were started 2–3 h after preparation. Except for experiments concerning monosynaptic inhibitory postsynaptic potentials (IPSPs), the concentration of $MgSO_4$ was lowered to1.2 mM (a value close to physiological Mg^{2+} concentrations; Windmuller et al. 2005) 1 h before starting the recordings for all experiments. Since a reduction of the IPSP conductance has been described during prolonged epileptiform activity on lowering of extracellular magnesium concentration $[Mg^{2+}]_o$ to 0 mM in the aCSF (Whittington et al. 1995), we investigated whether lowering of $[Mg^{2+}]_o$ from 1.8 to 1.2 mM in aCSF resulted in changes in GABAergic inhibition. Control experiments were performed in CA3 pyramidal cells, where changes in $GABA_A$-mediated inhibition were tested while $[Mg^{2+}]_o$ was lowered from 1.8 to 1.2 mM Mg^{2+}. This had no significant effect on the conductance of IPSPs, which was slightly but not significantly reduced (Ctl: 25.2 ± 3.6 nS; after 15 min: 22.6 ± 3.6 nS; after 30 min: 26.1 ± 1.2 nS; and after 45 min: 24.7 ± 2.4 nS, $P > 0.05$, $n = 5$; data not shown).

Electrophysiological recordings

Extracellular field potentials (FPs) were recorded under interface conditions using a custom-made amplifier from the stratum pyramidale of area CA3, with microelectrodes filled with 154 mM NaCl (5–10 MΩ). For intracellular recordings, sharp microelectrodes (70–90 mΩ) were pulled from borosilicate glass (OD 1.2 mm) and filled with 2.5 M K^+-acetate. The sharp microelectrode technique was chosen because it allows stable recordings demanded for long-term intracellular recordings during SPW-Rs. Extra- and intracellular signals were amplified by a SEC 05L amplifier (NPI Electronic Instruments, Tamm, Germany). All data were low-pass filtered at 3 kHz, digitized at 10 kHz, and stored on computer disk using a CED 1401 interface (Cambridge Electronic Design [CED], Cambridge, UK). Intracellular recordings were accepted when membrane potentials of the cells were < −60 mV, action potentials (APs) exceeded 75 mV, and input resistance was >25 MΩ. Input resistance was determined by hyperpolarizing current injection pulses of 0.2–0.4 nA for 0.2–0.6 s.

To measure changes in $[K^+]_o$, we used double-barreled K^+-sensitive microelectrodes for DC-coupled recordings in area CA3. K^+-sensitive microelectrodes were manufactured as previously described (Heinemann and Arens 1992). In brief, K^+-sensitive microelectrodes were tip-filled with the potassium ionophore cocktail A (60031; Fluka Chemie, Buchs, Switzerland) and accepted when they responded with 59 ± 1 mV to a change in $[K^+]_o$ from 3 to 30 mM.

In recordings where we tested for effects mediated by nicotine, bicuculline, or elevation of $[K^+]_o$ from 3 to 8.5 mM on GABAergic inhibition onto CA3 pyramidal cells DL-APV (50 μM) was coapplied with 6-cyano-7-nitroquinoxaline-2,3-dione (CNQX, 25 μM), to block glutamatergic synaptic transmission. To study evoked IPSPs, depolarizing and hyperpolarizing current steps (0.06 to −0.12 nA of 0.5-s duration; interval: 1.7 s) were applied. An extracellular single pulse stimulus (0.1 ms, 1–4 V, 75% of the maximal cell response) was applied with a delay of 0.25 s to the onset of each current pulse. Monosynaptic IPSPs were evoked by stimulation of either stratum radiatum (SR) or stratum oriens (SO) of area CA3 (see Davies and Collingridge 1993; Romo-Parra et al. 2008).

Induction of SPW-Rs

SPW-Rs were induced by high-frequency stimulation (HFS, containing three tetani of 40 pulses applied at 100 Hz, each; pulse duration: 0.1 ms; intertetanus interval: 40 s; HFS was repeated every 5 min) using a bipolar platinum electrode (25 μm, tip separation: 100–150 μm) placed in the SR of area CA1. Slices were stimulated using submaximal (70%) stimulus intensity (1.5–3 V) of that required to evoke maximal amplitude field responses.

Data analysis

To analyze different components of the SPW-Rs and REDs, raw data were filtered using the digital filter function in Spike2 software (CED) as previously described (Behrens et al. 2005). In brief, for ripple detection, we used a band-pass filter of 40–400 Hz with a threshold set to 4- to 6 SD of eventless baseline noise. For sharp wave detection, recordings were low-pass filtered at 20 Hz (Spike2 software). Ripple frequency was determined using custom-made software (H. Siegmund).

In the experiments where we tested for the modulation of the GABAergic inhibition onto CA3 pyramidal cells, changes in the amplitude of evoked IPSPs were measured during positive and negative current steps. Because sharp microelectrodes were used for long-term recordings of single-cell responses during SPW-Rs, we also used this method to calculate the membrane conductance. To determine the effects on synaptic conductance, a linear regression of the evoked potentials as a function of depolarizing and hyperpolarizing current injection was calculated using Origin software (Version 6, Microcal Software, Northampton, MA). For each condition (control, 100 and 500 μM nicotine, 1 and 2 μM BMI, $[K^+]_o$ 8.5 mM) the slope ± SD was calculated. The IPSP conductance was estimated by regression analysis from the plotted slope of the relation between the membrane potential deflection at the peak of the IPSPs versus injected current, minus the resting conductance of the cell (Luhmann and Prince, 1991). For statistical comparison, absolute data, obtained from each experiment, were normalized. To analyze changes in cellular timing during ripple oscillations, we measured the jitter between a given field ripple and the corresponding intracellular recorded AP. For that purpose, we measured the latency between the negative peak of the field ripple and the positive peak of a given AP. The calculated jitter was determined as the SD of the measured mean latencies between ripples and APs under defined conditions (control, 100 and 500 μM

nicotine). For comparison, changes in the jitter were normalized. All data are reported as means ± SE. Statistical significance was determined using one-way ANOVA (Origin 6.0; Microcal); $P < 0.05$ (*) was considered to indicate a significant difference.

Drugs

All drugs were dissolved in aCSF and applied by continuous bath perfusion. Nicotine tartrate (100 and 500 μM) was applied for 25–40 min; methyllycaconitine citrate hydrate (MLA, a specific α7 receptor antagonist, 10 nM) and mecamylamine hydrochloride (MEC, an unspecific nAChR antagonist, 25 μM) were used to test for specificity of nicotine effects. To mimic the effects of nicotine by acetylcholine (ACh) we used acetylcholine chloride (10 μM) in presence of atropine (1 μM) and physostigmine (2 μM). To investigate the effects of nicotine, BMI, or elevation in $[K^+]_o$ to 8.5 mM on evoked monosynaptic IPSPs on pyramidal cells, DL-2-amino-5-phosphonopentanoic acid (DL-APV sodium salt, 50 μM) and 6-cyano-7-nitroquinoxaline-2,3-dione (CNQX disodium salt, 25 μM) were applied to block the glutamatergic transmission. To investigate the α7-nAChR specificity of nicotine-mediated effects on evoked IPSPs, we added the α7-nAChR antagonist MLA to the bath solution, including DL-APV and CNQX prior to the application of nicotine. Bicuculline methiodide (BMI, 1–3 μM) was applied to determine which amount of fractional loss of inhibition was required for transformation of SPW-Rs into REDs and to verify that evoked IPSPs were $GABA_A$-dependent. Sodium phenobarbital (20 μM, courtesy of Dr. Holtkamp) was applied to test effects of increases in inhibition on SPW-R activity by modulation of $GABA_A$ receptors. All drugs were purchased from Sigma-Aldrich (Taufkirchen, Germany), except DL-APV and CNQX (Ascent Scientific, Bristol, UK).

RESULTS

Nicotine-mediated effects on area CA3 in naïve slices

Nicotine has recently been shown to evoke synchronized network oscillations in the cerebellum (Middleton et al. 2008). To test whether in hippocampal area CA3 nicotine application resulted in the induction of synchronized network activity, nicotine was bath applied in a concentration of 100 or 500 μM for 45 min to unstimulated, naïve slices. Extracellular field potential (FP) recordings obtained from the stratum pyramidale in area CA3 revealed that neither 100 μM ($n = 6$ slices) nor 500 μM of nicotine ($n = 5$ slices) induced synchronized network activity (data not shown). To investigate whether nicotine exerted effects on stimulus-evoked FPs in area CA3, single-pulse stimulation was applied to the stratum radiatum (SR) in area CA1 (Fig. 1*A*), thereby activating Schaffer collaterals, which originate from CA3 pyramidal cells. This stimulation induced antidromic FP responses in area CA3, which consisted of two population spikes (PSs): a first antidromic PS due to direct activation of CA3 pyramidal cell axons and a second PS, representing the population response generated by transmission via short, recurrent axon collaterals onto neighboring CA3 cells within the associational CA3 network (see Fig. 1*B*). We found that nicotine applied in 100 and 500 μM did not significantly affect the antidromically evoked first PS (Fig. 1*C*). In contrast, the second PS was significantly and reversibly enhanced to 162.7 ± 8.5% ($P < 0.004$) and to 179.8 ± 11.0% of control ($P < 0.001$) when nicotine was applied at 100 and 500 μM, respectively (washout: 102.4 ± 15.1%, $n = 6$ slices, $P > 0.05$; Fig. 1, *C* and *D*). In addition, in the presence of 500 μM nicotine, we observed the occurrence of multiple recurrent PSs (Fig. 1*C*), suggesting a loss of inhibition.

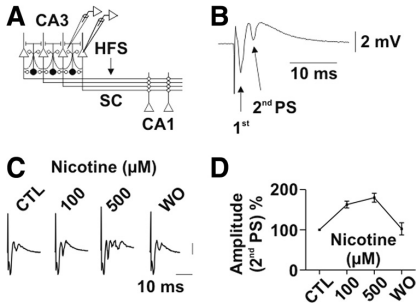

FIG. 1. Dose-dependent effects of nicotine (100–500 μM) on population spike response in area CA3 following stimulation of Schaffer collaterals in area CA1. *A*: scheme of hippocampus showing extra and intracellular recording sites in area CA3 and stimulation (Stim.) applied to Schaffer collaterals (SCs) in the stratum radiatum (SR) of area CA1. *B*: representative population spike (PS) response in area CA3 following antidromic stimulation applied to the SR of area CA1. Arrows: 1st (arrow) antidromic PS due to direct activation of CA3 pyramidal cell axons and 2nd PS superimposed on recurrent field excitatory postsynaptic potential (EPSP), representing population response generated within area CA3 associational recurrent collateral network. *C*: dose-dependent and reversible effects of nicotine on PS responses in area CA3. Note that nicotine significantly increased the amplitude of the 1st PS, whereas 500 μM nicotine reversibly induced multiple 2nd PSs. *D*: plot of normalized amplitude of the 2nd PS in area CA3 under control conditions, during application of 100 and 500 μM nicotine, and during washout.

Nicotine facilitates stimulus-dependent induction of SPW-Rs and modulates their properties

As previously reported, hippocampal sharp wave–ripple complexes (SPW-Rs) could be induced by repeated high-frequency stimulation (HFS), which reliably induced long-term potentiation (LTP) (Behrens et al. 2005). Simultaneous triple FP recordings obtained from stratum pyramidale in area CA3 and CA1 and stratum granulare in the dentate gyrus (DG) revealed that stimulus-induced SPW-Rs originated in the CA3 region, whereas they orthodromically spread into the CA1 region as previously shown (Behrens et al. 2005). In dentate gyrus, rather small negative potentials were observed. Such events presented with amplitudes <150–200 μV, and usually followed events in area CA3, whereas they occurred relatively simultaneously with CA1 events where transients were negative in SR neighboring the DG. These events may therefore represent far field effects or a back-propagation from CA3 to the dentate gyrus (Scharfman 2007). We did not further analyze these oscillations in the present study (data not shown).

Since the cholinergic agonist nicotine is known to facilitate induction of LTP in various brain regions including the hippocampal formation (Fujii et al. 2000; Nashmi and Lester 2006; Séguéla et al. 1993), we first investigated whether nicotine showed any effects on the induction of SPW-Rs (Supplemental Fig. S1).[1] In this set of experiments, nicotine was regularly administrated 30 min before HFS was started (HFS consisted of three short tetani applied at 100 Hz; see METHODS). Under control conditions, SPW-Rs appeared after 5.8 ± 0.4 tetanic stimulations ($n = 6$ slices), whereas in the presence of nicotine (100 and 500 μM) the threshold for

[1] The online version of this article contains supplemental data.

induction of SPW-Rs was reduced (Supplemental Fig. S1). In the presence of 100 μM nicotine, the number of tetani required to induce SPW-Rs was 3.0 $\pm$ 0.0 (n = 6 slices; $P < 0.0001$, Supplemental Fig. S1, *B* and *E*). The number of tetani required to induce SPW-R further decreased to 2.0 $\pm$ 0.7 when slices were pretreated with 500 μM nicotine (n = 6 slices; $P < 0.0001$, Supplemental Fig. S1, *C* and *E*). As shown in Supplemental Fig. S1*D*, prior application of the α7-NACh receptor antagonist methyllycaconitine (MLA, 10 nM) prevented the effect of 100 μM (n = 6; Supplemental Fig. S1, *D* and *E*). Importantly, in the absence of any stimulation, 500 μM nicotine did not cause any kind of spontaneous synchronized epileptiform discharges (data not shown).

To test potential nicotine-mediated effects on established SPW-Rs, HFS was repeated every 5 min as previously reported (Behrens et al. 2005). Following the sixth HFS, when stable SPW-Rs were induced, they occurred with an incidence of 12.2 $\pm$ 0.3 events/min and showed an average amplitude of 2.7 $\pm$ 0.1 mV (Fig. 2, *Aa–Ac*). SPW-Rs lasted on average for 54.8 $\pm$ 0.3 ms (n = 11 slices, Fig. 2, *Ab* and *Ac*). Ripple oscillations, which were superimposed on sharp waves, showed a mean frequency of 181.1 $\pm$ 2.0 Hz (n = 11 slices; Fig. 2*Ac*). To test whether nicotine affected stimulus-induced SPW-Rs, the drug was applied for 30–40 min during ongoing SPW-R activity. Nicotine applied in a concentration of 10 and 50 μM had no significant effects on the incidence, amplitude, or duration of established SPW-Rs (n = 6, $P > 0.05$, each; data not shown). In the presence of 100 μM nicotine, the incidence of SPW-Rs was slightly but not significantly increased to 13.5 $\pm$ 1.1 SPW-Rs/min (n = 5 slices, Fig. 2, *Aa* and *Ac*; washout: 5.3 $\pm$ 0.9 SPW-Rs/min). In contrast, 100 μM of nicotine caused a significant and reversible increase of the SPW-Rs amplitude to 4.1 $\pm$ 0.5 mV (n = 5 slices, $P < 0.005$, Fig. 2, *Aa–Ac*; washout: 2.3 $\pm$ 0.2 mV) with a duration of 56.1 $\pm$ 3.6 ms (n = 11 slices, Fig. 2, *Ab* and *Ac*). In this concentration, nicotine did not significantly change the frequency of ripple oscillations, which was 183.2 $\pm$ 4.8 Hz (n = 5 slices, Fig. 2*Ac*; washout: 185.5 $\pm$ 5.0 Hz).

When nicotine was applied at a concentration of 500 μM (n = 6 slices) SPW-Rs were transformed into recurrent epileptiform discharges (REDs), which occurred with an incidence of 9.2 $\pm$ 1.0 REDs/min ($P < 0.02$, Fig. 2, *Ba* and *Bc*; washout: 9.1 $\pm$ 0.7 REDs/min). REDs showed an amplitude of 5.4 $\pm$ 0.7 mV, which was significantly larger than that of control SPW-Rs ($P < 0.001$, washout: 3.1 $\pm$ 0.5 mV) and lasted on average 117.4 $\pm$ 11.3 ms ($P < 0.001$, Fig. 2, *Ba–Bc*; washout: 45.8 $\pm$ 5.9 ms). Under this condition, the ripple frequency was significantly increased to 210.8 $\pm$ 5.0 Hz ($P < 0.04$, Fig. 2*Bc*; washout 183.9 $\pm$ 3.6 Hz; the transition from SPW-R to REDs induced by 500 μM nicotine is shown later in Fig. 6). Usually, this transition began 20 min after onset of application, as indicated by an increase in amplitude, first, and subsequently the duration of single events, and was nearly complete after 30 min. As a measure for the underlying network activation, we analyzed changes in the extracellular potassium concentration ($[K^+]_o$) accompanying SPW-Rs, before and after application of 100 and 500 μM of nicotine since pronounced increases in $[K^+]_o$ are characteristic for REDs both in vivo and in vitro (Behrens et al. 2007; Futamachi and Pedley 1976; Heinemann et al. 1977). As illustrated in Fig. 2*C*, 100

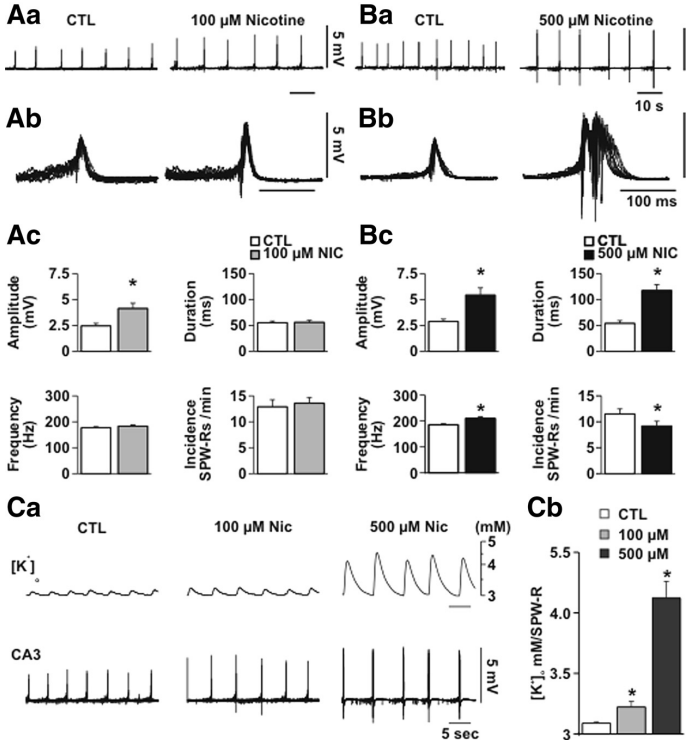

FIG. 2. Effects of nicotine on stimulus-induced sharp wave–ripple complexes (SPW-Rs). *Aa*: sample recording of 100 μM nicotine-mediated effects on established SPW-Rs. *Left*: control. *Right*: 100 μM nicotine; scale bars: 5 mV, 10 s. *Ab*: overlay of 10 samples of SPW-Rs before (*left*) and during application of 100 μM nicotine (*right*); scale bars: 5 mV, 0.1 s. *Ac*: plots summarizing 100 μM nicotine-mediated effects on SPW-Rs. Note that 100 μM nicotine caused an increase only in amplitude without major effects on ripple frequency, SPW-R incidence, and duration. *Ba*: analogous to *Aa–Ac*. Sample recording of 500 μM nicotine-mediated effects on SPW-Rs (*Left*: control; *Right*: 500 μM nicotine); scale bars: 5 mV, 10 s. *Bb*: overlay of 10 samples of SPW-Rs before (*left*) and during application of 500 μM nicotine (*right*); scale bars: 5 mV, 0.1 s, each. *Bc*: plots summarizing the effects of 500 μM nicotine on SPW-Rs. Note that 500 μM nicotine markedly prolonged SPW-Rs, transforming them into recurrent epileptiform discharges (REDs; $^*P < 0.05$). *Ca*: representative samples of increases in $[K^+]_o$ (*top*) accompanying SPW-Rs (*bottom*) under control condition (*left*) and during application of 100 μM (*middle*) and 500 μM nicotine (*left*). Note massive increases in $[K^+]_o$ during 500 μM nicotine-induced REDs. *Cb*: plot summarizing $[K^+]_o$ increases under different conditions according to *Ca* (n = 5 slices, each, $P < 0.05$).

μM nicotine elevated the increases in $[K^+]_o$ from 0.09 ± 0.01 to 0.22 ± 0.04 mM ($n = 5$, $P < 0.05$), whereas 500 μM of nicotine caused an elevation of increases in $[K^+]_o$ to 1.12 ± 0.14 mM ($n = 5$, $P < 0.001$; Fig. 2*C*).

To test whether ACh application mimicked nicotine-mediated effects on SPW-Rs, we applied 10 μM ACh in the presence of atropine (1 μM) to block muscarinic receptors. Selective activation of nAChR by ACh during blocked muscarinic transmission did not cause significant changes in the properties of SPW-Rs ($n = 4$; see Supplemental Fig. S2, *A* and *B*; amplitude: control: 2.8 ± 0.3 mV, wash in: 2.7 ± 0.5 mV, washout: 2.4 ± 0.65 mV; duration: control: 54.0 ± 2.0 ms, wash in: 53.0 ± 3.1 ms, washout: 54.0 ± 2.0 ms; incidence: control: 13.1 ± 3.2 SPW-Rs/min, wash in: 8.9 ± 2.3 SPW-Rs/min, washout: 7.5 ± 2.1 SPW-Rs/min; ripple frequency: control: 197.5 ± 17.2 Hz, wash in: 186.7 ± 16.3 Hz, washout: 189.7 ± 21.8 Hz). Since ACh may be degraded by the acetylcholine esterase (ACh-E), we then coapplied the ACh-E blocker physostigmine (2 μM). This resulted in similar changes of SPW-Rs properties compared with those resulting from 100 μM nicotine application (Supplemental Fig. S2, *A* and *B*). In these experiments we found a significant and reversible increase in the SPW-Rs amplitude from 2.8 ± 0.3 to 4.2 ± 0.2 mV ($n = 5$, $P > 0.005$, washout: 3.1 ± 0.2 mV) and incidence from 8.2 ± 1.0 to 13.1 ± 1.7 SPW-Rs/min (washout 6.1 ± 0.7), whereas duration and frequency were not significantly altered, similar to the experiments with 100 μM nicotine (for details see Supplemental Fig. S2).

Effects of 100 μM nicotine are α7-nACh receptor-dependent

To investigate in more detail the profile of the receptor subtypes involved in the observed nicotine-mediated effects, we performed experiments with two different, more specific, nACh receptor antagonists. We applied the nonspecific antagonist mecamylamine (MEC, 25 μM) (Giocomo and Hasselmo 2005) to block the two main types of nicotine receptors in the hippocampus, namely α7 and α4-β2 subunit containing receptors (Nott and Levin 2006). In these experiments, MEC was added to aCSF for ≥20 min before 100 μM of nicotine was coapplied during established SPW-R activity. MEC prevented the nicotine-mediated effects on the incidence, amplitude, and duration of SPW-Rs as well as on ripple frequency ($n = 6$ slices, $P > 0.05$, each; Supplemental Fig. S3, *A* and *B*). Importantly, application of methyllycaconitine (MLA, 10 nM), a specific antagonist for the α7 subunit containing nicotinic receptors, which are strongly expressed in hippocampal interneurons (Séguéla et al. 1993), also blocked effects caused by 100 μM nicotine ($n = 5$ slices; for details see Supplemental Fig. S3). Importantly, the application of MLA did not generate changes in the control activity (Supplemental Fig. S3). However, effects on SPW-Rs mediated by 500 μM of nicotine could not be fully antagonized by both nAChR antagonists, in part due to unspecific effects of the nAChR antagonist (data not shown).

Nicotine dose-dependently modulates single-cell responses during SPW-Rs

To study how nicotine affected the underlying cellular behavior during SPW-R activity, we performed simultaneous extra- and intracellular recordings from CA3 pyramidal cells (see Fig. 3). Under control conditions, 7 of 11 cells displayed compound excitatory postsynaptic potentials (EPSPs) superimposed by one to two APs. We found that nicotine dose-dependently increased the number of APs generated during SPW-Rs (Fig. 3, *Aa* and *Ab*). Thus the number of APs was increased from 1.6 ± 0.4 APs/SPW-R under control to 3.2 ± 0.4 APs/SPW-R during application of 100 μM of nicotine ($P < 0.001$) and to 19.8 ± 2.6 APs/SPW-R on 500 μM ($n = 7$ cells, $P < 0.001$, Fig. 3, *Aa* and *Ab*). Moreover, we found that the amplitude of SPW-R-associated compound EPSPs was almost unchanged during 100 μM nicotine (14.1 ± 1.3 mV under control vs. 15.0 ± 0.9 mV during 100 μM nicotine, $P > 0.05$), whereas 500 μM nicotine caused a significant increase to 20.2 ± 0.8 mV ($P < 0.001$; Fig. 3, *Aa* and *Ab*). Notably, the four cells, which displayed IPSPs during SPW-Rs, did not change their behavior in the presence of 100 μM nicotine ($n = 4$ cells, Fig. 3, *Ba* and *Bb*). In contrast, when exposed to 500 μM nicotine, cells that originally generated IPSPs during SPW-Rs switched their response into SPW-R-associated EPSPs, generating 4.3 ± 1.4 APs/SPW-R ($P < 0.001$, $n = 4$ cells, Fig. 3, *Ba* and *Bb*). However, in those cells there were no paroxysmal depolarization shifts. In two cells that were recorded during washout for ≥50 min, we observed that the transition into SPW-R-associated EPSPs was fully reversible (data not shown). In both concentrations, nicotine did not significantly change the input resistance (R_i) of recorded CA3 pyramidal cells (control: 35.7 ± 3.9 MΩ; 100 μM: 38.7 ± 2.7 MΩ; 500 μM: 38.8 ± 3.2 MΩ; and washout: 34.4 ± 3.8 MΩ; $n = 11$ cells, $P > 0.5$, each). Similarly, the membrane potential in stimulated slices was not significantly changed before and after application of nicotine in both concentrations ($n = 11$ cells, $P > 0.05$; data not shown).

Nicotine dose-dependently affects spike timing of CA3 pyramidal cells during ripple oscillations

To investigate whether nicotine had any effects on the temporal relation of APs to the network ripples, we also determined the jitter between the AP peaks recorded from single CA3 pyramidal cells and the trough of extracellularly recorded ripples during the course of a given SPW-R ($n = 1,376$; Fig. 4*A*). Notably, we observed that the increased cellular firing caused by 100 μM nicotine was accompanied by a significant reduction in the jitter between APs to the corresponding ripple oscillations (Fig. 4*B*). Thus in the presence of 100 μM nicotine, the jitter of the latency was significantly reduced to 76.0 ± 8.9% of control ($n = 358$ ripples in 7 cells, $P < 0.05$; Fig. 4*C*). In contrast, 500 μM nicotine significantly increased the jitter of the latency to 139.1 ± 10.5% of control ($n = 852$ ripples in 7 cells, $P < 0.05$; Fig. 4, *B* and *C*).

Nicotine reduces the GABAergic input onto CA3 principal cells

Based on our observations that during 500 μM nicotine. SR stimulation induced multiple PSs in area CA3 and that $GABA_A$ergic disinhibition had previously been shown to cause similar changes in area CA3 (Hablitz 1984), we hypothesized that nicotine might reduce $GABA_A$ receptor-mediated inhibition onto CA3 pyramidal cells. To test for nicotine-mediated

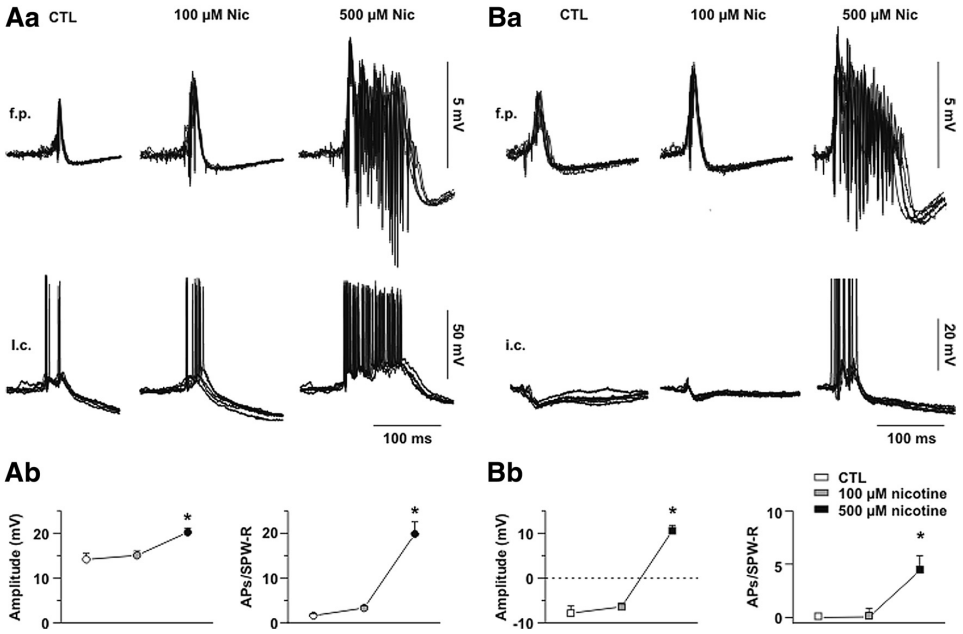

FIG. 3. Dose-dependent effects of nicotine on intracellular responses during sharp-wave ripples in CA3 pyramidal cells. *Aa*: overlay of 5 samples of simultaneous extra (*top*) and intracellular recordings (*bottom*) showing cellular responses of EPSP-generating CA3 pyramidal cell during SPW-Rs under control condition (*left*) and during application of 100 μM (*middle*) and 500 μM nicotine. *Ab*: plotted EPSP amplitude (*left*) and number of action potential (AP)/SPW-Rs (*right*) under control (white) and during application of 100 μM (gray) and 500 μM (black) nicotine. *Ba*: analogous to *A*, overlay of 5 samples of simultaneous extra (*top*) and intracellular recordings (*bottom*) of inhibitory postsynaptic potential (IPSP)–generating CA3 pyramidal cells during SPW-Rs (APs are truncated). *Bb*: plotted IPSP amplitude (*left*) and number of AP/SPW-Rs (*right*) under control (white) and during application of 100 μM (gray) and 500 μM (black) nicotine. Note that in the presence of 500 μM nicotine, IPSP-generating cells switch their response into suprathreshold EPSPs, which under this condition do not represent paroxysmal depolarization shifts as observed in EPSP-generating cells.

effects on inhibition, we performed sharp microelectrode recordings of evoked IPSPs during constant positive and negative current pulses in the absence of glutamatergic transmission due to coapplication of DL-APV (50 μM) and CNQX (25 μM). In these experiments, the SR and SO in area CA3 were alternatively stimulated during application of 100 and 500 μM nicotine ($n = 7$ cells; Fig. 5, *A–C*). IPSPs evoked by SR and SO stimulation did not show significant differences (data not shown). However, in the absence of glutamatergic transmission, six of seven cells showed a depolarization of the resting membrane potential of -63.2 ± 0.9 to -60.5 ± 1.5 mV ($P < 0.02$) and to -58.9 ± 1.8 mV ($P < 0.003$) on 100 and 500 μM nicotine, respectively (Fig. 5*A*). During nicotine application, the amplitudes of evoked IPSPs evoked at depolarizing and hyperpolarizing membrane potentials were reduced in a dose-dependent manner (Fig. 5*A*). The remaining IPSPs were completely abolished by BMI (5 μM; data not shown). These changes were not accompanied by a major shift of the chloride reversal potential (E_{IPSP}) during nicotine application, which was -74.3 ± 1.5 mV (control), -75.1 ± 1.6 mV (100 μM; Fig. 5, *A* and *B*), and -75.7 ± 1.7 mV (500 μM, $n = 7$ cells, $P > 0.05$; Fig. 5, *C* and *D*). When we calculated the synaptic

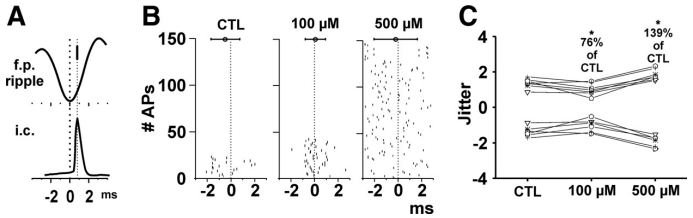

FIG. 4. Dose-dependent effects of nicotine on the jitter between the peak of APs generated by CA3 pyramidal cells and the through during synchronized ripple oscillations. *A*: scheme of an AP generated by a CA3 pyramidal cell and its corresponding field ripple showing latency between the ripple through and AP peak. *B*: plots showing the occurrence of APs (black streaks) during the time windows of ripple-oscillations in seven cells generating EPSP-associated APs during SPW-R activity in the presence of 100 and 500 μM nicotine. Note that in control conditions all cells already fired in a preferential interval during field ripples (CTL, *top trace*). During 100 μM nicotine (*middle trace*) cells generated a significantly higher number of APs. Note that the SD around the averaged latency (○) was smaller under these conditions, indicating a decreased jitter. In contrast, application of 500 μM nicotine resulted in a significant augmentation of APs (*bottom trace*), accompanied by an expansion of the SD around the averaged jitter between the AP peak and the corresponding ripple trough, indicating a loss of spike-timing precision. *C*: normalized SD of the jitter between APs and ripple troughs from 1,528 ripples (from 7 cells). Note the significantly decreased SD, indicating an increased spike-timing precision in the presence of 100 μM nicotine ($P < 0.05$).

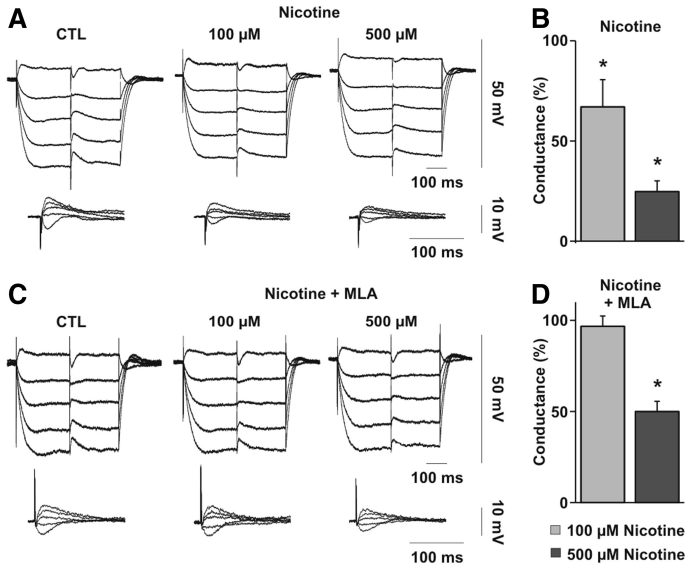

FIG. 5. Effects of nicotine on isolated IPSPs. *A*: sample recordings of isolated IPSPs in CA3 pyramidal cells during application of nicotine in the absence of glutamatergic transmission. *Bottom traces*: overlay of IPSPs evoked during depolarizing and hyperpolarizing current steps showing dose-dependent decreases in the amplitude of evoked IPSPs by nicotine. *B*: normalized changes in synaptic conductance for experiments with 100 μM (light gray) and 500 μM nicotine (dark gray). *C*: sample recordings of evoked IPSPs in the presence of 10 nM methyllycaconitine (MLA) preapplied to nicotine in the absence of glutamatergic transmission. *Bottom traces*: overlay of IPSPs evoked during depolarizing and hyperpolarizing current steps showing blockade of 100 μM nicotine-mediated effects on evoked IPSPs. *D*: normalized changes in synaptic conductance for experiments with 100 μM (light gray) and 500 μM nicotine (dark gray) in the presence of the α7-nicotinic acetylcholine receptor (nAChR) antagonist. Note that MLA blocked the decrease in inhibitory conductance mediated by 100 μM nicotine (*$P < 0.05$), whereas 500 μM nicotine-mediated effects were only partially antagonized (for comparison see *B*).

conductance underlying the generation of IPSPs (see METHODS), we found that this was dose-dependently decreased by nicotine from 31.3 ± 5.3 nS (control) to 21.0 ± 5.6 nS (100 μM) and 7.6 ± 1.7 nS (500 μM, $n = 7$ cells; Fig. 5). Normalization of the absolute data revealed that nicotine caused a significant reduction in the IPSP conductance to 67.0 ± 17.3% of control (100 μM, $P < 0.05$; Fig. 5*B*) and to 24.7 ± 4.5% of control (500 μM, $P < 0.001$, Fig. 5*B*).

To test whether nicotine-mediated effects on evoked IPSPs were α7-nACh receptor-specific, we applied 100 and 500 μM nicotine in the presence of MLA (10 nM). These experiments revealed that MLA prevented the effect mediated by 100 μM nicotine ($n = 6$ slices, $P > 0.07$), indicating that the observed attenuation of the IPSP was α7-nAChR-dependent (Fig. 5, *C* and *D*). However, a significant decrease of the evoked IPSP amplitude could not be fully prevented by MLA when 500 μM nicotine was applied ($n = 6$ slices, $P < 0.001$). Accordingly, in the presence of MLA, normalized synaptic conductance was not significantly reduced during application of 100 μM of nicotine (97.5 ± 9.1% of control), whereas this was decreased to 49.3 ± 9.2% of control ($n = 6$, $P < 0.001$) when 500 μM nicotine was applied (control: 17.6 ± 4.3 nS, 100 μM: 16.8 ± 4.3 nS, 500 μM: 11.0 ± 3.3 nS, $n = 6$).

Dose-dependent effects of bicuculline on stimulus-induced SPW-Rs

Based on our finding that partial disinhibition, caused by nicotine, could lead to a transition of stimulus-induced SPW-Rs into REDs, we investigated whether partial disinhibition, induced by increasing concentrations of BMI, similarly affected SPW-Rs in area CA3. To detect the threshold of disinhibition needed to induce spontaneous REDs, we applied BMI to naïve slices. Application of 1 μM BMI did not result in the generation of REDs in area CA3 ($n = 11$ slices; data not shown). When BMI was applied in a concentration of 2 μM, REDs occurred in 54.0% of recorded slices ($n = 13$ slices), with an incidence of 8.4 ± 1.2 events/min and an amplitude of 5.1 ± 1.1 mV ($n = 7$, each). Ripple frequency was 237.2 ± 11.6 Hz ($n = 7$ slices). They lasted on average for 135.3 ± 9.0 ms ($n = 7$ slices). Notably, in a concentration of 3 μM, BMI reliably induced REDs in all recorded naïve slices. Properties of spontaneous REDs were well comparable to those observed during 2 μM BMI; they occurred with an incidence of 8.4 ± 2.0, showed an amplitude of 6.3 ± 1.5 mV, and lasted for 131.4 ± 7.2 ms, whereas the frequency of superimposed ripples was 241.0 ± 7.2 Hz ($n = 5$ slices, $P > 0.05$, each).

Subsequently, we tested for dose-dependent effects of BMI in slices where SPW-Rs had been induced (data not shown) prior to BMI application. When BMI was applied in a concentration of 1 μM, SPW-Rs were transformed into REDs in 36% of 14 slices, whereas in 64% SPW-Rs were increased only in amplitude and ripple frequency (data not shown). In the latter slices, the amplitude of SPW-Rs was enlarged from 3.1 ± 0.2 to 5.0 ± 0.5 mV ($P < 0.001$) and the frequency of ripples was increased from 190.2 ± 3.2 to 213.0 ± 9.6 Hz ($P < 0.02$). In contrast, the incidence and duration of SPW-Rs remained unaffected ($n = 9$, $P > 0.09$ and $P > 0.6$, respectively). In the remaining 5 of 14 slices, 1 μM BMI transformed SPW-R into REDs, which lasted for 142.0 ± 7.6 ms ($P < 0.001$), with an amplitude of 5.5 ± 0.2 mV ($n = 5$ slices, $P < 0.001$). Incidence decreased to 7.1 ± 0.3 REDs/min ($n = 5$ slices). In these slices, the frequency of ripple oscillations was slightly but nonsignificantly increased to 202.9 ± 5.5 Hz ($n = 5$, $P > 0.06$). BMI (2 μM) reliably converted SPW-Rs into REDs in all tested slices (data not shown). In these experiments the incidence of REDs was significantly reduced to 7.1 ± 0.7 REDs/min ($n = 5$ slices, $P < 0.004$), whereas they showed an amplitude of 7.3 ± 1.3 mV ($n = 5$ slices, $P < 0.02$) and lasted for 147.7 ± 3.1 ms ($n = 5$ slices, $P < 0.001$; data not shown). As expected, the ripple frequency was significantly increased from 198.2 ± 7.7 Hz during SPW-Rs to 266.3 ± 7.0 Hz ($n = 5$ slices, $P < 0.001$). A further increase of BMI concentration to 3 μM showed that properties of REDs were well comparable

to those recorded during 2 μM BMI [incidence: 7.3 $\pm$ 0.8 REDs/min ($P < 0.02$); amplitude: 8.2 $\pm$ 1.3 mV ($P < 0.01$); duration: 145.8 $\pm$ 9.2 ms ($P < 0.01$); ripple frequency: 262.9 $\pm$ 8.4 Hz ($P < 0.001$), $n = 5$ slices, each; P values resulting from comparison to SPW-Rs]. In Fig. 6, the time course of these alterations is depicted. The transformation of SPW-Rs into REDs started 10 min after onset of 2 μM BMI application and was nearly complete 5 min later.

Bicuculline-mediated effects on inhibitory conductance in CA3 pyramidal cells are dose-dependent

To investigate in more detail dose-dependent effects of BMI on inhibitory synaptic transmission onto CA3 pyramidal cells, we next applied BMI at concentrations of 1 and 2 μM on monosynaptic IPSPs evoked in the absence of glutamatergic transmission (see Fig. 7). BMI reduced the amplitude of evoked IPSPs in a dose-dependent manner (see Fig. 7, *A* and *B*). Comparison of the inhibitory conductance before and after BMI application revealed that this was reduced, respectively, to 43.3 $\pm$ 3.6% of control (1 μM, $n = 8$ cells, $P < 0.001$) and to 15.5 $\pm$ 4.3% of control (2 μM, $n = 6$ cells, $P < 0.001$, Fig. 7*C*; control: 14.5 $\pm$ 1.0 nS, 1 μM: 6.0 $\pm$ 0.3 nS, 2 μM: 3.2 $\pm$ 1.1 nS). In these experiments input resistance of CA3 cells was not significantly changed (control: 33.2 $\pm$ 2.9 MΩ, 1 μM: 34.7 $\pm$ 2.5 MΩ, 2 μM: 35.7 $\pm$ 2.0 MΩ, $P > 0.05$, each; see Fig. 7*A*).

Effects of phenobarbital on induced SPW-Rs

Phenobarbital (PB) enhances IPSPs by increasing mean open time of Cl^- channels (Macdonald et al. 1989). To determine whether SPW-Rs are influenced by phenobarbital we investigated the effects of 20 μM PB on established SPW-R activity (Fig. 8). These experiments revealed a significant reduction of amplitudes and incidence of SPW-Rs in area CA3

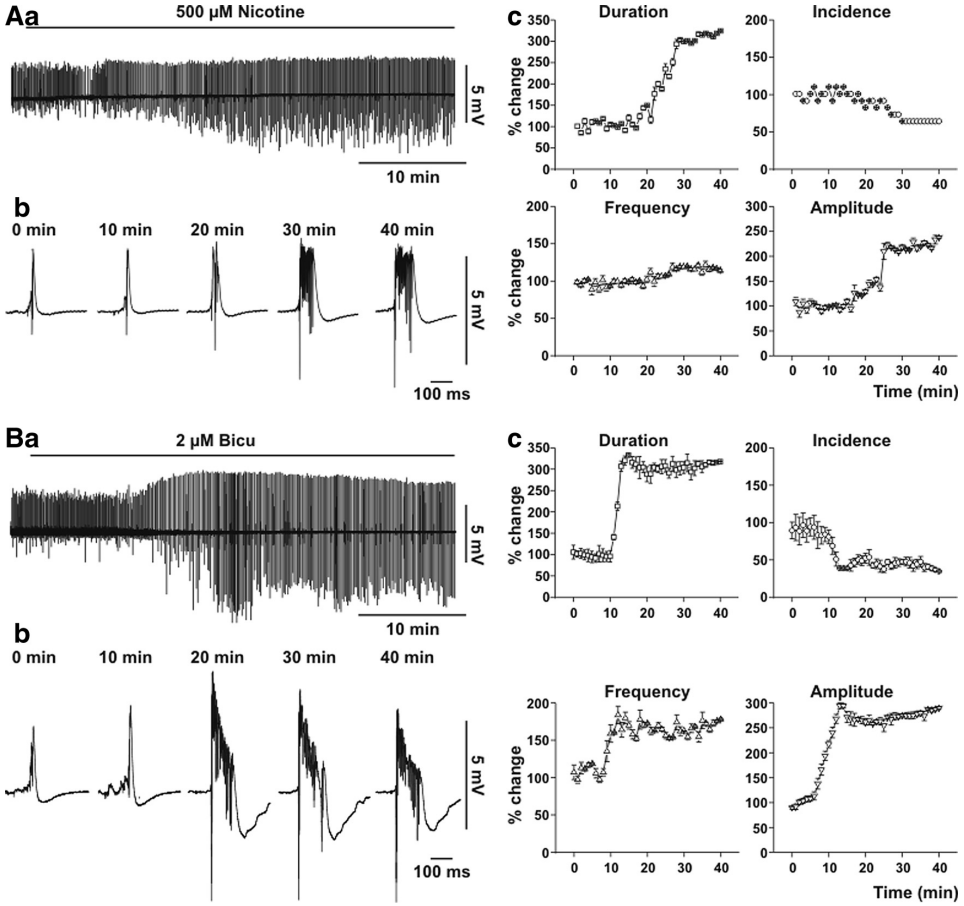

FIG. 6. Comparison of SPW-R transition into hypersynchronized network activity caused by nicotine (500 μM) or low-dose bicuculline (2 μM). *Aa*: sample recording showing transition of SPW-Rs into hypersynchronized network discharges during wash in of 500 μM nicotine. *Ab*: representative CA3 network discharges depicted on enlarge timescale before and during wash in of 500 μM nicotine. *Ac*: normalized, plotted time courses of duration, incidence, and amplitude of synchronized events and frequency of superimposed network fast oscillations. *Ba*: analogous to *Aa*, transition of SPW-Rs into hypersynchronized network discharges following 2 μM bicuculline methiodide (BMI) application. *Bb*: representative CA3 network discharges shown on enlarge timescale before and during wash in of 2 μM BMI. *Bc*: normalized, plotted time courses of duration, incidence, and amplitude of synchronized discharges and frequency of superimposed network fast oscillations. Note abrupt occurrence of massively prolonged discharges was observed only during BMI application.

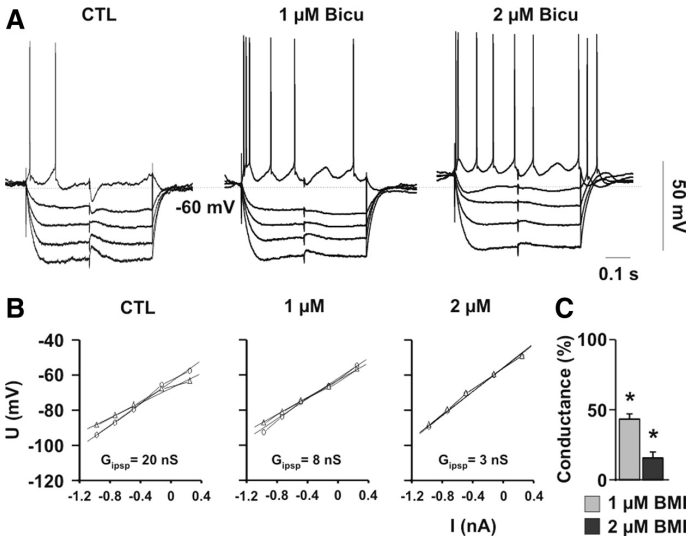

FIG. 7. Effects of low doses of BMI on isolated IPSPs in CA3 pyramidal cells. *A*: sample recordings of isolated IPSPs in CA3 pyramidal cells during application of low concentrations of BMI (1 and 2 μM) in the absence of glutamatergic transmission. Note dose-dependent decreases in the amplitude of evoked IPSPs by bicuculline. *B*: plotted current–voltage (*I–V*) curves under control condition (*left*) and during 1 μM (*middle*) and 2 μM of BMI (*right*), indicating dose-dependent BMI-mediated decrease in inhibitory conductance. *C*: normalized changes in the synaptic conductance for experiments with 1 μM (light gray) and 2 μM BMI (dark gray). Note the dose-dependent decrease in normalized inhibitory conductance (*$P < 0.05$).

($n = 8$, $P < 0.05$). Notably, the frequency of ripple oscillations superimposed on sharp waves (SWs) was not significantly altered, although a small reversible decrease of the ripple frequency was observed in the presence of PB and subsequent washout (for details see Fig. 8).

Effects of elevated extracellular potassium concentration on induced SPW-Rs

The KCC2 transporter exploits the transmembrane potassium gradient to extrude chloride (Cl^-) from cells (Misgeld et al. 1986; Rivera et al. 1999), thereby setting the reversal potential E_{IPSP} to potentials more negative than the resting membrane potential. As previously reported, increasing $[K^+]_o$ shifts the GABA reversal potential in a depolarizing direction (Thompson and Gähwiler 1989) possibly resulting in a reduced efficacy of inhibition (Lopantsev et al. 2009; Staley and Proctor 1999). We therefore tested whether 8.5 mM $[K^+]_o$ converted stimulus-induced SPW-Rs into REDs (see Fig. 9).

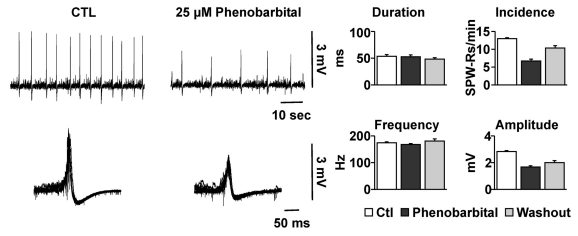

FIG. 8. Effects of phenobarbital (PB) on established SPW-Rs. *A*: sample recording obtained from stratum pyramidale of the CA3b region under control condition (*top*) and representative SPW-R taken from the same recording shown on expanded timescale (*bottom*); scale bars: 3 mV, 10 s (*top*), 0.1 s (*bottom*). *B*: analogous to *A*, established SPW-Rs in the presence of PB (20 μM, *top*), and individual SPW-R depicted on expanded timescale. *C*: plots summarizing effects on the SPW-R amplitude, duration, and incidence and on the frequency of SPW-associated ripple oscillations under control condition (white), in the presence of PB (black), and during washout (gray) according to recordings shown in *A* and *B*. Note that both the incidence and amplitude are reversibly reduced by the barbiturate ($n = 8$ slices, $P < 0.05$).

Elevation of $[K^+]_o$ from 3 to 8.5 mM resulted in a significant increase of the SPW-R incidence from 10.1 ± 1.6 to 47.8 ± 5.0 events/min ($n = 11$ slices, $P < 0.001$; Fig. 9*A*). Similarly, in the presence of 8.5 mM $[K^+]_o$ the duration of SPW-Rs was prolonged from 45.2 ± 4.7 to 61.6 ± 7.0 ms ($n = 11$ slices, $P < 0.001$), and caused a significant increase in the amplitude from 2.9 ± 0.1 to 6.8 ± 0.8 mV ($n = 11$ slices, $P < 0.00$, Fig. 9*B*). Using ion-sensitive microelectrodes, we found that transient, SPW-R-associated increases in $[K^+]_o$ were augmented from 0.9 ± 0.01 to 0.13 ± 0.02 mM ($P < 0.05$) in the presence of 8.5 mM $[K^+]_o$ (Fig. 9*C*). Interestingly, the frequency of SPW-R-associated ripple oscillation was not significantly altered (180.3 ± 6.8 to 192.6 ± 7.7 Hz, $n = 11$ slices, $P > 0.3$; Fig. 9*B*).

Simultaneous intracellular recordings from CA3 pyramidal cells revealed that 8.5 mM $[K^+]_o$ did not significantly change either the resting membrane potential (62.1 ± 0.4 vs. 60.6 ± 2.8 mV, $n = 9$ cells, $P > 0.05$) or the input resistance (44.8 ± 3.3 vs. 41.0 ± 8.4 MΩ, $n = 9$ cells, $P > 0.05$). In line with previous findings (Staley et al. 1998), in the presence of 8.5 $[K^+]_o$, CA3 cells showed an increased intrinsic excitability, as indicated by a significantly increased firing rate associated with a high incidence of spontaneous burst discharges (see Fig. 9*D*). In particular, comparison of cellular responses to SPW-Rs in EPSP-generating cells revealed that elevated $[K^+]_o$ caused a significant increase in the number of APs generated during SPW-Rs from 1.6 ± 0.1 to 5.8 ± 0.2 APs/SPW-R ($n = 5$ cells, $P < 0.001$; see Fig. 9*D*). Notably, intracellular recordings from these cells did not reveal prolonged depolarizing responses during network discharges, as observed following application of nicotine and BMI (see Fig. 9*D*). EPSPs, associated with SPW-Rs, lasted for 51.5 ± 2.7 and 67.9 ± 1.8 ms during 3 and 8.5 mM $[K^+]_o$, respectively ($n = 5$ cells, $P < 0.01$). That GABAergic inhibition was preserved under these conditions was indicated by the fact that cells, which displayed IPSPs during SPW-Rs in the presence of 3 mM $[K^+]_o$, also did not generate APs during SPW-Rs when $[K^+]_o$ was elevated ($n = 4$ cells; see Fig. 9*E*).

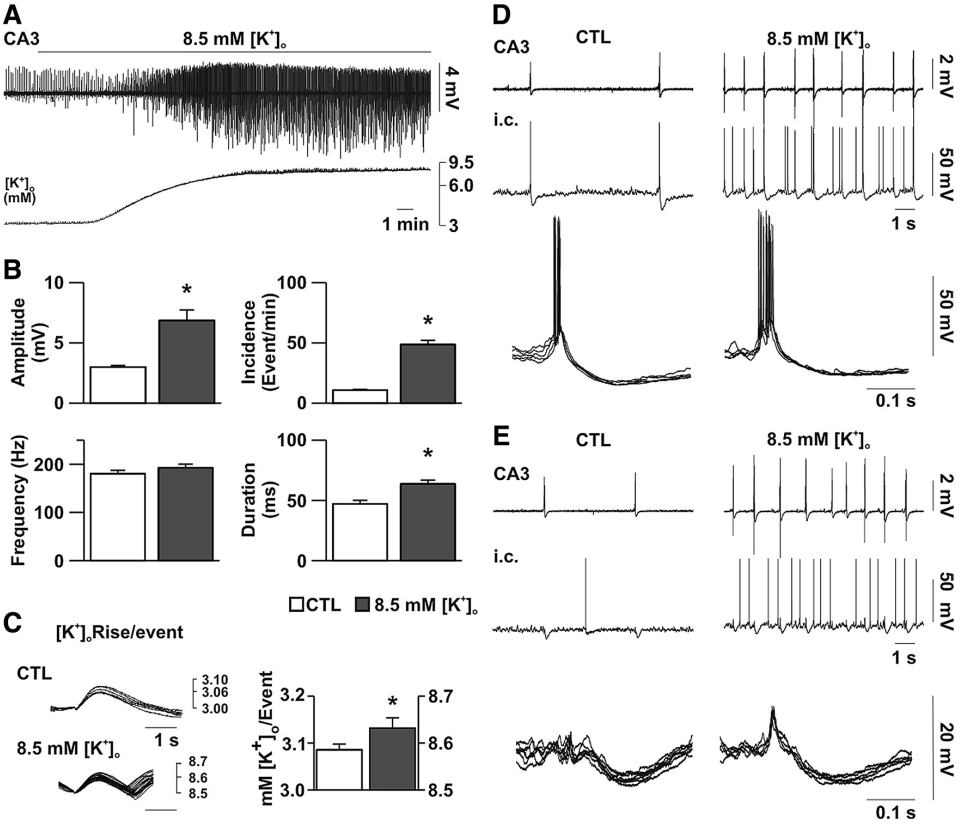

FIG. 9. Effects of high $[K^+]_o$ on SPW-Rs and associated intracellular responses. *A*: sample recording of high $[K^+]_o$-mediated effects on established SPW-Rs. *Bottom trace*: simultaneous recording showing increase in $[K^+]_o$ during wash in. *B*: plots summarizing the effects of elevated $[K^+]_o$ on SPW-Rs. Note that high $[K^+]_o$ caused a marked increase in the SPW-R incidence. *C*: effects of 8.5 mM $[K^+]_o$ on SPW-R-induced $[K^+]_o$ increases. *Left*: overlay of 5 sample traces of $[K^+]_o$ increase accompanying SPW-Rs during 3 mM (*top*) and 8.5 mM $[K^+]_o$ (*bottom*). *Right*: plot showing significant increase in $[K^+]_o$ in accordance with SPW-R before and after wash in of 8.5 mM $[K^+]_o$; $*P < 0.05$, applying to *B* and *C*. *D*: simultaneous extra (*top*) and intracellular recordings (*bottom*) showing cellular responses of EPSP-generating CA3 pyramidal cell during SPW-Rs under control condition (*left*) and following wash in of 8.5 mM $[K^+]_o$ (*right*). Overlay of 5 samples of SPW-R-associated EPSPs shown on expanded timescale under control condition (*left*) and during elevated $[K^+]_o$ (*right*). Note increased AP firing during 8.5 mM $[K^+]_o$. *E*: analogous to *A*, simultaneous extra (*top*) and intracellular recordings (*bottom*) showing cellular responses of IPSP-generating CA3 pyramidal cell during SPW-Rs. Overlay of 5 samples of SPW-R-associated IPSPs shown on expanded timescale. Note that during elevated $[K^+]_o$ CA3 cell still displays IPSPs in response to SPW-Rs.

Since SPW-Rs were not transformed into REDs during elevated $[K^+]_o$, we tested for 8.5 mM $[K^+]_o$-mediated effects on isolated IPSPs in the absence of glutamatergic transmission (see Fig. 10, *A* and *B*). Intracellular recordings revealed that in the presence of DL-APV and CNQX the resting membrane potential of CA3 pyramidal cells was significantly depolarized during 8.5 mM $[K^+]_o$ from 64.7 ± 1.4 to 57.1 ± 1.7 mV (n = 7 cells, $P < 0.001$). We found that the E_{IPSP} was shifted from −74.7 ± 1.8 to −60.8 ± 1.3 mV (n = 7, $P < 0.001$, Fig. 10). However, in contrast to experiments where both nicotine and BMI caused a significant decrease of the inhibitory conductance in the absence of glutamatergic transmission, we noted a profound increase of inhibitory conductance to 215.2 ± 38.4% of control during elevated $[K^+]_o$ (from 23.1 ± 7.2 to 45.8 ± 12.0 nS, n = 7 cells, $P < 0.05$; Fig. 10, *B* and *C*). Moreover, due to the $[K^+]_o$-induced depolarization of the resting membrane potential, we still observed hyperpolarizing IPSPs, as indicated by the overlay of isolated IPSPs evoked at depolarizing and hyperpolarizing potentials (see Fig. 10*A*). These recordings also indicated a significant prolongation of evoked IPSPs, in line with previous findings for CA1 neurons (Jensen et al. 1993). The input resistance of CA3 cells was significantly reduced from 41.4 ± 3.2 to 28.1 ± 2.6 MΩ (n = 7 cells, $P <$ 0.005) during elevated $[K^+]_o$.

As previously reported, elevation of $[K^+]_o$ induced spontaneous seizure-like events (SLEs) in different preparations, including human hippocampal tissue (Gabriel et al. 2004; Jandova et al. 2006; Jensen and Yaari 1997; Leschinger et al. 1993). We tested whether under our experimental conditions elevation of $[K^+]_o$ could also induce SLEs. In the presence of 1.2 mM $[Mg^{2+}]_o$, elevation of $[K^+]_o$ to 8.5 mM caused spontaneous SLEs in 6 of 14 naïve slices (43%; see Fig. 11), whereas this was the only case in one of 12 stimulated slices (8%) expressing SPW-Rs.

DISCUSSION

The aim of the present study was to determine the relationship between hypersynchronized REDs and SPW-Rs. We

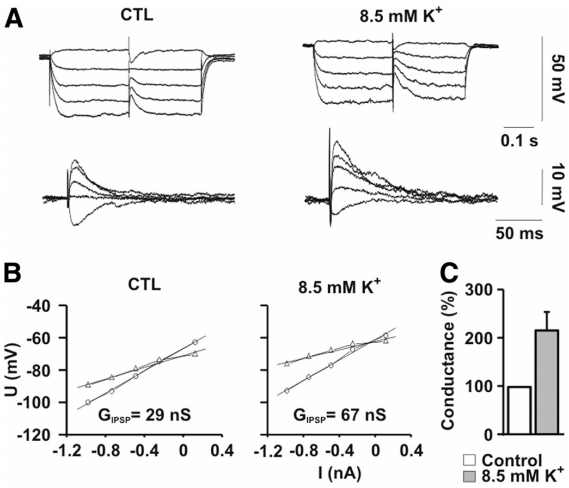

FIG. 10. Effects of high $[K^+]_o$ on isolated IPSPs. *A*: sample recordings of isolated IPSPs in CA3 pyramidal cells during elevated $[K^+]_o$ in the absence of glutamatergic transmission. *Bottom traces*: overlay of intracellular responses evoked during depolarizing and hyperpolarizing current steps showing increases in the amplitude of evoked IPSPs by high $[K^+]_o$. *B*: plotted *I–V* curves showing 8.5 mM $[K^+]_o$-induced increase in inhibitory conductance. *C*: normalized changes in synaptic conductance in the presence of 3 and 8.5 mM $[K^+]_o$. Note the increase in normalized inhibitory conductance during elevated $[K^+]_o$ (*$P < 0.05$).

found that partial disinhibition can convert SPW-Rs into REDs and, interestingly, that SPW-Rs, once induced by a recurrent stimulation protocol reminiscent of a short-term kindling protocol, prevented generation of seizure-like events induced by elevation of $[K^+]_o$. A better understanding of the relationship between SPW-Rs and REDs gained even more importance as spontaneous events, superimposed by ripple network oscillations, have previously been observed in humans and rodents with epilepsy. Thus the question has been posed under what conditions such events indicate the epileptogenic zone in temporal lobe epilepsy. In such regions, inhibition is usually, to some extent, compromised. In the present study, we therefore particularly investigated whether and when partial disinhibition might cause transition of SPW-Rs into interictal, proconvulsant, epileptiform discharges in area CA3 of adult rat hippocampal slices. This study builds on a previous study from our lab (Behrens et al. 2007) in which we showed that high concentrations of bicuculline and of gabazine transformed SPW-Rs into REDs. In that study, we were interested whether disinhibition leads to generation of high-frequency ripples, frequently observed in chronic epileptic tissue. However, although synchronized ripple oscillations could reach frequencies near 400 Hz during the very initial phase of a given RED (Bragin et al. 1999), even complete blockade of $GABA_A$ receptors did not cause generation of ultrafast ripples of ≤600 Hz, as previously observed in epileptic animals and humans (Behrens et al. 2007). In the present study, partial disinhibition led only to a moderate increase in ripple frequencies.

Properties of SPW-R

As previously reported, hippocampal SPW-Rs can be induced in vitro by recurrent electrical stimulation used to induce LTP in area CA3 (Behrens et al. 2005), irrespective of stimulation site and irrespective of whether HFS or TBS were used. Induction of SPW-Rs followed induction of LTP and this process was associated with a reorganization within hippocampal networks (Behrens et al. 2005). In a subset of cells, induction of SPW-Rs was associated with augmentation of compound EPSPs, whereas in others inhibition was augmented. Simultaneous intracellular recordings showed that one

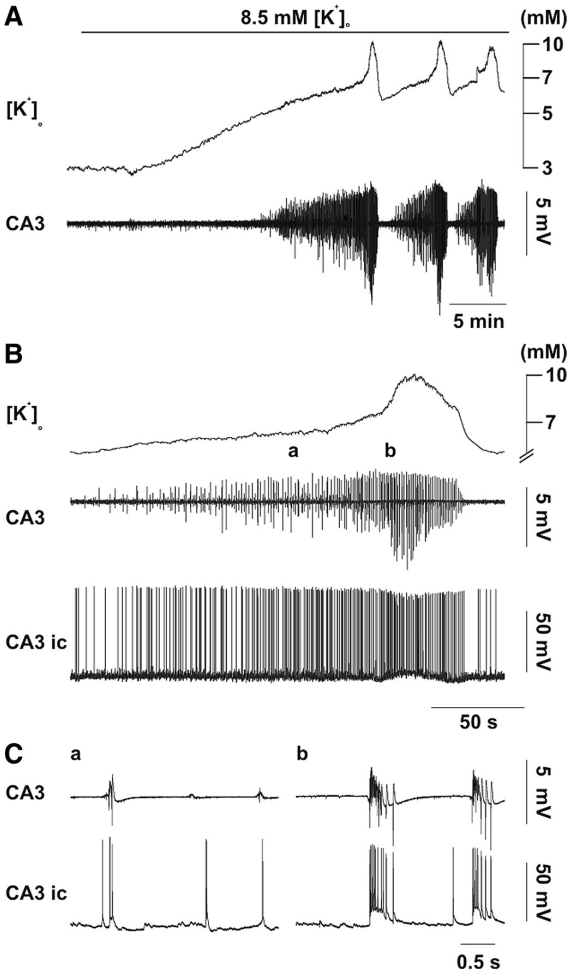

FIG. 11. 8.5 mM $[K^+]_o$-induced seizure-like events in naïve, unstimulated slices. *A*: sample recording of $[K^+]_o$ (*top*) and seizure-like events (SLEs) in area CA3 (*bottom*) induced by elevating $[K^+]_o$ from 3 to 8.5 mM in naïve slice (*top*). Note marked increases in $[K^+]_o$ accompanying SLEs during 8.5 mM $[K^+]_o$ (under these conditions, SLEs occurred in 43% of unstimulated slices). *B*: simultaneous extra (*middle*) and intracellular recording obtained from a CA3 pyramidal cell (*bottom*) during 8.5 mM $[K^+]_o$-induced SLE in area CA3; increase in $[K^+]_o$ accompanying SLE is shown in *top trace*. Note that CA3 cell increases firing and transiently depolarizes during SLE, whereas $[K^+]_o$ increases due to increased network activity. *C*: analogous to *B*, simultaneous recording of network activity in area CA3 (*top*) and intracellular responses of CA3 pyramidal cell (*bottom*) shown on enlarged timescale according to *a* and *b* as shown in *B*. Note spontaneous AP generation of CA3 cell during elevated $[K^+]_o$ and synchronous firing during network discharges (*a*). Note also that CA3 cell markedly increases burst firing in response to prolonged epileptiform network discharge during SLE (*b*).

to two APs were observed in about half of the CA3 pyramidal cells, whereas transition into a hypersynchronized network state was prevented by counterbalanced increase of inhibition in others (Behrens et al. 2005). Thus during ongoing SPW-R activity many cells in area CA3 and even more in area CA1 presented with large and long-lasting inhibitory potentials in contrast to epileptiform discharges (Behrens et al. 2005; Maier et al. 2003). In the present study, we confirmed the finding that SPW-Rs propagated into area CA1. In addition to that, we also report a slight propagation of SPW-Rs from area CA3 into the granular cell layer of the DG. This was increased in the absence of $GABA_A$-mediated inhibition. However, the observed signals were generally small and might potentially have represented far-field effects or activation of interneurons through recurrent collaterals from CA3 pyramidal cells.

Nicotine in high concentrations transforms SPW-Rs into REDs

Single-pulse stimulation applied to the SR in area CA1 induced network responses in area CA3, which were characterized by two PSs, a first short-latency, antidromic PS followed by a second PS due to the extensive recurrent axon collateral network in area CA3 (Wittner et al. 2007). Although 100 μM of nicotine caused an increase in the amplitude of the second PS, application of 500 μM resulted in the generation of multiple PSs, suggesting removal of recurrent inhibition.

Application of 100 μM of nicotine caused a significant increase in the amplitude of SPW-Rs. Interestingly, this effect of nicotine was sensitive to the α7-nAChR antagonist MLA, a specific antagonist of α7-nAChRs (Alkondon et al. 1992). In the hippocampus, α7-nAChRs are highly expressed in cholecystokinin (CCK)-expressing GABAergic basket cells (Frazier et al. 1998; Freedman et al. 1993). Paired recordings of synaptically coupled interneurons recently showed that activation of CCK-positive basket cells was indeed able to interrupt AP firing in PV-positive interneurons (Karson et al. 2009), thereby causing a reduced inhibitory transmission onto pyramidal cells. Together with this, the present data suggest that nicotine-mediated activation of CCK-positive interneurons might have caused a partial disinhibition of CA3 pyramidal cells. This effect was dramatically increased when nicotine was applied at a dose of 500 μM. Under this condition the amplitude of stimulus-induced SPW-Rs and the duration of SPWs were increased. Cells that presented with compound EPSPs following induction of SPW-Rs generated paroxysmal depolarization shifts (PDSs) accompanied by superimposed high-frequency discharges when 500 μM nicotine was present (see Fig. 6*A*). This conversion of SPW-Rs into REDs was associated with a large increase of rises in $[K^+]_o$, which were $\leq$15-fold larger than those observed during SPW-Rs. Such large increases in $[K^+]_o$ are characteristic for REDs in vivo and in vitro (Behrens et al. 2007; Futamachi and Pedley 1976; Heinemann et al. 1977). Interestingly, cells, which were inhibited during SPW-Rs prior to nicotine application, generated only up to six APs and did not exhibit PDSs (see Fig. 3*B*). Thus transition from SPW-Rs into REDs apparently is not an all or none effect. The transformation of SPW-Rs into REDs is a rather abrupt change in duration and amplitude, which occurs within 10 min following application of 2 μM bicuculline and more like 20 min when nicotine is applied at 500 μM. Since equilibration in slices with a given agent under interface conditions is slow (Müller et al. 1988) the concentrations required to sufficiently transform SPW-Rs into REDs is probably lower.

Facilitatory effects of nicotine on the HFS induction of SPW-Rs

As previously reported, hippocampal SPW-Rs can be induced by electrical stimulation where the induction of such SPW-R activity is closely linked to the induction of long-lasting LTP in associational fibers between CA3 pyramidal cells (Behrens et al. 2005). Since nicotine is known to modulate LTP in various brain regions including the hippocampal formation (Buhler and Dinwiddie 2001; Jones and Yakel 1999; Nakauchi et al. 2007), we tested whether nicotine facilitated induction of SPW-Rs. We found that nicotine significantly reduced the number of stimuli needed to induce SPW-Rs and that this facilitation was dose-dependent. This may depend, to some extent, on the calcium (Ca^{2+}) permeability of nAChR since intracellular Ca^{2+} signals have been shown to play a pivotal role in nAChR-mediated neuromodulatory effects (jas-Bailador and Wonnacott 2004). Previous studies also showed that nAChRs augment intracellular Ca^{2+} by activating voltage-operated Ca^{2+} channels (VOCCs) (Mulle et al. 1992) and by causing Ca^{2+}-induced Ca^{2+} release from internal stores (Le and Cherubini 2007; Welsby et al. 2006). Interestingly, the facilitation of SPW-R induction was prevented by MLA, a specific antagonist at α7-nAChR (Alkondon et al. 1992). This suggests that nicotine might facilitate induction of SPW-Rs via modulation of CCK-positive GABAergic basket cells that, indeed, express high levels of α7-nAChR (Frazier et al. 1998; Freedman et al. 1993). These cells innervate fast spiking parvalbumine-positive basket cells and pyramidal cells (Freund 2003) and might, by disinhibition, facilitate induction of LTP.

Nicotine modulates the $GABA_A$-mediated inhibition onto CA3 pyramidal cells

Experiments on isolated IPSPs in the absence of glutamatergic transmission revealed that nicotine indeed reduced IPSPs in CA3 pyramidal cells. The 100 μM nicotine-mediated reduction of inhibitory conductance was α7-nAChR-dependent. Nicotine, used in similar concentrations as applied here, showed an α7-nAChR-dependent reduction of the GABAergic inhibition in area CA1, where this effect was suggested to contribute to a facilitated induction of LTP in the Schaffer collateral pathway (Zhang and Berg 2007). However, reduction of inhibition mediated by 500 μM of nicotine was not fully sensitive to MLA in the chosen concentration. This may relate to a concentration of the antagonist, which is potentially too low under conditions when 500 μM nicotine is applied. However, MLA developed rather unspecific effects not causally related to nAChR activation when applied in high concentration (data not shown). The observed reduction in inhibition might be due to reduced GABA release resulting from depolarization blockade of interneurons (Alkondon et al. 2000), but might also involve effects on the presynaptic GABA release (Radcliffe et al. 1999) and increased inhibition of soma-inhibiting GABAergic neurons by CCK-positive basket cells, which inhibit both the soma of pyramidal cells (for review see Freund 2003) and other

interneurons (Karson et al. 2009). It is noteworthy that the majority of nicotine-mediated effects observed in the present study are of toxicological interest only because concentrations of 100 and 500 μM nicotine are presumably never reached during consumption of cigarettes. Interestingly, however, 10 μM of ACh has already demonstrated effects similar to those of 100 μM nicotine when ACh esterase activity was reduced by physostigmine coapplication. These effects could be ascribed to activation of nicotinergic receptors because the effects persisted in the presence of the muscarinic receptor antagonist atropine.

Comparison of nicotine- and BMI-mediated effects on the transition of SPW-Rs into REDs

Although 500 μM of nicotine did not induce spontaneous REDs in naïve slices, 3 μM of BMI reliably induced such events. Also 2 μM of BMI induced REDs in a relatively large proportion of naïve slices. At this concentration BMI reliably transformed SPW-Rs into REDs accompanied by increases in $[K^+]_o$ of about 1.8 mM. As shown by the present results of isolated IPSPs recorded in CA3 pyramidal cells, this compared with a reduction of the inhibitory conductance by 85%, which was more than the 76% reduction required for the nicotine-mediated transformation of SPW-Rs into REDs. We suggest that this might in part be due to additional effects of BMI. This $GABA_A$ receptor antagonist not only affects phasic inhibition but also blocks tonic inhibition (Bai et al. 2001). Reduced tonic inhibition has been shown to be involved in the induction of REDs in area CA3 (Glykys and Mody 2006). Moreover, BMI has previously been shown to affect glycinergic inhibition (Shirasaki et al. 1991) as well as SK channels (Debarbieux et al. 1998; Johnson and Seutin 1997; Stocker et al. 1999). Whether these effects are sufficient to explain the differences between nicotine and BMI-mediated effects observed here needs further investigation. Notably, comparison of the kinetics of transformation from SPW-Rs into hypersynchronized network discharges revealed that both BMI and 500 μM nicotine exerted similar effects on the transition of CA3 network activity. Under both conditions, an initial slow increase in the SPW-R amplitude was followed by a rather sudden switch into prolonged network discharges.

Nicotine-mediated effects on the jitter between ripple oscillations and action potentials generated in CA3 pyramidal cells

We found that nicotine, applied after induction of SPW-Rs, reversibly increased the amplitude and number of ripple oscillations during SPW-Rs, with rather mild effects on the amplitude of the underlying SPWs. In the presence of 100 μM nicotine this effect was in part due to an increase in the number of APs from 1.6 $\pm$ 0.3 to 3.1 $\pm$ 0.7 per SPW-R. On the other hand, we observed a significant change in the jitter of CA3 cells to a given ripple trough during the augmented ripple oscillations. This finding was based on our observation that during 100 μM nicotine the distribution of the latencies between APs and their corresponding extracellular ripple troughs became significantly narrower, as indicated by the reduction of the SD of their distribution (see Fig. 4). In contrast, the latency distribution became wider and the SD increased when 500 μM nicotine was applied. Thereby, the increase in ripple amplitude as observed under these conditions could be ascribed to a significantly increased AP firing rate during a given SPW-R up to about 15.8 $\pm$ 2.2 APs/SPW-R. We suggest that an increase in the reliability of spike timing, indicated by changes in the jitter, and the moderate increased number of APs both contribute to the increase in ripple amplitudes, observed in the presence of 100 μM nicotine. In particular, changes observed under conditions of 500 μM nicotine were also related to an increase in the number of ripples and APs but, nevertheless, the observed jitter was significantly increased. This compares to a previous study where we studied the effects of high concentrations of BMI and GABAzine, which showed that spike timing to ripple troughs was relatively imprecise presumably due to back and forward propagation within the recurrent excitatory CA3 network. Our findings also suggest that ripple frequency is not primarily determined by interactions between excitatory and inhibitory cells, as is the case in generation of theta and gamma oscillations in the hippocampus. In fact, augmenting inhibition by barbiturate or by potassium did not result in major changes in the ripple frequency and only when inhibition was completely blocked did ripple frequencies increase to nearly 300 Hz. Thus the ripple frequency seems to be determined by the interaction between excitatory cells in area CA3.

Effects of elevated $[K^+]_o$ in naïve and stimulated slices

When $[K^+]_o$, was elevated to 8.5 mM the incidence of SPW-Rs was strongly increased possibly due to the fact that all recorded CA3 pyramidal cells were converted into burster cells, which presented with three to five action potentials superimposed on a depolarizing envelope. In the presence of 3 mM $[K^+]_o$, bursting in CA3 pyramidal cells is relatively rare but already increased when recordings are performed in 5 mM $[K^+]_o$ (see Miles and Wong 1983). Interestingly, increasing $[K^+]_o$ to 8.5 mM resulted in the induction of SLEs in 43% of naïve slices but only in 8% of stimulated slices expressing SPW-Rs. As previously shown, during the stimulus induction of SPW-Rs, repeated application of HFS caused an increase in the amplitude of IPSPs in CA3 pyramidal cells that were inhibited during SPW-Rs (Behrens et al. 2005), indicating an activity-dependent increase in inhibition onto CA3 pyramidal cells. Together with the present finding that the propensity of elevated $[K^+]_o$ to induce SLEs was markedly higher in naïve slices than in stimulated slices that expressed SPW-Rs, our data suggest that activity-dependent augmentation of inhibition can prevent transition into SLEs. Since the generation of SPW-Rs is presumably due to mutual interaction among synaptically coupled neurons in area CA3 (Buzsáki et al. 1983), increase in excitatory synaptic input during burst discharges will augment synaptic drive for synchronous depolarization via the extensive recurrent axon collateral network in area CA3 (Wittner et al. 2007). The increase in the amplitude of SPW-Rs observed during elevated $[K^+]_o$ might also be related to an increase in excitability of neurons, as suggested by the increased baseline firing rate noted in all recorded neurons (see Fig. 9). In the presence of 8.5 mM $[K^+]_o$, the frequency of ripple oscillations was not increased. Notably, increases in $[K^+]_o$ induced by single SPW-Rs during elevated $[K^+]_o$ were much smaller than those observed during BMI- and 500 μM

nicotine-induced REDs, suggesting that inhibition was still preserved. This was also suggested by our finding that in cells that were inhibited during SPW-Rs, AP generation was still prevented when $[K^+]_o$ was elevated to 8.5 mM (see Fig. 9). As previously reported, increasing $[K^+]_o$ shifts the GABA reversal potential in a depolarizing direction (Thompson and Gähwiler 1989), possibly resulting in a reduced efficacy of inhibition (Staley and Proctor 1999) due to effects on the KCC2 transporter, which exploits the transmembrane potassium gradient to extrude chloride (Cl^-) from cells (Misgeld et al. 1986; Rivera et al. 1999). Notably, in the present study, we found that under conditions of elevated $[K^+]_o$, the inhibitory conductance was significantly increased, as indicated by effects on evoked IPSPs in the absence of glutamatergic transmission. This finding suggests that the 8.5 mM $[K^+]_o$-mediated increase in the inhibitory transmission prevented a transition of SPW-Rs into REDs. However, we found that elevating $[K^+]_o$ to 8.5 mM could result in the generation of SLEs in a subset of slices, although inhibition was increased. This implies that other mechanisms might contribute to the generation of ictaform activity, potentially involving generation of cellular bursting behavior (Jensen et al. 1994; Korn et al. 1987; Rutecki et al. 1985), altered $GABA_B$-mediated inhibition (Swartzwelder et al. 1986), depolarization-induced increase in presynaptic glutamate release (Oltedal et al. 2008; Staley et al. 1998), and/or reduced glutamate uptake into depolarized astrocytes (Kimelberg et al. 1995).

Comparison of SPW-Rs and REDs

It is noteworthy that SPW-Rs recorded in vivo and in vitro differ in some aspects. SPW-Rs induced by our stimulation protocol are prominent in area CA3 from where they propagate through area CA1 to the subiculum (Behrens et al. 2005). In contrast, sharp wave–associated ripple oscillations in vivo are less pronounced in area CA3 (Csicsvari et al. 1999). Moreover, in hippocampal slices, repeated stimulation is used to activate a limited neuronal network, which differs from in vivo conditions where a fully preserved network is involved in the generation of SPW-Rs. That most cells are inhibited during SPW-Rs in area CA1 in vivo compares well with experimental in vitro data (Maier et al. 2003). During the induction of SPW-Rs in vitro $\geq$50% of CA3 pyramidal cell receive strong synaptic inhibition during SPW-Rs. Notably, the majority of these cells showed increased IPSP amplitudes during given SPW-Rs on repeated stimulation, indicating an activity-dependent augmentation of GABAergic transmission (Behrens et al. 2005). This is in stark contrast to network activity during REDs, where inhibition is usually substantially impaired (Behrens et al. 2007; Hablitz 1984; Schwartzkroin and Prince 1978; Traub and Wong 1982), indicating that stimulus-induced SPW-Rs do not represent classical interictal discharges. Indeed, REDs prominently differ from SPW-Rs by a prolonged duration of hypersynchronized network discharges, the development of paroxysmal depolarization shifts accompanied with high-frequency AP firing during epochs of fast ripple oscillations $>$250 Hz, and prominent increases in $[K^+]_o$ (Behrens et al. 2007) as well as by a significantly increased oxygen consumption detected within the CA3 pyramidal layer during REDs (unpublished data). Interestingly, ripple oscillations in vivo have also been observed in epileptic humans and rodents (Bragin et al. 1999a,b; Staba et al. 2004). In epileptic patients high-frequency oscillations (HFOs) were reported presenting either with ripple frequencies of 80–250 Hz, similar to those recorded during SPW-Rs in our experiments, or fast ripple frequencies (250–500 Hz) (Le Van et al. 2008; Staba et al. 2002). A recent study investigated whether the incidence of HFOs occurring with ripple frequencies might specifically indicate the site of epileptogenesis (Jacobs et al. 2008), which was not the case. Indeed, network events, involving synchronized inhibitory activity, seem to slow spread of SLEs (Trevelyan et al. 2007) and interfere with ictogenesis (Barbarosie et al. 2002). However, since SPW-Rs are usually associated with robust network inhibition, they might represent an intrinsic, dynamic mechanism to modulate the threshold for seizure induction.

ACKNOWLEDGMENTS

We thank Drs. H. J. Gabriel and K. Schulze for skilled technical assistance and Prof. K. Albus for critical comments on the manuscript.

GRANTS

This work was supported by a joint Bernstein Center/Deutsche Forschungsgemeinschaft Research Training Group Grant GRK 1123 (Bernstein Focus Learning: "Cellular Mechanisms of Learning and Memory Consolidation") through the NeuroCure cluster, the Hertie Foundation, and European Union Epicure.

DISCLOSURES

No conflicts of interest, financial or otherwise, are declared by the authors.

REFERENCES

Albuquerque EX, Pereira EF, Castro NG, Alkondon M, Reinhardt S, Schroder H, Maelicke A. Nicotinic receptor function in the mammalian central nervous system. *Ann NY Acad Sci* 757: 48–72, 1995.

Alkondon M, Braga MF, Pereira EF, Maelicke A, Albuquerque EX. alpha7 nicotinic acetylcholine receptors and modulation of gabaergic synaptic transmission in the hippocampus. *Eur J Pharmacol* 393: 59–67, 2000.

Alkondon M, Pereira EF, Wonnacott S, Albuquerque EX. Blockade of nicotinic currents in hippocampal neurons defines methyllycaconitine as a potent and specific receptor antagonist. *Mol Pharmacol* 41: 802–808, 1992.

Bai D, Zhu G, Pennefather P, Jackson MF, MacDonald JF, Orser BA. Distinct functional and pharmacological properties of tonic and quantal inhibitory postsynaptic currents mediated by gamma-aminobutyric acid(A) receptors in hippocampal neurons. *Mol Pharmacol* 59: 814–824, 2001.

Barbarosie M, Louvel J, D'Antuono M, Kurcewicz I, Avoli M. Masking synchronous GABA-mediated potentials controls limbic seizures. *Epilepsia* 43: 1469–1479, 2002.

Behrens CJ, van den Boom LP, de Hoz L, Friedman A, Heinemann U. Induction of sharp wave–ripple complexes in vitro and reorganization of hippocampal networks. *Nat Neurosci* 8: 1560–1567, 2005.

Behrens CJ, van den Boom LP, Heinemann U. Effects of the GABA(A) receptor antagonists bicuculline and gabazine on stimulus-induced sharp wave–ripple complexes in adult rat hippocampus in vitro. *Eur J Neurosci* 25: 2170–2181, 2007.

Both M, Bähner F, von Bohlen und Halbach O, Draguhn A. Propagation of specific network patterns through the mouse hippocampus. *Hippocampus* 18: 899–908, 2008.

Bragin A, Engel J Jr, Wilson CL, Fried I, Buzsáki G. High-frequency oscillations in human brain. *Hippocampus* 9: 137–142, 1999a.

Bragin A, Engel J Jr, Wilson CL, Fried I, Mathern GW. Hippocampal and entorhinal cortex high-frequency oscillations (100–500 Hz) in human epileptic brain and in kainic acid–treated rats with chronic seizures. *Epilepsia* 40: 127–137, 1999b.

Buhler AV, Dunwiddie TV. Regulation of the activity of hippocampal stratum oriens interneurons by alpha7 nicotinic acetylcholine receptors. *Neuroscience* 106: 55–67, 2001.

Buzsáki G. Hippocampal sharp waves: their origin and significance. *Brain Res* 398: 242–252, 1986.

Buzsáki G. Memory consolidation during sleep: a neurophysiological perspective. *J Sleep Res* 7: 17–23, 1998.

Buzsáki G, Leung LW, Vanderwolf CH. Cellular bases of hippocampal EEG in the behaving rat. *Brain Res* 287: 139–171, 1983.

Chrobak JJ, Lorincz A, Buzsáki G. Physiological patterns in the hippocampo–entorhinal cortex system. *Hippocampus* 10: 457–465, 2000.

Csicsvari J, Hirase H, Czurko A, Mamiya A, Buzsáki G. Fast network oscillations in the hippocampal CA1 region of the behaving rat. *J Neurosci* 19: RC20, 1999.

Davies CH, Collingridge GL. The physiological regulation of synaptic inhibition by $GABA_B$ autoreceptors in rat hippocampus. *J Physiol* 472: 245–265, 1993.

Debarbieux F, Brunton J, Charpak S. Effect of bicuculline on thalamic activity: a direct blockade of I_{AHP} in reticularis neurons. *J Neurophysiol* 79: 2911–2918, 1998.

Frazier CJ, Rollins YD, Breese CR, Leonard S, Freedman R, Dunwiddie TV. Acetylcholine activates an alpha-bungarotoxin-sensitive nicotinic current in rat hippocampal interneurons, but not pyramidal cells. *J Neurosci* 18: 1187–1195, 1998.

Freedman R, Wetmore C, Stromberg I, Leonard S, Olson L. Alpha-bungarotoxin binding to hippocampal interneurons: immunocytochemical characterization and effects on growth factor expression. *J Neurosci* 13: 1965–1975, 1993.

Freund TF. Interneuron Diversity series: rhythm and mood in perisomatic inhibition. *Trends Neurosci* 26: 489–495, 2003.

Freund TF, Katona I. Perisomatic inhibition. *Neuron* 56: 33–42, 2007.

Frey U, Morris RG. Synaptic tagging and long-term potentiation. *Nature* 385: 533–536, 1997.

Fujii S, Jia Y, Yang A, Sumikawa K. Nicotine reverses GABAergic inhibition of long-term potentiation induction in the hippocampal CA1 region. *Brain Res* 863: 259–265, 2000.

Futamachi KJ, Pedley TA. Glial cells and extracellular potassium: their relationship in mammalian cortex. *Brain Res* 109: 311–322, 1976.

Gabriel S, Njunting M, Pomper JK, Merschhemke M, Sanabria ERG, Eilers A, Kivi A, Zeller M, Meencke HJ, Cavalheiro EA, Heinemann U, Lehmann TN. Stimulus and potassium-induced epileptiform activity in the human dentate gyrus from patients with and without hippocampal sclerosis. *J Neurosci* 24: 10416–10430, 2004.

Giocomo LM, Hasselmo ME. Nicotinic modulation of glutamatergic synaptic transmission in region CA3 of the hippocampus. *Eur J Neurosci* 22: 1349–1356, 2005.

Glykys J, Mody I. Hippocampal network hyperactivity after selective reduction of tonic inhibition in $GABA_A$ receptor alpha5 subunit-deficient mice. *J Neurophysiol* 95: 2796–2807, 2006.

Hablitz JJ. Picrotoxin-induced epileptiform activity in hippocampus: role of endogenous versus synaptic factors. *J Neurophysiol* 51: 1011–1027, 1984.

Hablitz JJ, Lundervold A. Hippocampal excitability and changes in extracelluar potassium. *Exp Neurol* 71: 410–420, 1981.

Heinemann U, Arens J. Production and calibration of ion-sensitive microelectrodes. In: *Practical Electrophysiological Methods: A Guide for In Vitro Studies in Vertebrate Neurobiology*, edited by Grantyn R, Kettenmann H. New York: Wiley–Liss, 1992, p. 206–212.

Heinemann U, Lux HD, Gutnick MJ. Extracellular free calcium and potassium during paroxysmal activity in the cerebral cortex of the cat. *Exp Brain Res* 27: 237–243, 1977.

Jacobs J, Levan P, Chander R, Hall J, Dubeau F, Gotman J. Interictal high-frequency oscillations (80–500 Hz) are an indicator of seizure onset areas independent of spikes in the human epileptic brain. *Epilepsia* 49: 1893–1907, 2008.

Jandova K, Pasler D, Antonio LL, Raue C, Ji S, Njunting M, Kann O, Kovacs R, Meencke HJ, Cavalheiro EA, Heinemann U, Gabriel S, Lehmann TN. Carbamazepine-resistance in the epileptic dentate gyrus of human hippocampal slices. *Brain* 129: 3290–3306, 2006.

Jarolimek W, Lewen A, Misgeld U. A furosemide-sensitive K^+-Cl^- cotransporter counteracts intracellular Cl^- accumulation and depletion in cultured rat midbrain neurons. *J Neurosci* 19: 4695–4704, 1999.

jas-Bailador F, Wonnacott S. Nicotinic acetylcholine receptors and the regulation of neuronal signalling. *Trends Pharmacol Sci* 25: 317–324, 2004.

Jensen MS, Azouz R, Yaari Y. Variant firing patterns in rat hippocampal pyramidal cells modulated by extracellular potassium. *J Neurophysiol* 71: 831–839, 1994.

Jensen MS, Cherubini E, Yaari Y. Opponent effects of potassium on $GABA_A$-mediated postsynaptic inhibition in the rat hippocampus. *J Neurophysiol* 69: 764–771, 1993.

Jensen MS, Yaari Y. Role of intrinsic burst firing, potassium accumulation, and electrical coupling in the elevated potassium model of hippocampal epilepsy. *J Neurophysiol* 77: 1224–1233, 1997.

Ji D, Lape R, Dani JA. Timing and location of nicotinic activity enhances or depresses hippocampal synaptic plasticity. *Neuron* 31: 131–141, 2001.

Johnson SW, Seutin V. Bicuculline methiodide potentiates NMDA-dependent burst firing in rat dopamine neurons by blocking apamin-sensitive Ca^{2+}-activated K^+ currents. *Neurosci Lett* 231: 13–16, 1997.

Jones S, Yakel JL. Inhibitory interneurons in hippocampus. *Cell Biochem Biophys* 31: 207–218, 1999.

Karson MA, Tang AH, Milner TA, Alger BE. Synaptic cross talk between perisomatic-targeting interneuron classes expressing cholecystokinin and parvalbumin in hippocampus. *J Neurosci* 29: 4140–4154, 2009.

Kimelberg HK, Rutledge E, Goderie S, Charniga C. Astrocytic swelling due to hypotonic or high K^+ medium causes inhibition of glutamate and aspartate uptake and increases their release. *J Cereb Blood Flow Metab* 15: 409–416, 1995.

Korn SJ, Giacchino JL, Chamberlin NL, Dingledine R. Epileptiform burst activity induced by potassium in the hippocampus and its regulation by GABA-mediated inhibition. *J Neurophysiol* 57: 325–340, 1987.

Le MC, Cherubini E. Presynaptic calcium stores contribute to nicotine-elicited potentiation of evoked synaptic transmission at CA3–CA1 connections in the neonatal rat hippocampus. *Hippocampus* 17: 316–325, 2007.

Leschinger A, Stabel J, Igelmund P, Heinemann U. Pharmacological and electrographic properties of epileptiform activity induced by elevated K^+ and lowered Ca^{2+} and Mg^{2+} concentration in rat hippocampal slices. *Exp Brain Res* 96: 230–240, 1993.

Le Van QM, Bragin A, Staba R, Crepon B, Wilson CL, Engel J Jr. Cell type-specific firing during ripple oscillations in the hippocampal formation of humans. *J Neurosci* 28: 6104–6110, 2008.

Lopantsev V, Both M, Draguhn A. Rapid plasticity at inhibitory and excitatory synapses in the hippocampus induced by ictal epileptiform discharges. *Eur J Neurosci* 29: 1153–1164, 2009.

Luhmann HJ, Prince DA. Postnatal maturation of the GABAergic system in rat neocortex. *J Neurophysiol* 65: 247–263, 1991.

Lux HD, Heinemann U, Dietzel I. Ionic changes and alterations in the size of the extracellular space during epileptic activity. *Adv Neurol* 44: 619–639, 1986.

Macdonald RL, Rogers CJ, Twyman RE. Barbiturate regulation of kinetic properties of the $GABA_A$ receptor channel of mouse spinal neurones in culture. *J Physiol* 417: 483–500, 1989.

Maier N, Nimmrich V, Draguhn A. Cellular and network mechanisms underlying spontaneous sharp wave–ripple complexes in mouse hippocampal slices. *J Physiol* 550: 873–887, 2003.

Middleton SJ, Racca C, Cunningham MO, Traub RD, Monyer H, Knopfel T, Schofield IS, Jenkins A, Whittington MA. High-frequency network oscillations in cerebellar cortex. *Neuron* 58: 763–774, 2008.

Miles R, Wong RKS. Single neurones can initiate synchronized population discharge in the hippocampus. *Nature* 306: 371–373, 1983.

Misgeld U, Deisz RA, Dodt HU, Lux HD. The role of chloride transport in postsynaptic inhibition of hippocampal neurons. *Science* 232: 1413–1415, 1986.

Mulle C, Choquet D, Korn H, Changeux J-P. Calcium influx through nicotinic receptor in rat central neurons: its relevance to cellular regulation. *Neuron* 8: 135–143, 1992.

Müller W, Misgeld U, Heinemann U. Carbachol effects on hippocampal neurons in vitro: dependence on the rate of rise of carbachol tissue concentration. *Exp Brain Res* 72: 287–298, 1988.

Nakauchi S, Brennan RJ, Boulter J, Sumikawa K. Nicotine gates long-term potentiation in the hippocampal CA1 region via the activation of alpha2* nicotinic ACh receptors. *Eur J Neurosci* 25: 2666–2681, 2007.

Nashmi R, Lester HA. CNS localization of neuronal nicotinic receptors. *J Mol Neurosci* 30: 181–184, 2006.

Nimmrich V, Maier N, Schmitz D, Draguhn A. Induced sharp wave–ripple complexes in the absence of synaptic inhibition in mouse hippocampal slices. *J Physiol* 563: 663–670, 2005.

Nott A, Levin ED. Dorsal hippocampal alpha7 and alpha4beta2 nicotinic receptors and memory. *Brain Res* 1081: 72–78, 2006.

Oltedal L, Haglerod C, Furmanek T, Davanger S. Vesicular release of glutamate from hippocampal neurons in culture: an immunocytochemical assay. *Exp Brain Res* 184: 479–492, 2008.

Radcliffe KA, Fisher JL, Gray R, Dani JA. Nicotinic modulation of glutamate and GABA synaptic transmission of hippocampal neurons. *Ann NY Acad Sci* 868: 591–610, 1999.

Rivera C, Voipio J, Payne JA, Ruusuvuori E, Lahtinen H, Lamsa K, Pirvola U, Saarma M, Kaila K. The K^+/Cl^- co-transporter KCC2 renders GABA hyperpolarizing during neuronal maturation. *Nature* 397: 251–255, 1999.

Romo-Parra H, Trevino M, Heinemann U, Gutierrez R. GABA actions in hippocampal area CA3 during postnatal development: differential shift from depolarizing to hyperpolarizing in somatic and dendritic compartments. *J Neurophysiol* 99: 1523–1534, 2008.

Rutecki PA, Lebeda FJ, Johnston D. Epileptiform activity induced by changes in extracellular potassium in hippocampus. *J Neurophysiol* 54: 1363–1374, 1985.

Scharfman HE. The CA3 "backprojection" to the dentate gyrus. *Prog Brain Res* 163: 627–637, 2007.

Schwartzkroin PA, Prince DA. Cellular and field potential properties of epileptogenic hippocampal slices. *Brain Res* 147: 117–130, 1978.

Séguéla P, Wadiche J, Dineley-Miller K, Dani JA, Patrick JW. Molecular cloning, functional properties, and distribution of rat brain alpha 7: a nicotinic cation channel highly permeable to calcium. *J Neurosci* 13: 596–604, 1993.

Shirasaki T, Klee MR, Nakaye T, Akaike N. Differential blockade of bicuculline and strychnine on GABA- and glycine-induced responses in dissociated rat hippocampal pyramidal cells. *Brain Res* 561: 77–83, 1991.

Staba RJ, Wilson CL, Bragin A, Fried I, Engel J Jr. Quantitative analysis of high-frequency oscillations (80–500 Hz) recorded in human epileptic hippocampus and entorhinal cortex. *J Neurophysiol* 88: 1743–1752, 2002.

Staba RJ, Wilson CL, Bragin A, Jhung D, Fried I, Engel J Jr. High-frequency oscillations recorded in human medial temporal lobe during sleep. *Ann Neurol* 56: 108–115, 2004.

Staley KJ, Dudek FE. Interictal spikes and epileptogenesis. *Epilepsy Curr* 6: 199–202, 2006.

Staley KJ, Longacher M, Bains JS, Yee A. Presynaptic modulation of CA3 network activity. *Nat Neurosci* 1: 201–209, 1998.

Staley KJ, Proctor WR. Modulation of mammalian dendritic $GABA_A$ receptor function by the kinetics of Cl^- and HCO_3^- transport. *J Physiol* 519: 693–712, 1999.

Stocker M, Krause M, Pedarzani P. An apamin-sensitive Ca^{2+}-activated K^+ current in hippocampal pyramidal neurons. *Proc Natl Acad Sci USA* 96: 4662–4667, 1999.

Swartzwelder HS, Sutch CP, Wilson WA. Attenuation of epileptiform bursting by baclofen: reduced potency in elevated potassium. *Exp Neurol* 94: 726–734, 1986.

Thompson SM, Gähwiler BH. Activity-dependent disinhibition. II. Effects of extracellular potassium, furosemide, and membrane potential on E_{Cl^-} in hippocampal CA3 neurons. *J Neurophysiol* 61: 512–523, 1989.

Traub RD, Wong RKS. Cellular mechanism of neuronal synchronization in epilepsy. *Science* 216: 745–747, 1982.

Trevelyan AJ, Sussillo D, Yuste R. Feedforward inhibition contributes to the control of epileptiform propagation speed. *J Neurosci* 27: 3383–3387, 2007.

Welsby P, Rowan M, Anwyl R. Nicotinic receptor-mediated enhancement of long-term potentiation involves activation of metabotropic glutamate receptors and ryanodine-sensitive calcium stores in the dentate gyrus. *Eur J Neurosci* 24: 3109–3118, 2006.

Whittington MA, Traub RD, Jefferys JGR. Erosion of inhibition contributes to the progression of low magnesium bursts in rat hippocampal slices. *J Physiol* 486: 723–734, 1995.

Windmuller O, Lindauer U, Foddis M, Einhaupl KM, Dirnagl U, Heinemann U, Dreier JP. Ion changes in spreading ischaemia induce rat middle cerebral artery constriction in the absence of NO. *Brain* 128: 2042–2051, 2005.

Wittner L, Henze DA, Zaborszky L, Buzsáki G. Three-dimensional reconstruction of the axon arbor of a CA3 pyramidal cell recorded and filled in vivo. *Brain Struct Funct* 212: 75–83, 2007.

Zhang J, Berg DK. Reversible inhibition of $GABA_A$ receptors by alpha7-containing nicotinic receptors on the vertebrate postsynaptic neurons. *J Physiol* 579: 753–763, 2007.

Publication II

Neuroscience Letters 574 (2014) 15–20

Contents lists available at ScienceDirect

Neuroscience Letters

journal homepage: www.elsevier.com/locate/neulet

$GABA_B$ receptor dependent modulation of sharp wave-ripple complexes in the rat hippocampus in vitro

Jan Oliver Hollnagel[a], Anna Maslarova[a], Rizwan ul Haq[a,c], Uwe Heinemann[a,b,*]

[a] Institute of Neurophysiology, Charité-Universitätsmedizin Berlin, 14195 Berlin, Germany
[b] NeuroCure Research Center, Charité-Universitätsmedizin Berlin, 14195 Berlin, Germany
[c] Department of Pharmacy, Hazara University, Havelian Campus, Abbottabad 22500, Pakistan

HIGHLIGHTS

- $GABA_B$ agonist baclofen transiently suppresses sharp wave-ripple oscillations.
- Induction of sharp wave-ripple activity in presence of baclofen is possible.
- Baclofen affects presynaptic Ca^{2+} dependent transmitter release.
- $GABA_B$ antagonist CGP55846 does not increase incidence of SPW-R activity.
- Associative LTP permits delayed aggregation into neural assemblies.

ARTICLE INFO

Article history:
Received 16 January 2014
Received in revised form 8 April 2014
Accepted 26 April 2014
Available online 4 May 2014

Keywords:
Slow inhibition
CA3
Calcium-signaling
High frequency oscillations

ABSTRACT

Sharp wave-ripple complexes (SPW-R) are observed in vivo during resting immobility, consummatory behavior and during slow wave sleep, and they have been proposed to support memory consolidation. It has been suggested that GABAergic cells play important roles in controlling incidence of sharp waves and of ripple frequency. We report here that the $GABA_B$ agonist baclofen reversibly suppresses SPW-R activity in rat hippocampal slices, presumably affecting the strength of neuronal coupling in the associative network of area CA3. The effect is specific as the $GABA_B$ receptor antagonist CGP55846 prevents this effect; however, CGP55846 application had no major effect on incidence of SPW-R. Interestingly, repetitive stimulation in the presence of baclofen is able to induce SPW-R activity, which only appears after washout of baclofen. Our findings suggest that GABA levels through activation of $GABA_B$ receptors may be involved in the transition from theta-gamma to SPW-R working mode in the hippocampus.

1. Introduction

The two stage model of memory formation suggests that spatial memories in rodents are formed during theta and gamma activity in the local EEG, while memory consolidation was proposed to be dependent on off-line replay of previously stored information during SPW-R activity [1–3]. The transition between these two stages is often rather abrupt [2]. It was previously shown that switching between these two states may be dependent on the systemic neuromodulator ACh [4]. Moreover, it was shown that blocking of SPW-Rs could be achieved by another systemic neuromodulator, namely norepinephrine [5]. Locally acting neuromodulators, however, also seem to be able to block SPW-R activity. This was shown for adenosine and for canabinnoids [6].

SPW-Rs occur in mouse hippocampal slices spontaneously [7] while in rat hippocampal slices SPW-Rs can be induced by protocols that induce LTP, provided suprathreshold stimulation for generation of action potentials in the CA3 region is used [8]. These SPW-R complexes are more uniform than those observed in mice hippocampal slices and therefore permit facilitated analysis of mechanisms that control their appearance. Intracellular recordings have revealed that both interneurons and principal cells participate in their generation [9,10] raising the possibility that GABAergic neurons control ripple frequency on one hand and incidence of SPW-Rs on the other. However, GABAergic mechanisms are less likely to control ripple frequency as studies with barbiturates and $GABA_A$ receptor blockers revealed little influence on ripple frequency [13]. Nevertheless, both stimulus-induced and spontaneous SPW-Rs can be transiently suppressed by $GABA_A$ receptor agonists

* Corresponding author at: Institute of Neurophysiology, Garystraße 5, 14195 Berlin, Germany. Tel.: +49 30 450 528 091.
E-mail address: Uwe.Heinemann@charite.de (U. Heinemann).

http://dx.doi.org/10.1016/j.neulet.2014.04.045
0304-3940/

[11,12]. This effect might be due to activation of $GABA_B$ receptors as during block of $GABA_A$ receptors the synaptically released GABA may more readily reach extrasynaptic $GABA_B$ receptors. Indeed, in presence of $GABA_A$ receptor blockers $GABA_B$ mediated IPSPs can be augmented [14,15], and thereby lead to the blocking of SPW-R activity. $GABA_B$ receptors are G-protein coupled heptahelical transmembrane proteins which, upon activation, form dimers. They postsynaptically activate GIRK channels, which mediate a slow hyperpolarization of neurons [16,17]. Presynaptically it was suggested that $GABA_B$ receptors reduce presynaptic calcium entry and thereby regulate homosynaptically GABA release and heterosynaptically glutamate release [18,19]. We therefore became interested in studying effects of $GABA_B$ receptor modulating drugs on stimulus-induced SPW-Rs.

2. Material and methods

All animal procedures were performed in accordance with the guidelines of the European Communities Council and were approved by the regional Landesamt for Gesundheit and Soziales, Berlin (T0096/02). We used adult male Wistar rats (aged 6–8 weeks, > 200 g) that were purchased from Charles River Laboratories (Sulzfeld, Germany) or from Janvier (Saint Berthevin, France). Slices were prepared following previously published procedures [13] and maintained in ACSF containing (in mM): NaCl 129, $NaHCO_3$ 21, KCl 3, $CaCl_2$ 1.6, $MgSO_4$ 1.8, NaH_2PO_4 1.25, glucose 10, saturated with 95% O_2—5% CO_2 at 36 ± 0.2 °C (flow rate: ~1.8 ml/min, pH 7.4, osmolarity: 295–300 mosmol/kg). Slices were allowed to recover for 2–3 h before experiments were started. For each experimental condition up to two slices per animal were used. However, different protocols were often employed in slices from the same animal in order to minimize the overall number of individual animals sacrificed.

Extracellular field potentials (FP) were recorded from the stratum pyramidale of the CA3 and CA1 with microelectrodes filled with 154 mM NaCl (5–10 MΩ). Alternatively carbon fiber electrodes were used (0.4–1.2 MΩ). For intracellular recordings, sharp microelectrodes (70–90 MΩ) were pulled from borosilicate glass (o.d. 1.2 mm) and filled with 2.5 M potassium acetate and signals were amplified using a SEC-05L amplifier (NPI Instruments, Tamm, Germany). Sharp microelectrodes were preferred over patch recordings as the required measurement often took considerable time. All data were low-pass filtered at 3 kHz, digitized at 10 kHz and stored on computer disk using a CED 1401 interface (Cambridge Electronic Design, Cambridge, UK). Intracellular recordings were accepted when membrane potentials were negative to −62 mV, action potential (AP) amplitudes exceeded 70 mV and input resistance was >25 MΩ. For paired pulse stimulation experiments, stimulation intensities subthreshold for induction of action potentials were used to reduce feed-forward and feedback inhibition. Additionally, for paired pulse experiments in the presence of bicuculline, CA3 was surgically removed to prevent generation of epileptiform discharges.

In some experiments the effects of baclofen were studied on presynaptic calcium entry. In these experiments double barreled Ca^{2+} selective microelectrodes were inserted into SR of area CA1, synaptic transmission was blocked by CNQX and DL-2-APV, and short trains of repetitive stimulation (20 Hz, 2s) were employed. This results in a decrease of extracellular calcium concentration ($[Ca^{2+}]_o$), which has been attributed to presynaptic Ca^{2+} uptake [5].

All drugs were purchased from Sigma-Aldrich (Taufkirchen Germany). Baclofen was applied in concentrations of 0.5–5 μM, CGP55846 in concentrations of 2–5 μM, CNQX was applied with 25 μM and DL-2-APV with 50 μM. All agents were dissolved in ACSF to their final concentration.

SPW-Rs were induced by high frequency stimulation (HFS; three trains of 40 pulses with 100 Hz, 100 μs duration, 40 s intertrain interval, repeated every 5 min) with a bipolar platinum electrode (25 μm, tip separation 100–150 μm) placed in the stratum radiatum (SR) of CA1. Such stimulation evokes antidromic action potentials, and recurrent EPSPs and population spikes in the associative network of area CA3 due to relatively strong collateral interaction between different CA3 pyramidal cells. Slices were stimulated using a submaximal (70%) stimulus intensity (1.5–3 V) for induction of population spike responses in area CA1 or CA3. In most experiments SPW-Rs were induced with 1.2 mM Mg, which is closer to normal Mg concentration than the 1.8 mM Mg used in most other experiments.

We analyzed different components of SPW-Rs by filtering the raw data using the digital filter function in Spike2 software (Cambridge Electronic Design, Cambridge, UK). Data were analyzed using custom-made software. For ripple detection, we used a band pass filter of 120 - 400 Hz. For sharp wave detection, recordings were low pass filtered at 45 Hz. For analysis of amplitude and duration of SPW-Rs, at least 40 events from a given slice and condition were analyzed and data were averaged per slice before calculation of group averages.

In order to locate the site of baclofen-mediated modulation of SPW-R activity, we investigated the paired pulse ratio (PPR) and the coefficient of variance (CV) of evoked EPSPs [20]. We calculated PPR by dividing the amplitude of the second evoked EPSP by that of the first evoked EPSP. For comparison of the PPR before and after drug application, we averaged 10 values for each condition per cell. In order to analyze coefficients of variance (CV), we analyzed data of evoked EPSPs before and after drug application. In summary, ratio of coefficients of variance squared (r) was plotted against the modification factor (π) where r = (CV^2 before drug application)/(CV^2 after drug application) and π = (M after drug application)/(M before drug application) with CV = (standard deviation of the amplitude of evoked EPSPs)/(mean of the amplitude of evoked EPSPs), and with M = mean amplitude of evoked EPSPs [20]. All data were reported as mean ± standard error of mean (SEM). Statistical significance was determined using paired T-tests following tests confirming normal distribution; $p < 0.05$ (*) was considered to indicate a significant difference.

3. Results

Recurrent repetitive high frequency stimulation induced reliably sharp wave-ripple activity provided the intensity of stimulation was high enough to induce population spikes and LTP in area CA3 [8]. The properties of SPW-R complexes compared well to those that we have reported previously [8]. The incidence of SPW-R was 8.5 ± 1.0 per minute; the amplitudes of sharp waves were 2.9 ± 0.3 mV lasting for 73.4 ± 0.9 ms with a ripple incidence of 2.9 ± 0.1 per SPW-R (n = 7 slices). As shown in Fig. 1A application of baclofen (0.5 μM) reliably and reversibly suppressed SPW-Rs within 5 min of wash in. When SPW-R complexes reappeared after washout of baclofen (taking on average 25 min), events within a time window of 1 h were analyzed. In this period of observation, the incidence did not reach the original level (4.3 ± 0.9 events per minute, p = 0.029). All other parameters of SPW-R complexes compared well to control (amplitude: p = 0.080, duration: p = 0.648, n of ripples: p = 0.100) as shown in Fig. 1D. In five experiments where CGP55846 (5 μM) was applied prior to and during baclofen application we found that the blocking effect of baclofen on SPW-Rs was prevented (data not shown).

We next asked whether intrinsic background GABA through activation of $GABA_B$ receptors would affect the incidence and properties of sharp wave-ripples. We found that CGP55846 applied with 5 μM had no major effect on incidence of SPW-Rs. Only

Publication II

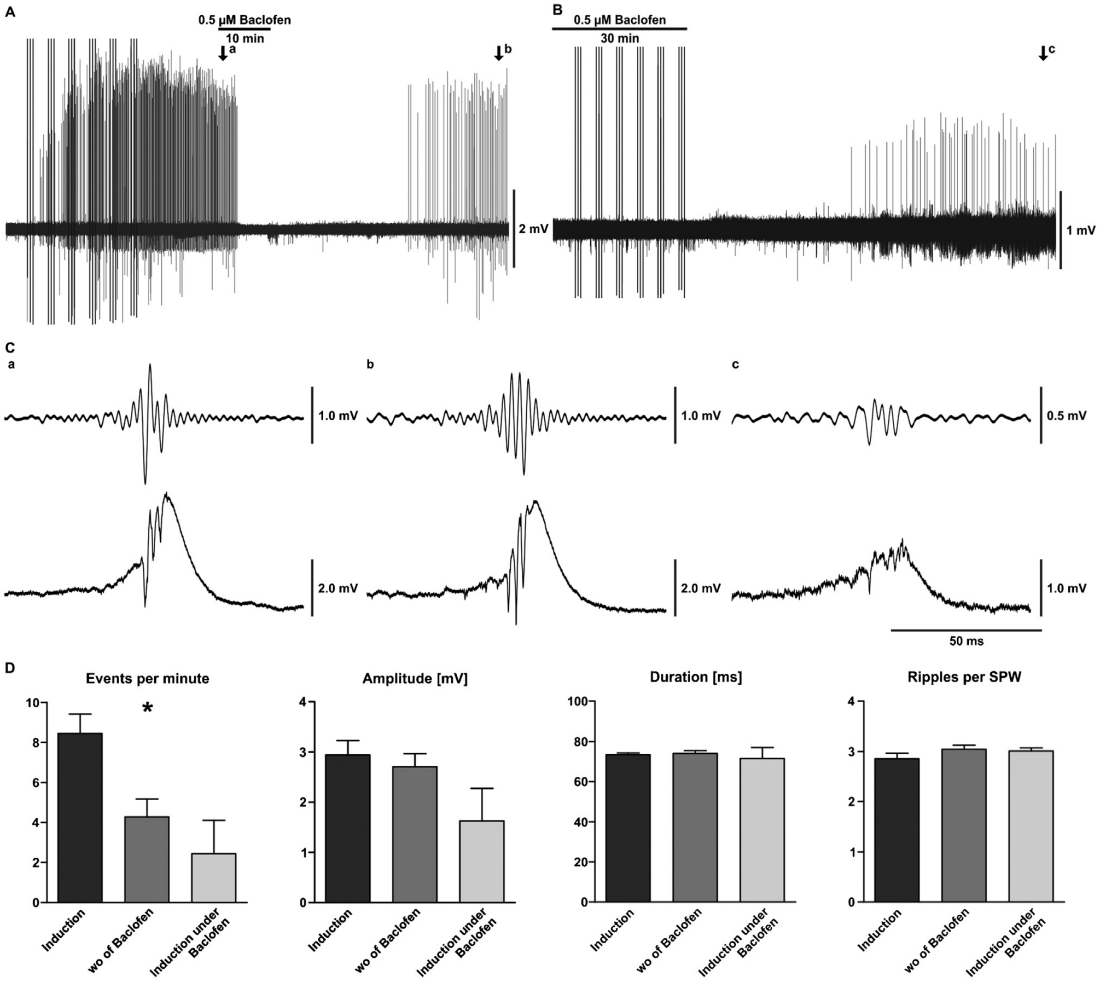

Fig. 1. *SPW-Rs and baclofen.* (A) Field potentials (FP) in hippocampal area CA3. Baclofen [0.5 µM] reversibly suppressed induced SPW-Rs. Arrows signify for SPW-Rs shown in (C). (B) Baclofen suppressed the appearance of SPW-Rs but did not prevent their induction, as SPW-Rs develop spontaneously after wash out of baclofen. Arrow signifies for SPW-R shown in (C). (C) Representative examples for SPW-Rs shown in (A and B). The upper panel represents the band-pass filtered (120–400 Hz) signals. (D) Synopsis of properties of SPW-Rs under control conditions and following washout of baclofen. Asterisk in (D) marks significance with $p < 0.05$.

the negative after-potential of a SPW-R complex was somewhat increased. We next asked whether in the presence of baclofen LTP and SPW-R activity could still be induced. With 0.5 µM baclofen, lasting LTP could only be induced in 3 out of 10 experiments. Statistical analysis was therefore omitted. Interestingly in those cases where lasting LTP was induced, SPW-R activity appeared; however, only at about 25 min after washout out of baclofen and not as promptly during ongoing stimulation as under control conditions (Fig. 1B). The incidence (2.4 ± 1.7 events per minute) and the amplitude (1.6 ± 0.7 mV) of these SPW-Rs was reduced. Duration and ripple numbers per sharp wave were comparable to control conditions (Fig. 1D).

The blocking of SPW-Rs can in principle be explained by postsynaptic hyperpolarization and an increase in membrane conductance, as well as by effects on presynaptic transmitter release thereby uncoupling neurons that under other conditions associate with each other into a neuronal ensemble. We therefore performed intracellular recordings and accepted cells that had an input resistance larger than 25 MΩ and a membrane potential more negative than −62 mV with overshooting action potentials. We found that baclofen hyperpolarized CA3 pyramidal cells by 7.1 ± 0.7 mV and decreased input resistance from 31.1 ± 4.1 to 23.0 ± 1.6 MΩ ($n = 10$ cells). Also in the presence of bicuculline, baclofen hyperpolarized membrane potentials and increased membrane conductance.

To test for the possibility that presynaptic mechanisms also contribute to this blocking effect, we analyzed paired pulse evoked excitatory postsynaptic potentials (EPSPs) in Schaffer collateral pyramidal cell synapses, with Schaffer collaterals originating from the axons of CA3 pyramidal cells. These were thought to have similar synaptic properties as those axons which interconnect CA3 pyramidal cells with each other and with interneurons. In intracellular recordings we noted a paired pulse ratio (Fig. 2C) of 1.1 ± 0.1 under control conditions with stimulus intensities subthreshold for induction of action potentials. In the presence of baclofen this ratio significantly increased to 1.5 ± 0.1 ($n = 10$ cells, $p = 0.002$). We repeated these experiments in the presence of bicuculline and found under conditions of stimulation intensities subthreshold for induction of action potentials a paired pulse ratio of 1.5 ± 0.2 that

Publication II

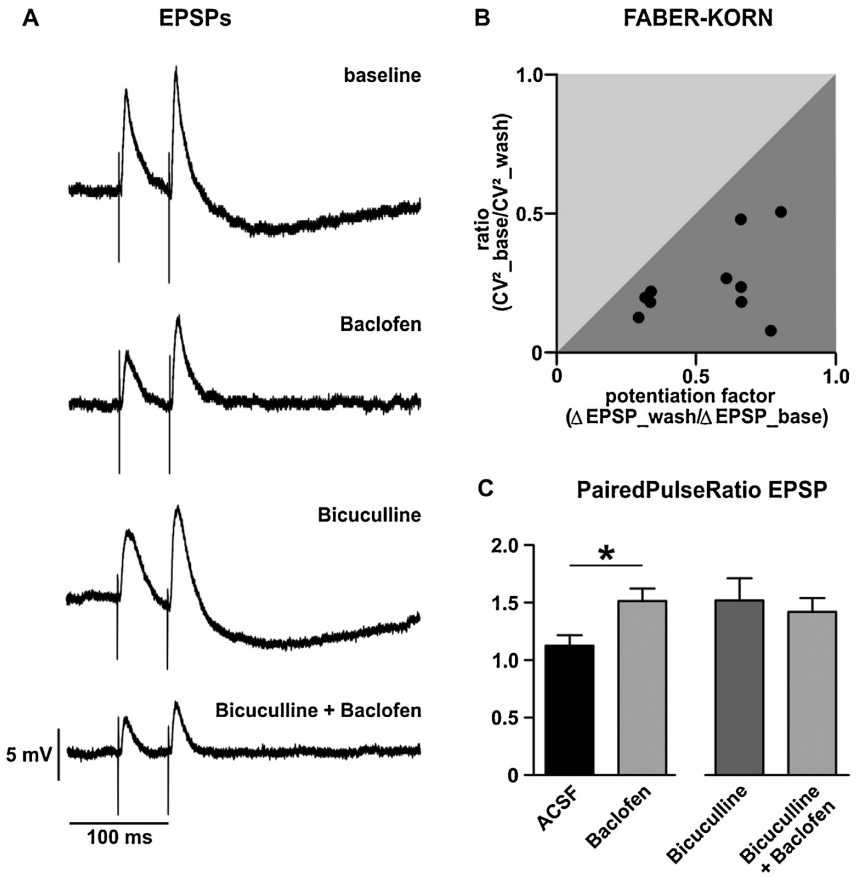

Fig. 2. *Baclofen and EPSPs.* (A) EPSPs recorded in CA1 evoked by paired stimulation of stratum radiatum (50 ms interval). (B) Coefficient of variation analysis. Data indicates presynaptic depressive modulation by of baclofen. (C) Paired pulse ratio of EPSPs is significantly increased by baclofen under control condition but not in presence of bicuculline. Asterisks mark significance with $p < 0.05$.

did no longer change significantly after application of baclofen (1.4 ± 0.1; $n = 4$ cells, $p = 0.673$). When we analyzed the ratio of evoked EPSPs under control condition versus drug conditions we noted that all values were in the lower right segment of the plot indicating a presynaptic effect of baclofen (Fig. 2B). This could be due to a number of effects of baclofen including presynaptic hyperpolarization, decreased Ca^{2+} influx and altered fusion processes. We therefore determined whether baclofen had any effect on antidromically induced population spikes in area CA3. This was not the case (data not shown). We next tested whether baclofen had an effect on presumed presynaptic Ca^{2+} entry. In order to isolate this component, stimulus induced Ca^{2+} concentration changes

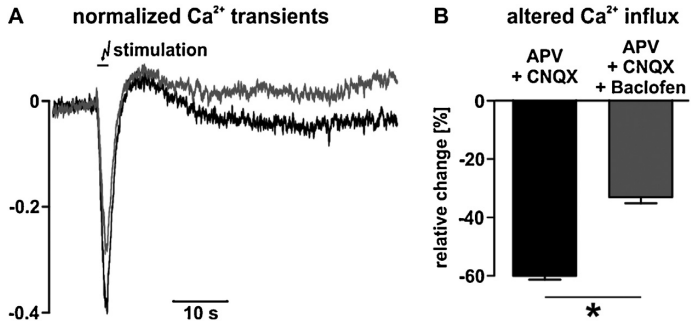

Fig. 3. *Calcium transients in stratum radiatum of CA1.* (A) Normalized medians of five stimulation trains (40 pulses @ 20 Hz) obtained with Ca^{2+}-sensitive electrodes after application of DL-2-APV and CNQX (black) and after coapplication of baclofen with DL-2-APV and CNQX (gray). B: Application of baclofen significantly reduced the influx of Ca^{2+} during stimulation. Asterisks indicate significant reduction ($p < 0.05$).

were measured in SR of area CA1 (Fig. 3A). Following application of CNQX (25 μM) and DL-2-APV (50 μM) stimulus evoked postsynaptic responses were blocked (see also [21]) and stimulus induced Ca^{2+} concentration changes were reduced by 59.5 ± 6% (n = 9). When baclofen (0.5 μM) was then added the remaining Ca^{2+} signal was significantly (p = 0.025) reduced by another 32.7 ± 6.4% (Fig. 3B).

4. Discussion

The present study shows that stimulus induced SPW-R complexes are reversibly blocked by application of the $GABA_B$ receptor agonist baclofen, an effect which could be prevented by the $GABA_B$ receptor antagonist CGP55846. This shows that $GABA_B$ receptors may be involved in regulation of incidence of SPW-R complexes. This effect might contribute to the blocking effect of $GABA_A$ receptor antagonists on SPW-R complexes previously observed both for stimulus and spontaneous SPW-R complexes in mice [9] and rats [12]. If $GABA_A$ receptors are blocked, released GABA can probably diffuse further away from release sites and thus activate extrasynaptic $GABA_B$ receptors. The fact that CGP55846 did not increase incidence of SPW-R activity suggested that under our experimental conditions interstitial GABA through activation of $GABA_B$ receptors is not strongly involved in regulating the incidence of SPW-Rs. Since ambient GABA may be reduced by slice perfusion, however, this might be different under in vivo conditions where ambient GABA is probably in the order of some μM [22].

The blocking effect of baclofen on SPW-Rs was associated with a hyperpolarizing change in membrane potential and a change in input resistance [23]. This compares to other agents that were previously shown to block SPW-R activity, such as adenosine [6] and norepinephrine [5]. However, SPW-Rs were found to be sensitive also to acetylcholine, which depolarizes hippocampal neurons, suggesting that also presynaptic effects might be involved [4]. Our findings on the reduction of stimulation induced Ca^{2+} concentration changes confirmed previous observations [24]. This effect could be due to modification of axonal excitability. However, antidromically propagating action potential amplitudes in Schaffer collaterals were not affected by baclofen. That would indicate that baclofen reduces Ca^{2+} signals by block of PQ- and/or N-type Ca^{2+} currents underlying presynaptic Ca^{2+} dependent transmitter release [25,26]. Indeed, baclofen can reduce Ca^{2+} transients in dendritic spines [27] and also suppress P/Q- and N-type Ca^{2+} currents [28]. Independent of such action of baclofen on Ca^{2+} currents, modulation of processes involved in fusion of vesicles [29] might also contribute to this effect. The SPW-R complexes seem to be generated in area CA3, which is an associative network characterized by recurrent excitatory synaptic interaction between pyramidal cells, and between pyramidal cells and interneurons. In such a network, strengthening of synaptic interaction by induction of LTP permits formation of neural assemblies in which previously activated cells generate action potentials in rapid succession. Weakening of transmitter release in such an associative network might therefore interrupt SPW-R generation. If these events are important for replay of previously stored information then these effects of baclofen could explain some of the memory disturbing effects that baclofen has [30]. We employed a baclofen concentration which is probably double of that achieved in CSF of patients. However, we applied baclofen for only relatively short times and the blocking effect was noted after about 5 minutes. This is way before the time when a slice maintained under interface conditions is fully equilibrated with a drug (see [31–33]). Effects of baclofen on SPW-Rs compare to the effects of norepinephrine via α1 receptors and to the effects of adenosine. These share both presynaptic effects and postsynaptic hyperpolarization [34]. Additionally, ACh can block SPW-Rs both in mice [35] and in rats [4], an effect which is, however, associated with postsynaptic depolarization pointing to the importance of presynaptic modulation.

Activation of $GABA_B$ receptors does not generally prevent induction of LTP. We show here that in the presence of baclofen induction of SPW-Rs is possible albeit rarely occurring in our hands and only in a delayed fashion at times when baclofen had been washed out. This suggests a delayed aggregation into neural assemblies in area CA3 following induction of associative LTP at a time when the probability of transmitter release is increased, thus permitting generation of SPW-R complexes. This compares well to similar observations, where in the presence of norepinephrine, due to activation of presynaptic α1 receptors the formation of SPW-R is delayed until washout of norepinephrine [5]. This proposes that the appearance of sharp wave ripples can be regulated by controlling efficacy of presynaptic transmitter release while postsynaptic mechanisms which regulate synaptic strength permit organization of ensemble activity generating SPW-R complexes for example at consummatory behavior or during slow wave sleep.

Acknowledgments

This work was supported by Bernstein Focus Learning Förderkennzeichen 01GQ0971 and the DFG grant He 1128/17-1. We are grateful for technical assistance to Dr. H.-J. Gabriel and to Dipl. Biol. Tanja Specowius.

References

[1] B. Shen, B.L. McNaughton, Modeling the spontaneous reactivation of experience-specific hippocampal cell assembles during sleep, Hippocampus 6 (1996) 685–692.
[2] G. Buzsaki, Two-stage model of memory trace formation: a role for noisy brain states, Neuroscience 31 (1989) 551–570.
[3] O. Eschenko, W. Ramadan, M. Molle, J. Born, S.J. Sara, Sustained increase in hippocampal sharp-wave ripple activity during slow-wave sleep after learning, Learn. Mem. 15 (2008) 222–228.
[4] M.E. Hasselmo, J. McGaughy, High acetylcholine levels set circuit dynamics for attention and encoding and low acetylcholine levels set dynamics for consolidation, Prog. Brain Res. 145 (2004) 207–231.
[5] R. ul Haq, A. Liotta, R. Kovacs, A. Rösler, M.J. Jarosch, U. Heinemann, C.J. Behrens, Adrenergic modulation of sharp wave-ripple activity in rat hippocampal slices, Hippocampus 22 (2012) 516–533.
[6] N. Maier, G. Morris, S. Schuchmann, T. Korotkova, A. Ponomarenko, C. Bohm, C. Wozny, D. Schmitz, Cannabinoids disrupt hippocampal sharp wave-ripples via inhibition of glutamate release, Hippocampus 22 (2011) 1350–1362.
[7] N. Maier, M. Guldenagel, G. Sohl, H. Siegmund, K. Willecke, A. Draguhn, Reduction of high-frequency network oscillations (ripples) and pathological network discharges in hippocampal slices from connexin 36-deficient mice, J.Physiol. 541 (2002) 521–528.
[8] C.J. Behrens, L.P. van den Boom, L. de Hoz, A. Friedman, U. Heinemann, Induction of sharp wave-ripple complexes in vitro and reorganization of hippocampal networks, Nat. Neurosci. 8 (2005) 1560–1567.
[9] N. Maier, V. Nimmrich, A. Draguhn, Cellular and network mechanisms underlying spontaneous sharp wave-ripple complexes in mouse hippocampal slices, J. Physiol. 550 (2003) 873–887.
[10] G. Buzsaki, D.L. Buhl, K.D. Harris, J. Csicsvari, B. Czeh, A. Morozov, Hippocampal network patterns of activity in the mouse, Neuroscience 116 (2003) 201–211.
[11] V. Nimmrich, N. Maier, D. Schmitz, A. Draguhn, Induced sharp wave-ripple complexes in the absence of synaptic inhibition in mouse hippocampal slices, J. Physiol. 563 (2005) 663–670.
[12] C.J. Behrens, L.P. van den Boom, U. Heinemann, Effects of the GABA(A) receptor antagonists bicuculline and gabazine on stimulus-induced sharp wave-ripple complexes in adult rat hippocampus in vitro, Eur. J. Neurosci. 25 (2007) 2170–2181.
[13] A. Liotta, G. Caliskan, R. ul Haq, J.O. Hollnagel, A. Rösler, U. Heinemann, C.J. Behrens, Partial disinhibition is required for transition of stimulus-induced sharp wave-ripple complexes into recurrent epileptiform discharges in rat hippocampal slices, J. Neurophysiol. 105 (2011) 172–187.
[14] R.M. Empson, U. Heinemann, The perforant path projection to hippocampal area CA1 in the rat hippocampal-entorhinal cortex combined slice, J. Physiol. 484 (1995) 707–729.
[15] S.M. Thompson, B.H. Gähwiler, Comparison of the actions of baclofen at pre- and postsynaptic receptors in the rat hippocampus *in vitro*, J. Physiol. 451 (1992) 329–345.

Publication II

[16] T. Bartoi, K.T. Rigbolt, D. Du, G. Kohr, B. Blagoev, H.C. Kornau, $GABA_B$ receptor constituents revealed by tandem affinity purification from transgenic mice, J. Biol. Chem. 285 (2010) 20625–20633.
[17] R. Kuner, G. Kohr, S. Grunewald, G. Eisenhardt, A. Bach, H.C. Kornau, Role of heteromer formation in $GABA_B$ receptor function, Science 283 (1999) 74–77.
[18] A. Konnerth, U. Heinemann, Effects of GABA on presumed presynaptic Ca^{2+} entry in hippocampal slices, Brain Res. 270 (1983) 185–189.
[19] H.-G. Schaible, B.D. Grubb, V. Neugebauer, M. Oppmann, The effects of NMDA antagonists on neuronal activity in cat spinal cord evoked by acute inflammation in the knee joint, Eur. J. Neurosci. 3 (1991) 981–991.
[20] D.S. Faber, H. Korn, Applicability of the coefficient of variation method for analyzing synaptic plasticity, Biophys. J. 60 (1991) 1288–1294.
[21] A. Liotta, J. Rösner, C. Huchzermeyer, A. Wojtowicz, O. Kann, D. Schmitz, U. Heinemann, R. Kovacs, Energy demand of synaptic transmission at the hippocampal Schaffer-collateral synapse, J. Cereb. Blood Flow Metab. 32 (2012) 2076–2083.
[22] B.M. Stell, S.G. Brickley, C.Y. Tang, M. Farrant, I. Mody, Neuroactive steroids reduce neuronal excitability by selectively enhancing tonic inhibition mediated by delta subunit-containing $GABA_A$ receptors, Proc. Nat. Acad. Sci. U.S.A. 100 (2003) 14439–14444.
[23] B.W. Connors, R.C. Malenka, L.R. Silva, Two inhibitory postsynaptic potentials, and $GABA_A$ and $GABA_B$ receptor-mediated responses in neocortex of rat and cat, J. Physiol. 406 (1988) 443–468.
[24] U. Heinemann, B. Hamon, A. Konnerth, GABA and baclofen reduce changes in extracellular free calcium in area CA1 of rat hippocampal slices, Neurosci. Lett. 47 (1984) 295–300.
[25] P. Igelmund, Y.Q. Zhao, U. Heinemann, Effects of T-type, L-type, N-type, P-type and Q-type calcium channel blockers on stimulus-induced pre- and postsynaptic calcium fluxes in rat hippocampal slices, Exp. Brain Res. 109 (1996) 22–32.
[26] K. Dunlap, J.I. Luebke, T.J. Turner, Exocytotic Ca^{2+} channels in mammalian central neurons, Trends Neurosci. 18 (1995) 89–98.
[27] E. Perez-Garci, M.E. Larkum, T. Nevian, Inhibition of dendritic Ca^{2+} spikes by $GABA_B$ receptors in cortical pyramidal neurons is mediated by a direct Gi/o-beta-subunit interaction with Cav1 channels, J. Physiol. 591 (2013) 1599–1612.
[28] S. Lei, C.J. McBain, $GABA_B$ receptor modulation of excitatory and inhibitory synaptic transmission onto rat CA3 hippocampal interneurons, J. Physiol. 546 (2003) 439–453.
[29] B.R. Rost, P. Nicholson, G. Ahnert-Hilger, A. Rummel, C. Rosenmund, J. Breustedt, D. Schmitz, Activation of metabotropic GABA receptors increases the energy barrier for vesicle fusion, J. Cell Sci. 124 (2011) 3066–3073.
[30] M.P. Arolfo, M.A. Zanudio, O.A. Ramírez, Baclofen infused in rat hippocampal formation impairs spatial learning, Hippocampus 8 (1998) 109–113.
[31] W. Müller, U. Misgeld, U. Heinemann, Carbachol effects on hippocampal neurons in vitro: dependence on the rate of rise of carbachol tissue concentration, Exp. Brain Res. 72 (1988) 287–298.
[32] K. Alici, T. Gloveli, D. Schmitz, U. Heinemann, Effects of glutamate receptor agonists and antagonists on Ca2+ uptake in rat hippocampal slices lesioned by glucose deprivation or by kainite, Neuroscience 77 (1997) 97–109.
[33] S. Sokolova, D. Schmitz, C.L. Zhang, W. Löscher, U. Heinemann, Comparison of effects of valproate and trans-2-en-valproate on different forms of epileptiform activity in rat hippocampal and temporal cortex slices, Epilepsia 39 (1998) 251–258.
[34] M. Scanziani, M. Capogna, B.H. Gähwiler, S.M. Thompson, Presynaptic inhibition of miniature excitatory synaptic currents by baclofen and adenosine in the hippocampus, Neuron 9 (1992) 919–927.
[35] M.M. Zylla, X. Zhang, S. Reichinnek, A. Draguhn, M. Both, Cholinergic plasticity of oscillating neuronal assemblies in mouse hippocampal slices, PLoS One 8 (2013) e80718.

Publication III

Neuroscience 284 (2015) 459–469

NO EVIDENCE FOR ROLE OF EXTRACELLULAR CHOLINE-ACETYLTRANSFERASE IN GENERATION OF GAMMA OSCILLATIONS IN RAT HIPPOCAMPAL SLICES *IN VITRO*

J. O. HOLLNAGEL,[a] R. UL HAQ,[a] C. J. BEHRENS,[a] A. MASLAROVA,[a] I. MODY[c,d] AND U. HEINEMANN[a,b]*

[a] *Institute of Neurophysiology, Charité Universitätsmedizin Berlin, 14195 Berlin, Germany*

[b] *NeuroCure Research Center, Charité Universitätsmedizin Berlin, 14195 Berlin, Germany*

[c] *Department of Neurology, The David Geffen School of Medicine at the University of California, Los Angeles, CA 90095, USA*

[d] *Department of Physiology, The David Geffen School of Medicine at the University of California, Los Angeles, CA 90095, USA*

Abstract—Acetylcholine (ACh) is well known to induce persistent γ-oscillations in the hippocampus when applied together with physostigmine, an inhibitor of the ACh degrading enzyme acetylcholinesterase (AChE). Here we report that physostigmine alone can also dose-dependently induce γ-oscillations in rat hippocampal slices. We hypothesized that this effect was due to the presence of choline in the extracellular space and that this choline is taken up into cholinergic fibers where it is converted to ACh by the enzyme choline-acetyltransferase (ChAT). Release of ACh from cholinergic fibers in turn may then induce γ-oscillations. We therefore tested the effects of the choline uptake inhibitor hemicholinium-3 (HC-3) on persistent γ-oscillations either induced by physostigmine alone or by co-application of ACh and physostigmine. We found that HC-3 itself did not induce γ-oscillations and also did not prevent physostigmine-induced γ-oscillation while washout of physostigmine and ACh-induced γ-oscillations was accelerated. It was recently reported that ChAT might also be present in the extracellular space (Vijayaraghavan et al., 2013). Here we show that the effect of physostigmine was prevented by the ChAT inhibitor (2-benzoylethyl)-trimethylammonium iodide (BETA) which could indicate extracellular synthesis of ACh. However, when we tested for effects of extracellularly applied acetyl-CoA, a substrate of ChAT for synthesis of ACh, physostigmine-induced γ-oscillations were attenuated. Together, these findings do not support the idea that ACh can be synthesized by an extracellularly located ChAT.

Key words: γ-oscillations in hippocampal area CA3, acetylcholine, physostigmine, hemicholinium-3 (HC-3), (2-benzoylethyl)-trimethylammonium iodide (BETA), acetyl-CoA.

INTRODUCTION

In the central nervous system acetylcholine (ACh) is critically involved in regulation of arousal, attention and rapid eye movement (REM) sleep (Metherate et al., 1987; Steriade et al., 1993). Elevated ACh levels during explorative behavior are likely to induce network oscillations in the theta (θ)- and γ-bands (Klinkenberg et al., 2011; Picciotto et al., 2012). These oscillations can be reproduced *in vitro* in hippocampal slices by application of cholinergic agonists such as carbachol (Fisahn et al., 1998; Weiss et al., 2003). Carbachol readily induces γ-oscillations in area CA3 in horizontal and parasagittal slices (Wójtowicz et al., 2009). While in longitudinal slices θ-oscillations emerge as reported also for kainate-induced oscillations (Gloveli et al., 2005a). In contrast to the basal ganglia and septum, cortex and hippocampus contain only few cholinergic neurons (Frotscher et al., 2000) whose function is presently unclear but which could contribute to cholinergic oscillations as suggested by the findings that both types of oscillations can coexist in hippocampal slice cultures (Fischer et al., 2002) without septal input. In the cortex, the main sources of ACh are terminals originating from the nucleus basalis (Johnston et al., 1979; Struble et al., 1986), and in the hippocampus, fibers which originate from the septum (Hasselmo and Bower, 1993). Stimulation of the nucleus basalis not only induces θ- and superimposed γ-oscillations (Lamour et al., 1986; McLin et al., 2003), but also leads to a rapid neurovascular response (Moro et al., 1995). Activation of the septum has similar effects in the hippocampus (Vandecasteele et al., 2014). ACh binds to both ionotropic nicotinic receptors, and metabotropic G protein-dependent muscarinic receptors. Nicotinic receptors containing α4 subunits found on hippocampal pyramidal cells show rapid desensitization (Liotta et al., 2011), while nicotinic receptors containing α7 subunits are typically expressed on parvalbumin-negative basket cells (Freund and Gulyás, 1997). Muscarinic receptors, on the other hand, are present in different types of neurons and can be blocked by atropine, and, in case of M1 receptors, by pirenzepine (Müller and Misgeld, 1989). ACh also exerts effects on non-neuronal non-excitable cells abundant in the brain, including microglia, astrocytes, oligodendrocytes,

*Correspondence to: U. Heinemann, Institute of Neurophysiology, Garystraße 5, 14195 Berlin, Germany. Tel: +49-30-450-528-091.
E-mail address: Uwe.Heinemann@charite.de (U. Heinemann).

Abbreviations: ACh, acetylcholine; AChE, acetylcholinesterase; aCSF, artificial cerebrospinal fluid; BETA, (2-benzoylethyl)-trimethylammonium iodide; ChAT, choline-acetyltransferase; DMSO, dimethyl sulfoxide; HC-3, hemicholinium-3.

http://dx.doi.org/10.1016/j.neuroscience.2014.10.016
0306-4522/

endothelia, and vascular smooth muscle cells (Wessler and Kirkpatrick, 2008; Kawashima and Fujii, 2008).

ACh is synthesized from choline by choline-acetyltransferase (ChAT), an enzyme which transfers acetate from acetyl-CoA onto choline. This enzyme is considered to be localized inside cholinergic terminals and serves as a marker of cholinergic neurons (Léránth and Frotscher, 1987). After synthesis, ACh is transported into vesicles and eventually released. Recently it has been suggested that ChAT is also present in the extracellular space thus permitting synthesis of ACh outside neurons (Vijayaraghavan et al., 2013). In presence of acetylcholinesterase (AChE) and butyrylcholinesterase (BuChE), ACh is very short-lived (Kaufer et al., 1999). AChE comes in different forms. The soluble read-through form is not anchored close to release sites, permitting wide-spread diffusion of ACh (Meshorer et al., 2002). Animals lacking AChE show a strong increase in extracellular ACh in the dorsal hippocampus which can be detected by microdialysis (Hartmann et al., 2008). These increased ACh levels are accompanied by decreased levels of extracellular choline. Addition of choline (10 μM) to the perfusion fluid, while ineffective in wild-type animals, more than doubles extracellular ACh levels in AChE-deficient mice suggesting that ACh synthesis is probably not saturated (Hartmann et al., 2008).

Additionally, it has been suggested that in brain slices choline originates also from the degradation of lipid membranes. Using Corning type tri- and tetra alkylated ammonia and K^+-sensitive electrodes in comparison to measurements with valinomycine-based K^+-selective microelectrodes suggested concentrations of about 10 μM choline in the extracellular space (Müller et al., 1988). We hypothesized that this source of choline is used for ACh synthesis after cellular uptake and thus may induce network oscillations, provided ACh degradation is inhibited.

In this study we tested for effects of physostigmine alone and physostigmine in combination with ACh on γ-oscillations in hippocampal slices. We found that physostigmine alone could dose-dependently induce γ-oscillations which were strongly augmented by ACh. Surprisingly, the choline uptake inhibitor hemicholinium-3 (HC-3) did not prevent generation of γ-oscillations by physostigmine but rather led to a slight augmentation suggesting that ACh synthesis can occur under conditions when choline transport is blocked.

To clarify whether additional ACh can be synthesized by extracellular ChAT we applied (2-benzoylethyl)-trimethylammonium iodide (BETA) which antagonizes the synthesis of ACh by blocking ChAT (Galea and Estrada, 1991; Chen et al., 1993). In another set of experiments we applied acetyl-CoA, a substrate for ChAT to form ACh. While we observed a (slight) reduction of physostigmine-induced γ-oscillations by BETA, there was no evidence for a facilitation of γ-oscillations in the presence of acetyl-CoA. Together these findings suggest that there is no evidence for an extracellularly located ChAT.

EXPERIMENTAL PROCEDURES

Slice preparation and solutions

Animal procedures were performed in accordance with the guidelines of the European Communities Council and approved by the State Office of Health and Social Affairs Berlin (Landesamt für Gesundheit und Soziales, LaGeSO, Berlin: T0096/02). Six to eight-week-old male Wistar rats were decapitated under deep isoflurane/laughing gas anesthesia. The brain was rapidly removed and then washed in ice-cold carbogenated (95% O_2–5% CO_2) artificial cerebrospinal fluid (aCSF) containing (in mM): NaCl 129, $NaHCO_3$ 21, KCl 3, $CaCl_2$ 1.6, $MgSO_4$ 1.8, NaH_2PO_4 1.25, and glucose 10. Horizontal hippocampal-entorhinal cortex slices, 400-μm thick, were prepared on a vibrating blade microtome (Leica Microsystems, Wetzlar, Germany) and immediately transferred to an interface chamber and perfused with carbogenated aCSF at 36 ± 0.5 °C (flow rate: ∼1.8 ml/min, pH 7.4, osmolarity: 300 ± 3 mosmol/kg). Slices were left to recover for at least 2 h before recording was started.

Recordings

Extracellular field potentials (FP) were recorded under interface conditions with carbon-fiber electrodes in AC mode. Electrodes were placed in the pyramidal layer of area CA3. Potentials were amplified 200 times using a custom-made amplifier, low-pass filtered at 3 kHz, digitized at 10 kHz using Spike2 software, and stored on a computer disk for offline analysis (1401 interface, CED, Cambridge, UK).

Data analysis

Signals were analyzed off-line using custom programs written in Matlab (The MathWorks, Natick, MA, USA). We performed power spectrum analyses on 1-min data epochs collected during the last 5 min in a given series of measurements. We determined peak power, peak frequency and power between 30 and 90 Hz. In addition we analyzed the 40–10-Hz quotient in a given treatment termed γ–θ ratio. Finally, we did autocorrelation analysis of 5 min of data and used the distance of nearest peak to corroborate dominant frequency. By fitting an exponential to the different peaks in the autocorrelation function we determined inner coherence following Stenkamp et al. in their analysis on carbachol-induced γ-oscillations (Stenkamp et al., 2001). All numerical data are expressed as mean ± standard error. If data were normally distributed, statistical evaluation was performed by a one-way analysis of variance (ANOVA) with Bonferroni's correction for multiple comparisons to identify significant differences between conditions. Non-parametric tests (Kruskal–Wallis as well as Friedman) were used and followed by Dunn's multiple comparisons, when data were not normally distributed. *p*-Values less than 0.05 were considered to indicate a significant difference between means (indicated by asterisks and/or plusses).

Drug application

The following drugs were used in the experiments: HC-3, acetyl-CoA, physostigmine, and ACh (all Sigma–Aldrich, Taufkirchen, Germany), dissolved in aCSF to their final concentration. For blocking choline-acetyltransferase, BETA (Angene, Hong Kong, China), was dissolved in dimethyl sulfoxide (DMSO) and applied with 100 µM (final DMSO concentration 0.1%).

RESULTS

ACh-dependent γ-oscillations

A previous study had indicated that choline concentration in slices may be around 10 µM (Müller et al., 1988). Since cholinergic receptor activation is well known to cause persistent network oscillations in hippocampal slices we hypothesized that application of physostigmine would raise extracellular ACh levels and thereby induce γ-oscillations. As shown in the sample recording of Fig. 1 this was indeed the case. When physostigmine was applied with increasing concentrations of ACh, γ-oscillations increased in amplitude while peak frequency became smaller. Fig. 1 also illustrates details of data evaluation used for this series of experiments. Application of physostigmine induced γ-oscillations with a very wide frequency distribution ranging from 30 to 60 Hz (Fig. 1a_2, b_2). Peak frequency of such oscillations was on average 47.3 ± 0.8 Hz (n = 34; Fig. 2a) in contrast to control without physostigmine where activity was pronounced in the 10–30-Hz range. Peak power at 46.3 Hz was 2.84 ± 0.4 × 10^{-5} mV^2 (n = 33, Fig. 2b). Fig. 2c indicates the variability of physostigmine-mediated effects. As shown, physostigmine caused an increase in peak power in all except for four out of 32 experiments. The summated power between 30 and 90 Hz significantly increased from 3.5 ± 0.4 (aCSF) to 9.0 ± 1.2 × 10^{-4} mV^2 (n = 58, n = 31; p < 0.01, Fig. 2d). In addition, application of physostigmine led to a shift in frequencies from θ/β like activity represented by power at 10 Hz to higher frequencies represented by power at 40 Hz (Fig. 2e). The γ–θ ratio increased from 0.47 ± 0.03 (aCSF; n = 58) to 2.50 ± 0.15 in the presence of physostigmine (n = 32). We also determined the inner coherence (as defined in Stenkamp et al., 2001) of the induced oscillation by an autocorrelation analysis (Fig. 1c). The plot of a decay time constant (Tau/τ) to the observed peaks in the autocorrelation function becomes longer as oscillations become more sinusoidal and would be infinite for a pure sinus oscillation with a fixed frequency. The plot in Fig. 1c_2 indicates a relatively weak inner coherence with an average τ of 10.1 ± 0.5 ms (n = 32; Fig. 2f).

When ACh was added to the physostigmine containing aCSF a more coherent and significantly more powerful γ-oscillation was induced (Fig. 1$a_{3–5}$). The peak frequency decreased with increasing concentrations of ACh (45.8 ± 1.7 Hz, 40.9 ± 1.1 Hz, 37.7 ± 1.3 Hz for 2, 5 and 10 µM ACh (n = 9, n = 11, n = 13 respectively; Fig. 2a)). At concentrations of 5

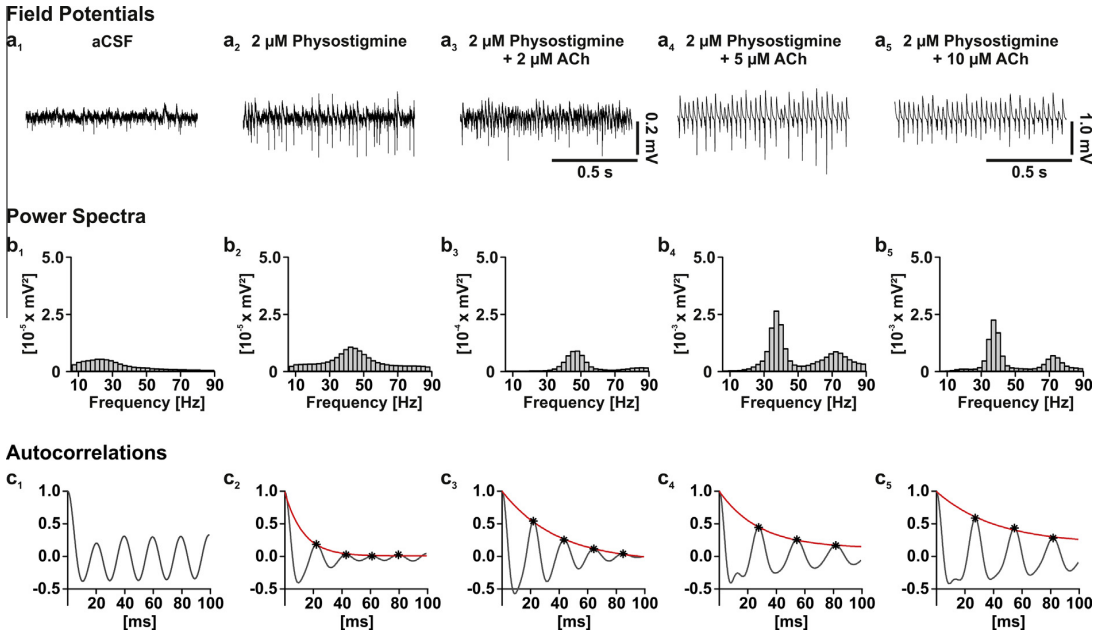

Fig. 1. ACh-dependent γ-oscillations. (a_1–a_5) CA3 field potentials (FP) in presence of different ACh concentrations and 2 µM physostigmine. Calibration in a_3 applies also to a_1, a_2; calibration in a_5 applies also to the recording in a_4. (b_1–b_5) Power spectra of 1-min data epochs represented in a_1–a_5. Note a second harmonic peak in b_4–b_5. Calibration of power spectra is different between b_1, b_2, b_3 and b_4–b_5. (c_1–c_5) Autocorrelograms of 5-min data epochs exemplified in a_1–a_5. Exponential fits (red) were calculated using maxima (asterisks) of the autocorrelograms. The resulting time constant of the exponential fit is related to the inner coherence of the oscillation itself. Note a second small fast peak in the autocorrelograms of c_4 and c_5 corresponding to the second peak in the power spectra. (For interpretation of the references to color in this figure legend, the reader is referred to the web version of this article.)

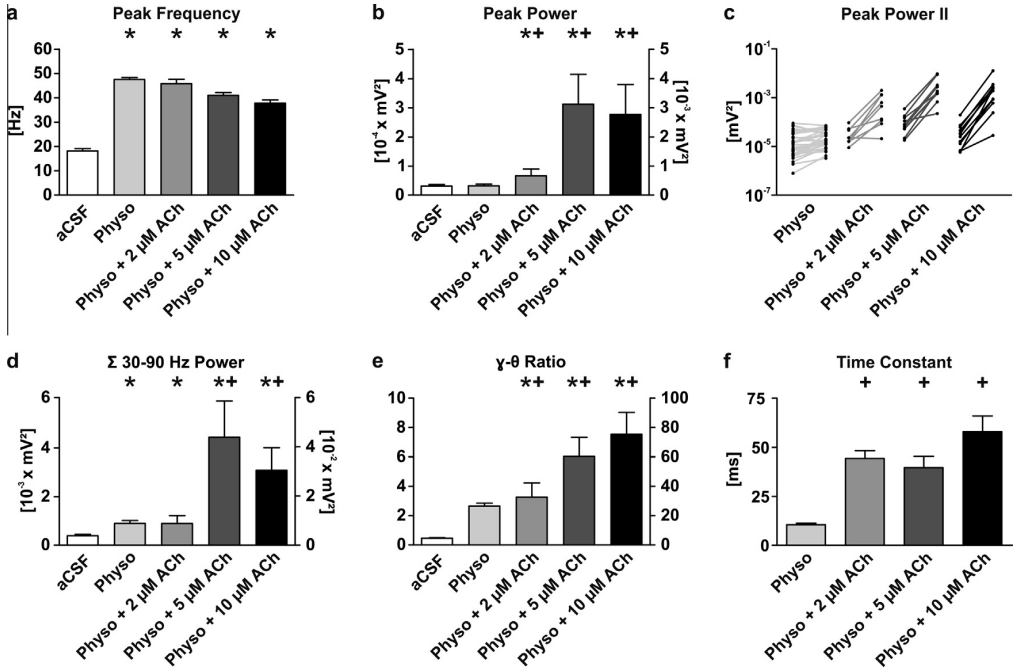

Fig. 2. Summary of ACh-dependent γ-oscillations. (a) Peak frequencies. Note a shift to lower peak frequencies at higher ACh concentrations. (b) Peak power. Presence of ACh led to significant increases compared to physostigmine alone. (c) Effects of different ACh concentrations on individual slice experiments. Note the logarithmic calibration of peak power. (d) Summated power between 30 and 90 Hz. ACh in concentrations of 5 and 10 µM significantly increased values compared to wash in of physostigmine alone. (e) Ratio of γ vs. θ (γ–θ ratio). Note that concentrations of 5 and 10 µM ACh significantly increased the γ–θ ratio when compared to 2 µM ACh. (f) Time constant representing inner coherence. Data are represented by mean and SEM (n = 58, 34, 9, 11 and 13; left to right). Asterisks denote significance against baseline, whereas plusses denote significance against application of 2 µM physostigmine ($p < 0.05$). Note that in b, d and e, calibration on the left applies to the first two columns and calibration on right to the last three columns.

and 10 µM ACh a harmonic peak at double frequency was regularly noted (Fig. 1b$_{4+5}$). Peak power significantly increased when 2, 5 and 10 µM ACh were co-applied ($p < 0.0001$ for all conditions, Fig. 2b). Compared to only physostigmine-treated slices ($2.8 \pm 0.4 \times 10^{-5}$ mV^2, n = 32), peak power values were about 24 times higher with 2 µM ACh ($6.6 \pm 2.3 \times 10^{-4}$ mV^2, n = 7) and around 100 times higher with 5 and 10 µM ACh ($3.1 \pm 1.0 \times 10^{-3}$ mV^2, n = 9 and $2.7 \pm 1.0 \times 10^{-3}$ mV^2, n = 9). Compared to physostigmine alone, co-application with ACh caused a significant increase in summated power between 30 and 90 Hz to $8.8 \pm 3.2 \times 10^{-3}$ mV^2 (2 µM ACh, $p < 0.01$), $4.4 \pm 1.5 \times 10^{-2}$ mV^2 (5 µM ACh, $p < 0.0001$) and $3.0 \pm 0.9 \times 10^{-2}$ mV^2 (10 µM ACh, $p < 0.0001$), indicating that power was saturated at about 5–10 µM (Fig. 2d). The γ–θ ratio also increased significantly with rising ACh concentrations and saturated at 5–10 µM (Fig. 2e). The time constant for the autocorrelograms indicating inner coherence, significantly increased when ACh was co-applied: τ was 44.3 ± 4.0 ms (2 µM ACh, n = 7), 39.6 ± 5.7 ms (5 µM ACh, n = 9) and 58.0 ± 8.0 ms (10 µM ACh, n = 9, $p < 0.0001$ for all conditions). While peak power stabilized at about 5 µM ACh the inner coherence still increased from 5 to 10 µM ACh (Fig. 2f).

Application of 2 µM physostigmine induced weak broad-band γ-oscillations. Higher concentrations of physostigmine (5 and 10 µM, n = 7 each) did not shift peak frequency but increased power of γ-oscillations dose dependently (Fig. 3) At 10 µM peak power was $5.5 \pm 0.1 \times 10^{-4}$ mV^2 (Fig. 3e). 30–90 Hz summated power was $1.0 \pm 0.2 \times 10^{-2}$ mV^2 (Fig. 3f) and γ–θ ratio was 32.1 ± 11.7 (Fig. 3g). Inner coherence also increased dose dependently (Fig. 3h). These values are still lower than those obtained with a combined application of 2 µM physostigmine with 5 or 10 µM ACh but compared to 2 µM physostigmine combined with 2 µM ACh, suggesting that extracellular ACh concentrations are in the order of 2 µM.

Influence of HC-3

We next tested for effects of the choline uptake inhibitor HC-3 on network oscillations as summarized in Figs. 4 and 5, based on the idea that choline is taken up into presynaptic cholinergic terminals and used for synthesis of ACh. Sole application of HC-3 did not induce γ-oscillations (Fig. 4a–f), but HC-3 co-applied with physostigmine did shift peak frequency from 25.0 ± 4.6 Hz to 56.3 ± 2.3 (n = 6, $p < 0.0001$; Fig. 4c) while summated power was significantly increased ($0.5 \pm 0.1 \times 10^{-3}$ mV^2 vs. $1.5 \pm 0.4 \times 10^{-3}$ mV^2, n = 6, $p < 0.05$; Fig. 4f). In order to determine whether HC-3 affected the time course of physostigmine washout on oscillations we compared

Publication III

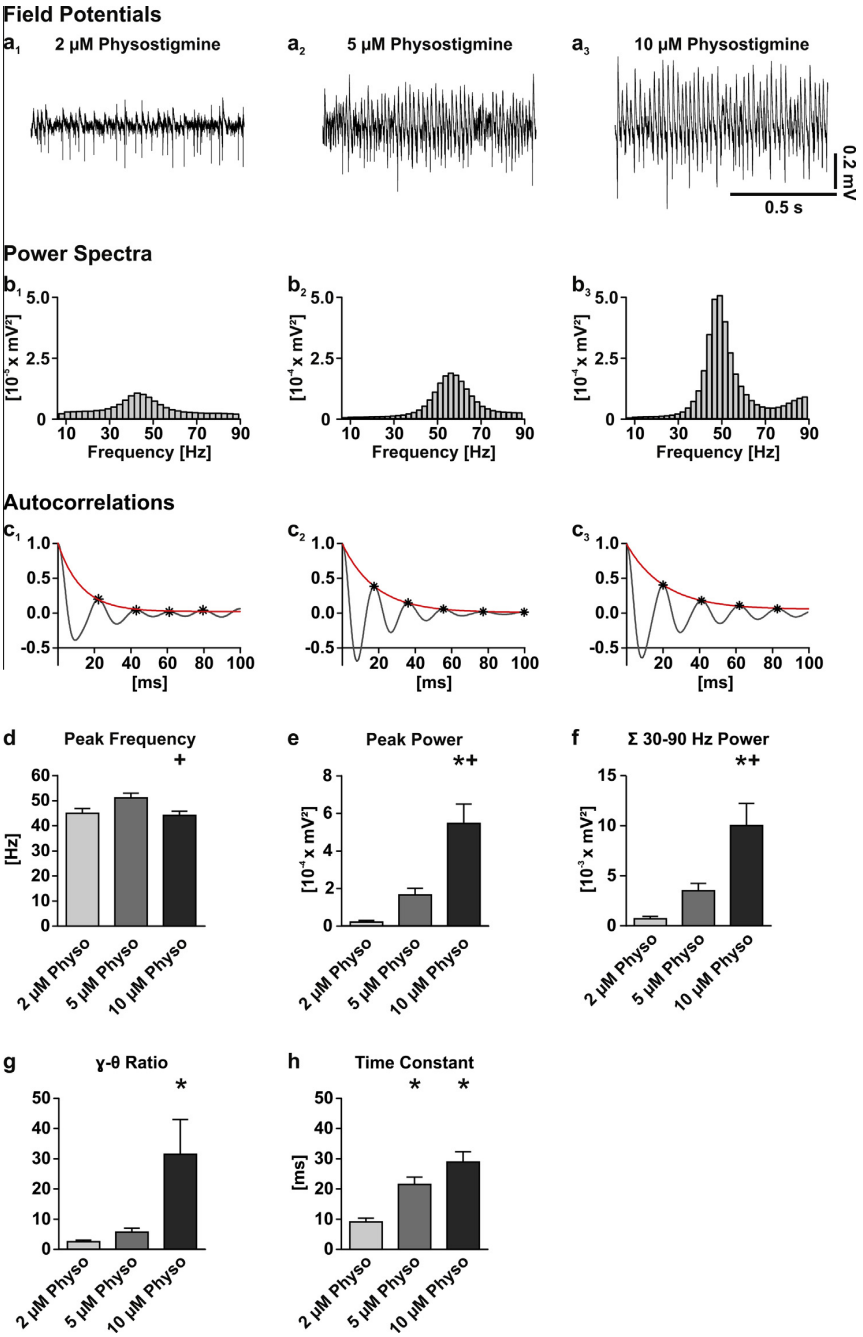

Fig. 3. Physostigmine-dose dependent γ-oscillations. (a_1–a_3) CA3 field potentials (FP) in presence of different physostigmine concentrations. (b_1–b_3) Power spectra off 1-min data epochs represented in a_1–a_3. Note a second harmonic peak in b_3 toward the end of the power spectrum. Note that calibration of power spectra is different between b_1 and b_2–b_3. (c_1–c_3) Autocorrelograms of 5-min data epochs exemplified in a_1–a_3. (d) Peak frequency of γ-oscillations. Peak frequencies differ significantly when comparing 5 µM physostigmine with 10 µM physostigmine. (e) Peak power of γ-oscillations shown in d. γ-oscillations induced with 10 µM physostigmine have significantly higher peak power compared to lower concentrations of physostigmine. (f) Σ 30–90 Hz. Summated power is significantly higher in the presence of 10 µM physostigmine. (g) γ–θ ratio. Compared to 2 µM physostigmine, γ–θ ratio is significantly higher following application of 10 µM physostigmine. (h) Time constant. Inner coherence of γ-oscillations induced by low concentration of physostigmine (2 µM) was significantly lower compared to other treatments (5 µM and 10 µM physostigmine). Data are represented by mean and SEM ($n = 7$). Asterisks and plusses denote significance with $p < 0.05$ between application of 2 µM physostigmine and 5 µM physostigmine respectively.

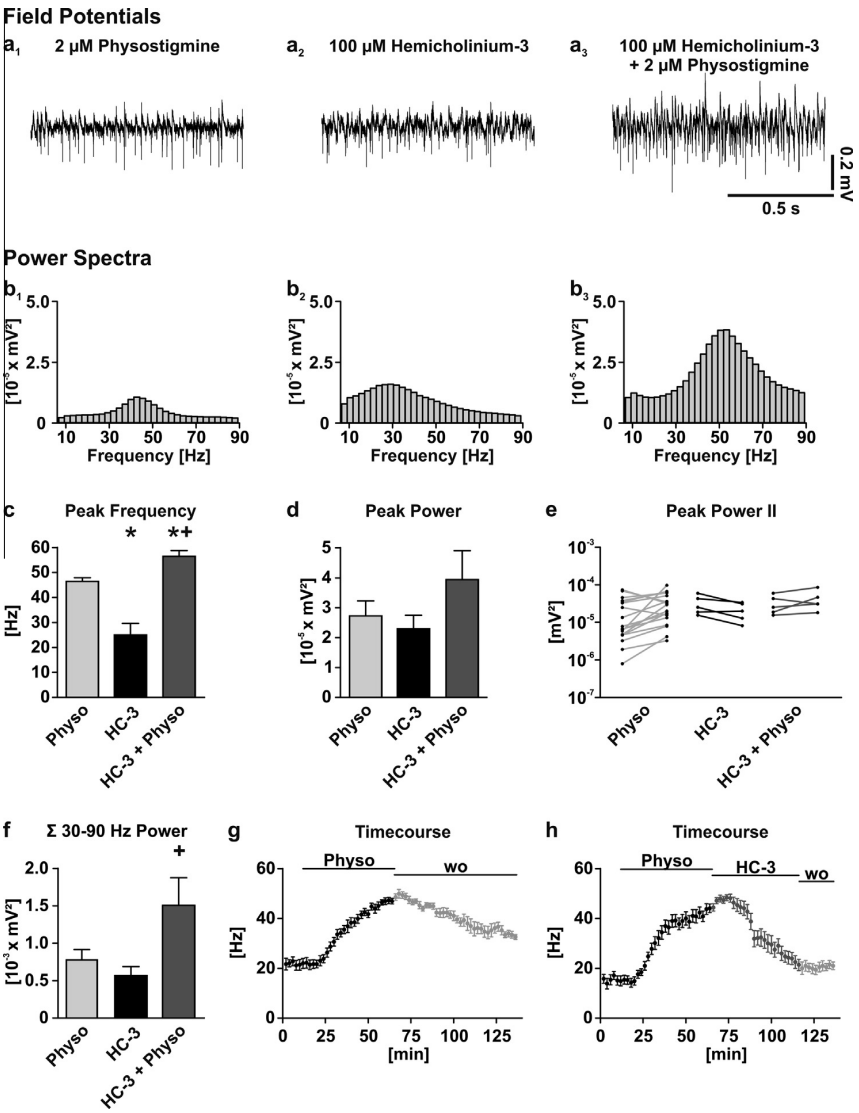

Fig. 4. Influence of hemicholinium-3 (HC-3) on induction of γ-oscillations. Synopsis and time course of wash out of γ-oscillations. (a_1–a_3) Representative FPs recorded in stratum pyramidale of area CA3. (b_1–b_3) Resulting power spectra of 1-min data epochs from the same experiment as in a. (c) Peak frequency of γ-oscillations. Compared to application of 2 µM physostigmine, peak frequencies were significantly lower when HC-3 was applied but significantly higher when HC-3 was co-applied with physostigmine. The difference between HC-3 + physostigmine vs. HC-3 alone is significant as well. (d) Peak power is not significantly different among treatments. (e) Effects of HC-3 on individual experiments. (f) Summated power 30–90 Hz. Co-application of HC-3 with physostigmine differs significantly from sole HC-3 application. (g) Time course of washout of physostigmine indicates that frequencies remain at elevated levels even 1 h after washout; average from five experiments. (h) Time course of replacement of 2 µM physostigmine by 100 µM HC-3 and washout. Under these conditions frequencies are reduced to baseline levels. Data are represented by mean and SEM (n = 16, 6 and 6; left to right). Asterisks and plusses denote significance with $p < 0.05$ between application of 2 µM physostigmine and 100 µM HC-3 respectively.

washout kinetics between experiments where HC-3 was co-applied with physostigmine to sole physostigmine. Physostigmine washout was clearly accelerated in the presence of HC-3 (Fig. 4g, h), a robust phenomenon that was independent of additional ACh (data not shown).

We further investigated whether 100 µM HC-3 affected γ-oscillations induced by co-application of physostigmine plus 10 µM ACh (Fig. 5). Under these conditions, a similar harmonic peak can be observed in the power spectra (Fig. 5b_{1+2}), which is also present in the autocorrelograms shown in Fig. 5c. Quantitative analysis revealed that HC-3 did not affect any of the parameters of γ-oscillations when physostigmine co-applied with 10 µM ACh was compared to the same treatment with HC-3 added (Fig. 5d–g).

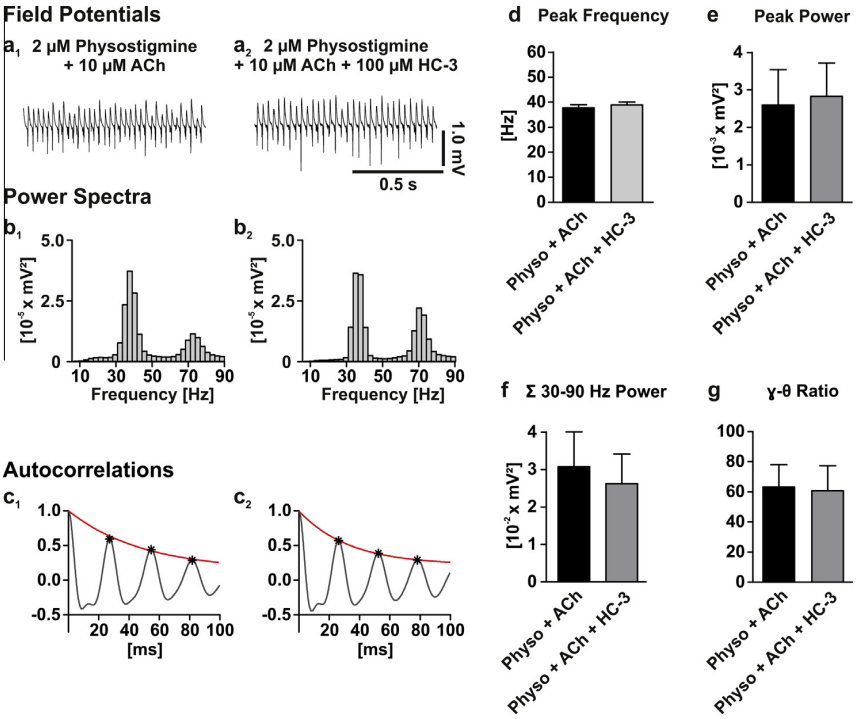

Fig. 5. γ-oscillations induced by high ACh concentrations are not affected by HC-3. (a_1, a_2) Representative FPs recorded in CA3. (b_1, b_2) Power spectra of 1-min data epochs shown in a. Under both conditions peak frequency (~38 Hz) and peak power (~2.7×10^{-3} mV^2) remain comparable. Peak amplitude of the harmonic is increased when 100 µM HC-3 is added (b_2). (c_1, c_2) Autocorrelograms corresponding to 5-min epochs from the same experiment as shown in a_1, a_2. Presence of HC-3 has no effect on the time constant obtained from exponential fits. (d) Peak frequency of γ-oscillations. (e) Peak power. (f) Σ 30–90 Hz. (g) γ–θ ratio. Data are represented by mean and SEM (n = 11 and 12; left to right).

BETA reduces physostigmine-induced γ-oscillations

Our finding that HC-3 did not prevent generation of γ-oscillations by physostigmine raised the possibility that ACh might be synthesized by an extracellularly located ChAT, as suggested previously (Vijayaraghavan et al., 2013). We therefore used the ChAT blocker BETA. Because BETA is quite lipophilic and its sole application does not permit discrimination between extra- and intracellular located ChAT, we applied BETA in the presence of HC-3 in order to prevent reuptake of choline. Co-application of BETA and HC-3 distorted the generation of physostigmine-dependent broad-band γ-oscillations (n = 8). Peak frequencies significantly decreased from 46.2 ± 0.9 Hz (2 µM physostigmine) to 29.2 ± 3.5 Hz when 100 µM HC-3 and 100 µM BETA were co-applied with physostigmine ($p < 0.01$). Accordingly, peak power, as well as summated power of frequencies between 30 and 90 Hz were significantly reduced after co-application of physostigmine with HC-3 and BETA (peak power: $1.5 \pm 0.3 \times 10^{-5}$ mV^2 vs. $1.1 \pm 0.2 \times 10^{-5}$ mV^2, $p < 0.01$; Σ 30–90 Hz power: $5.6 \pm 1.3 \times 10^{-4}$ mV^2 vs. $3.9 \pm 1.1 \times 10^{-4}$ mV^2, $p < 0.01$). The γ–θ ratio followed this trend with values of 2.5 ± 0.4 in the presence of physostigmine, whereas a significant reduction ($p < 0.01$) after additional application of HC-3 and BETA (1.2 ± 0.2) was observed, which was no longer different from baseline conditions.

Dose-dependent reduction of γ-oscillations by acetyl-CoA

We further hypothesized that extracellular application of acetyl-CoA, the coenzyme providing the acetate for the transformation of choline to ACh, to the extracellular fluid would enhance physostigmine-induced γ-oscillations. Acetyl-CoA was co-applied successively in concentrations of 10 and 50 µM (n = 7, each) after induction of γ-oscillations by 2 µM physostigmine (Fig. 6a). Induced γ-oscillations remained unaffected after 10 µM acetyl-CoA (Fig. 6a_2, b_2) but when 50 µM were co-applied, physostigmine no longer induced γ-oscillations (Fig. 6a_3, b_3), which contradicts the expectation of extracellular synthesis of ACh. Compared to application of 2 µM physostigmine there were no changes in peak frequency when co-applied with 10 µM acetyl-CoA, whereas 50 µM acetyl-CoA significantly decreased peak frequency which remained in the γ-range (36.3 ± 2.1 Hz, $p < 0.0001$; Fig. 6c). Peak power significantly decreased when 2 µM physostigmine were co-applied with 50 µM acetyl-CoA ($3.5 \pm 0.9 \times 10^{-5}$ mV^2 vs. $0.8 \pm 0.2 \times 10^{-5}$ mV^2, $p < 0.001$; Fig. 6d). Obtained peak power did not differ among other conditions (2 µM physostigmine alone: $3.5 \pm 0.9 \times 10^{-5}$ mV^2 and co-application of 2 µM physostigmine and 10 µM acetyl-CoA: $2.6 \pm 0.7 \times 10^{-5}$ mV^2). The summated power of frequencies

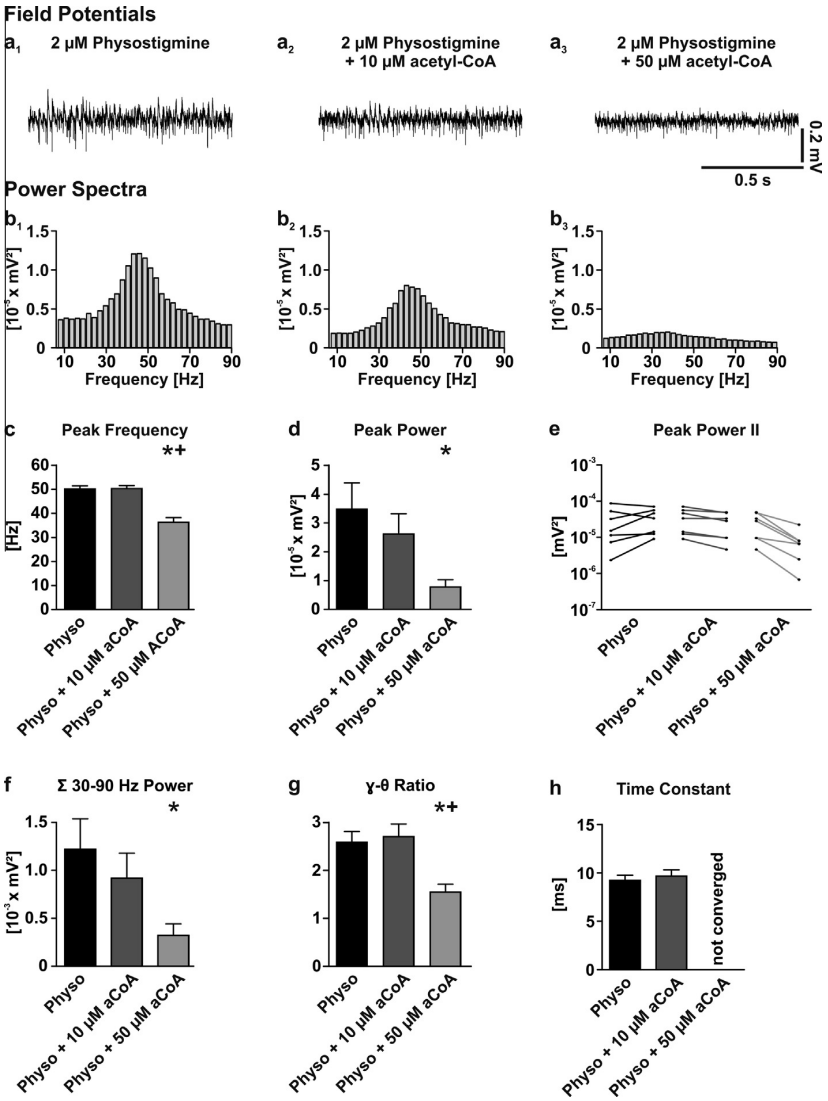

Fig. 6. Dose-dependent reduction of γ-oscillations by acetyl-CoA (aCoA) and synopsis. (a_1–a_3) CA3 field potentials (FP) in presence of different acetyl-CoA concentrations and 2 µM physostigmine (b_1–b_3) Power spectra of 1-min data epochs represented in a_1–a_4. (c) Peak frequency of γ-oscillations. The difference between values for co-application of 50 µM acetyl-CoA and all other conditions is significant. (d) Peak power is only significantly different for physostigmine alone vs. physostigmine plus 50 µM acetyl-CoA. (e) Changes in peak power of individual experiments. (f) Summated power 30–90 Hz. Σ 30–90 Hz is significantly different between physostigmine alone vs. physostigmine plus 50 µM acetyl-CoA. (g) γ–θ ratio. The difference between co-application of 50 µM acetyl-CoA and all other conditions is significant. (h) Time constants could only be calculated from converging fits. There is no significant difference between converged fits. Data are represented by mean and SEM (n = 7). Asterisks and plusses denote significance with $p < 0.05$ between application of 2 µM physostigmine alone and co-application of 2 µM physostigmine with 50 µM acetyl-CoA respectively.

between 30 and 90 Hz was $1.2 \pm 0.3 \times 10^{-3}$ mV^2 after application of 2 µM physostigmine (Fig. 6f). Addition of acetyl-CoA reduced this power to $0.9 \pm 0.3 \times 10^{-3}$ mV^2 (10 µM acetyl-CoA) and significantly further down to $0.3 \pm 0.1 \times 10^{-3}$ mV^2 (50 µM acetyl-CoA $p < 0.001$). The latter values compared well to baseline conditions. The resulting γ–θ ratio was 2.6 ± 0.2 after wash in of 2 µM physostigmine and remained at 2.7 ± 0.3 when 10 µM acetyl-CoA were added (Fig. 6g). Further increase of acetyl-CoA concentration to 50 µM significantly decreased ratio values to 1.5 ± 0.2 ($p < 0.01$ compared to 2 µM physostigmine and $p < 0.001$ compared to co-application of 2 µM physostigmine and 10 µM acetyl-CoA).

We also tested whether acetyl-CoA had any effects on baseline activity. We found that acetyl-CoA (10 and 100 µM) had no significant effect on spontaneous θ/β activity. In another set of experiments we first washed in the choline uptake inhibitor HC-3 (100 µM) followed by 10 µM acetyl-CoA to test whether accumulating choline

together with the added acetyl-CoA would lead to extracellular synthesis of ACh and thus induce γ-oscillations. However, all parameters remained at baseline levels (data not shown).

DISCUSSION

The present study confirms that application of physostigmine-like other ACh esterase inhibitors (Spencer et al., 2010) can induce a weak form of broadband γ-oscillations in rat hippocampal slices which is amplified in a dose-dependent manner when ACh is added. γ-oscillations induced by 10 μM physostigmine resemble those induced by 2 μM physostigmine combined with 2 μM ACh suggesting roughly 2 μM ACh are present in the extracellular space. The augmented γ-oscillations differ from low level ACh γ-oscillations in various parameters, such as peak power, inner coherence, narrow frequency distribution around peak power, and appearance of harmonic oscillations at double the frequency of the first peak. Higher ACh concentrations (5 and 10 μM) induced γ-oscillations with lower peak frequency than when induced by physostigmine, physostigmine combined with 2 μM ACh, or physostigmine combined with HC-3.

It is already known that ACh induces γ-oscillations in slices as demonstrated by the observation that carbachol induces stable and persistent γ-oscillations (Fisahn et al., 1998; Weiss et al., 2003). Previously we had shown that physostigmine combined with ACh induced γ-oscillations which propagate from CA3 to CA1 (Schulz et al., 2012) and are sensitive to a number of neuromodulators that can either augment, decrease or even block induced γ-oscillations. Along this line, ACh-induced γ-oscillations are facilitated by histamine release from histaminergic terminals (Fano et al., 2011). By contrast serotonin, dopamine and norepinephrine reduced these oscillations or even blocked them (Wójtowicz et al., 2009). In case of 5-HT it was sufficient to cause release of 5-HT by the 5-HT agonist fenfluramine. ACh-induced γ-oscillations were also found to be sensitive to adenosine through interaction with A1 receptors (Schulz et al., 2012). Some of these modulatory effects differed from kainate-induced γ-oscillations, which is of interest, as *in vivo* generation of γ-oscillations seems to be strongly dependent on elevated levels of ACh.

Much like kainate, ACh can also induce θ-oscillations in hippocampal slices (Gloveli et al., 2005a,b; Wójtowicz et al., 2009) when they are prepared in longitudinal direction. It was proposed that this is due to a particular activation of OLM interneurons (Gloveli et al., 2005b) while basket cells were more important in mediating γ-oscillations presumably by interactions among each other and with pyramidal cells (Bartos et al., 2007).

A striking finding in our study was that physostigmine alone could induce weak but significant γ-oscillations in rat hippocampal slices. We hypothesized that physostigmine-induced γ-oscillations are caused by increases in extracellular choline concentration. These increases could be a result of lipid membrane degradation (Müller et al., 1988) and/or of ACh release from cholinergic terminals of ChAT-positive neurons within the hippocampus and from cholinergic fibers from the septum. We expected choline uptake into presynaptic terminals to provide for increased ACh synthesis. Therefore, blocking choline uptake by HC-3 was supposed to reduce physostigmine-induced γ-oscillations. Surprisingly this was not the case and in fact γ-oscillation power in the 30–90-Hz band was even mildly (yet insignificantly) increased. This points to the possibility that a fraction of ACh synthesis can also occur in the extracellular space. Extracellular synthesis of ACh has recently been suggested in studies on cholinergic modulation of immune responses (Vijayaraghavan et al., 2013). Extracellular ChAT may originate from cells through export, for example, by inclusion into exosomes (An et al., 2013) or ChAT may be secreted from neurons similar to some forms of AChEs (Zimmerman et al., 2008). Alternatively, enzymes other than ChAT may be responsible for extracellular ACH synthesis. However, the demonstration of extracellular ChAT is still lacking at present, since classical immuno-gold electron microscopy cannot distinguish ChAT found in the extracellular space from that found in terminals (Michael Frotscher, personal communication). Whether such demonstration would be possible with fast freezing procedures and maintenance of the extracellular space has to be proven.

The effect of HC-3 was weak when ACh was co-applied with physostigmine in concentrations of 5 or 10 μM. However, HC-3 facilitated recovery from γ-oscillations induced by physostigmine alone or physostigmine plus ACh. This suggests that blocked reuptake of choline leads to reduced levels of intracellularly available choline which in turn limits recycling of ACh and thus explaining the accelerated washout kinetics observed in these experiments.

To establish whether ChAT alone was responsible for putative extracellular ACh synthesis, we attempted to block ChAT activity. Unfortunately, the ChAT blocker 4-(1-Naphthylvinyl)-pyridine is not soluble in water and dissolving in DMSO or cyclodextrin did not prevent immediate precipitation when added to the aCSF, which precluded us from performing such experiments. Instead, we employed BETA, another blocker of ChAT, which reliably blocked appearance of γ-oscillations. However, this agent is lipophilic, probably entering cells and therefore unable to discriminate between intra- and extracellular location of ChAT.

Synthesis of ACh not only depends on choline but also on the presence of acetyl-CoA. If ChAT would be present in the extracellular space, then application of acetyl-CoA should augment physostigmine-induced γ-oscillations. This was not the case and in fact, when applied with 50 μM γ-oscillations were reduced by a yet unknown mechanism, which is probably not related to simple modification of neuronal activity, since baseline activity in the θ/β range was not affected when sole acetyl-CoA was applied. We also tried to elevate extracellular choline levels by combining HC-3 with acetyl-CoA, again without any effect. We did not apply choline extracellularly as a recent study (Fischer et al., 2014) indicated direct activation of nicotinic and muscarinic receptors which would confound our conclusion.

CONCLUSION

Our study does not support the idea of extracellular synthesis of ACh. However, it shows that very low levels of ACh are already sufficient to produce broad-band γ-oscillations while narrow-band γ-oscillations require concentrations of ACh between 5 and 10 μM.

Acknowledgments—We are grateful to Dr. H.-J. Gabriel and Dipl. Biol. T. Specowius for technical help, to Prof. H. Soreq from the Hebrew University for helpful discussions, and to K. Schoknecht and M.L. Anderson for revision of the manuscript. This research was supported by the BMBF Bernstein Focus Learning, the NeuroCure Cluster of excellence and by the DFG grant He 1128/17-1.

REFERENCES

An K, Klyubin I, Kim Y, Jung JH, Mably AJ, O'Dowd ST, Lynch T, Kanmert D, Lemere CA, Finan GM, Park JW, Kim T, Walsh DM, Rowan MJ, Kim J (2013) Exosomes neutralize synaptic-plasticity-disrupting activity of Aβ assemblies in vivo. Mol Brain 6:47.

Bartos M, Vida I, Jonas P (2007) Synaptic mechanisms of synchronized gamma oscillations in inhibitory interneuron networks. Nat Rev Neurosci 8:45–56.

Chen YS, King RG, Rook TJ, Brennecke SP (1993) Effect of the choline acetyltransferase inhibitor (2-benzoylethyl)-trimethylammonium iodide (BETA) on human placental prostaglandin release and phospholipase A2 activity. Placenta 14:627–640.

Fano S, Çalışkan G, Behrens CJ, Heinemann U (2011) Histaminergic modulation of acetylcholine-induced γ oscillations in rat hippocampus. Neuroreport 22:520–524.

Fisahn A, Pike FG, Buhl EH, Paulsen O (1998) Cholinergic induction of network oscillations at 40 Hz in the hippocampus in vitro. Nature 394:186–189.

Fischer V, Both M, Draguhn A, Egorov AV (2014) Choline-mediated modulation of hippocampal sharp wave-ripple complexes in vitro. J Neurochem 129:792–805.

Fischer Y, Wittner L, Freund TF, Gähwiler BH (2002) Simultaneous activation of gamma and theta network oscillations in rat hippocampal slice cultures. J Physiol 539:857–868.

Freund TF, Gulyás AI (1997) Inhibitory control of GABAergic interneurons in the hippocampus. Can J Physiol Pharmacol 75:479–487.

Frotscher M, Vida I, Bender R (2000) Evidence for the existence of non-GABAergic, cholinergic interneurons in the rodent hippocampus. Neuroscience 96:27–31.

Galea E, Estrada C (1991) Periendothelial acetylcholine synthesis and release in bovine cerebral cortex capillaries. J Cereb Blood Flow Metab 11:868–874.

Gloveli T, Dugladze T, Rotstein HG, Traub RD, Monyer H, Heinemann U, Whittington MA, Kopell NJ (2005a) Orthogonal arrangement of rhythm-generating microcircuits in the hippocampus. Proc Natl Acad Sci USA 102:13295–13300.

Gloveli T, Dugladze T, Saha S, Monyer H, Heinemann U, Traub RD, Whittington MA, Buhl EH (2005b) Differential involvement of oriens/pyramidale interneurones in hippocampal network oscillations in vitro. J Physiol 562:131–147.

Hartmann J, Kiewert C, Duysen EG, Lockridge O, Klein J (2008) Choline availability and acetylcholine synthesis in the hippocampus of acetylcholinesterase-deficient mice. Neurochem Int 52:972–978.

Hasselmo ME, Bower JM (1993) Acetylcholine and memory. Trends Neurosci 16:218–222.

Johnston MV, McKinney M, Coyle JT (1979) Evidence for a cholinergic projection to neocortex from neurons in basal forebrain. Proc Natl Acad Sci USA 76:5392–5396.

Kaufer D, Friedman A, Seidman S, Soreq H (1999) Anticholinesterases induce multigenic transcriptional feedback response suppressing cholinergic neurotransmission. Chem Biol Interact 119–120:349–360.

Kawashima K, Fujii T (2008) Basic and clinical aspects of non-neuronal acetylcholine: overview of non-neuronal cholinergic systems and their biological significance. J Pharmacol Sci 106:167–173.

Klinkenberg I, Sambeth A, Blokland A (2011) Acetylcholine and attention. Behav Brain Res 221:430–442.

Lamour Y, Dutar P, Rascol O, Jobert A (1986) Basal forebrain neurons projecting to the rat frontoparietal cortex: electrophysiological and pharmacological properties. Brain Res 362:122–131.

Léránth C, Frotscher M (1987) Cholinergic innervation of hippocampal GAD- and somatostatin-immunoreactive commissural neurons. J Comp Neurol 261:33–47.

Liotta A, Çalışkan G, ul Haq R, Hollnagel JO, Rösler A, Heinemann U, Behrens CJ (2011) Partial disinhibition is required for transition of stimulus-induced sharp wave-ripple complexes into recurrent epileptiform discharges in rat hippocampal slices. J Neurophysiol 105:172–187.

McLin DE, Miasnikov AA, Weinberger NM (2003) CS-specific gamma, theta, and alpha EEG activity detected in stimulus generalization following induction of behavioral memory by stimulation of the nucleus basalis. Neurobiol Learn Mem 79:152–176.

Meshorer E, Erb C, Gazit R, Pavlovsky L, Kaufer D, Friedman A, Glick D, Ben-Arie N, Soreq H (2002) Alternative splicing and neuritic mRNA translocation under long-term neuronal hypersensitivity. Science 295:508–512.

Metherate R, Tremblay N, Dykes RW (1987) Acetylcholine permits long-term enhancement of neuronal responsiveness in cat primary somatosensory cortex. Neuroscience 22:75–81.

Moro V, Badaut J, Springhetti V, Edvinsson L, Seylaz J, Lasbennes F (1995) Regional study of the co-localization of neuronal nitric oxide synthase with muscarinic receptors in the rat cerebral cortex. Neuroscience 69:797–805.

Müller W, Misgeld U (1989) Carbachol and pirenzepine discriminate effects mediated by two muscarinic receptor subtypes on hippocampal neurons in vitro. In: Frotscher M, Misgeld U, editors. Central cholinergic synaptic transmission. Basel: Birkhäuser Basel. p. 114–122.

Müller W, Misgeld U, Heinemann U (1988) Carbachol effects on hippocampal neurons in vitro: dependence on the rate of rise of carbachol tissue concentration. Exp Brain Res 72:287–298.

Picciotto MR, Higley MJ, Mineur YS (2012) Acetylcholine as a neuromodulator: cholinergic signaling shapes nervous system function and behavior. Neuron 76:116–129.

Schulz SB, Klaft Z, Rösler AR, Heinemann U, Gerevich Z (2012) Purinergic P2X, P2Y and adenosine receptors differentially modulate hippocampal gamma oscillations. Neuropharmacology 62:914–924.

Spencer JP, Middleton LJ, Davies CH (2010) Investigation into the efficacy of the acetylcholinesterase inhibitor, donepezil, and novel procognitive agents to induce gamma oscillations in rat hippocampal slices. Neuropharmacology 59:437–443.

Stenkamp K, Palva JM, Uusisaari M, Schuchmann S, Schmitz D, Heinemann U, Kaila K (2001) Enhanced temporal stability of cholinergic hippocampal gamma oscillations following respiratory alkalosis in vitro. J Neurophysiol 85:2063–2069.

Steriade M, McCormick DA, Sejnowski TJ (1993) Thalamocortical oscillations in the sleeping and aroused brain. Science 262:679–685.

Struble RG, Lehmann J, Mitchell SJ, McKinney M, Price DL, Coyle JT, DeLong MR (1986) Basal forebrain neurons provide major cholinergic innervation of primate neocortex. Neurosci Lett 66:215–220.

Vandecasteele M, Varga V, Berényi A, Papp E, Barthó P, Venance L, Freund TF, Buzsáki G (2014) Optogenetic activation of septal cholinergic neurons suppresses sharp wave ripples and enhances

Publication III

theta oscillations in the hippocampus. Proc Natl Acad Sci USA 111:13535–13540.

Vijayaraghavan S, Karami A, Aeinehband S, Behbahani H, Grandien A, Nilsson B, Ekdahl KN, Lindblom RPF, Piehl F, Darreh-Shori T (2013) Regulated extracellular choline acetyltransferase activity – the plausible missing link of the distant action of acetylcholine in the cholinergic anti-inflammatory pathway. PLoS One 8:e65936.

Weiss T, Veh RW, Heinemann U (2003) Dopamine depresses cholinergic oscillatory network activity in rat hippocampus. Eur J Neurosci 18:2573–2580.

Wessler I, Kirkpatrick CJ (2008) Acetylcholine beyond neurons: the non-neuronal cholinergic system in humans. Br J Pharmacol 154:1558–1571.

Wójtowicz AM, van den Boom L, Chakrabarty A, Maggio N, Haq RU, Behrens CJ, Heinemann U (2009) Monoamines block kainate- and carbachol-induced gamma-oscillations but augment stimulus-induced gamma-oscillations in rat hippocampus in vitro. Hippocampus 19:273–288.

Zimmerman G, Njunting M, Ivens S, Tolner EA, Tolner E, Behrens CJ, Gross M, Soreq H, Heinemann U, Friedman A (2008) Acetylcholine-induced seizure-like activity and modified cholinergic gene expression in chronically epileptic rats. Eur J Neurosci 27:965–975.

(Accepted 12 October 2014)
(Available online 16 October 2014)

8 Curriculum Vitae

„Mein Lebenslauf wird aus datenschutzrechtlichen Gründen in der elektronischen Version meiner Arbeit nicht veröffentlicht.“

Curriculum Vitae

„Mein Lebenslauf wird aus datenschutzrechtlichen Gründen in der elektronischen Version meiner Arbeit nicht veröffentlicht.“

9 Complete list of own publications (in chronological order)

9.1 Published

Liotta A, Çalışkan G, ul Haq R, **Hollnagel JO**, Rösler A, Heinemann U, Behrens CJ (2011). Partial disinhibition is required for transition of stimulus-induced sharp wave-ripple complexes into recurrent epileptiform discharges in rat hippocampal slices. J Neurophysiol 105 (1): 172–187.
Impact Factor (2011)**: 3.316**

Hollnagel JO, Maslarova A, ul Haq R, Heinemann U (2014). $GABA_B$ receptor dependent modulation of sharp wave-ripple complexes in the rat hippocampus in vitro. Neurosci Lett 574: 15–20.
Impact Factor (2013/2014)**: 2.055**

Çalışkan G, Albrecht A, **Hollnagel JO**, Rösler A, Richter-Levin G, Heinemann U, Stork O (2015). Long-term changes in the CA3 associative network of fear-conditioned mice. Stress: 18(2):188-197.
Impact Factor (2014/2015)**: 2.715**

Grosser S, **Hollnagel JO**, Gilling KE, Bartsch JC, Heinemann U, Behr J (2015). Gating of hippocampal output by β-adrenergic receptor activation in the pilocarpine model of epilepsy. Neuroscience 286: 325–337.
Impact Factor (2014/2015)**: 3.357**

Hollnagel JO, ul Haq R, Behrens CJ, Maslarova A, Mody I, Heinemann U (2015). No evidence for role of extracellular choline-acetyltransferase in generation of gamma oscillations in rat hippocampal slices in vitro. Neuroscience 284: 459–469.
Impact Factor (2014/2015)**: 3.357**

Sandow N, Kim S, Raue C, Päsler D, Klaft Z, Antonio LL, **Hollnagel JO**, Kovács R, Kann O, Horn P, Vajkoczy P, Holtkamp M, Meencke H, Cavalheiro EA, Pragst F, Gabriel S, Lehmann T, Heinemann U (2015). Drug resistance in cortical and hippocampal slices from resected tissue of epilepsy patients: no significant impact of p-glycoprotein and multidrug resistance-associated proteins. Front Neurol 6: 30.
Impact Factor (2015)**:** not yet available

ul Haq R, **Hollnagel JO**, Anderson ML, Worschech F, Sherkheli M, Behrens CJ, Heinemann U (2016). Serotonin dependent masking of hippocampal sharp wave ripples. Neuropharmacology 101: 188-203.
Impact Factor (2014/2015)**: 5.106**

Çalışkan G, Müller I, Semtner M, Winkelmann A, Raza A, **Hollnagel JO**, Rösler A, Heinemann U, Stork O, Meier JC (2016). Identification of parvalbumin interneurons as cellular substrate of fear memory persistence. Cereb Cortex 26 (5): 2325–2340.
Impact Factor (2014/2015)**: 8.665**

Salar S, Lapilover E, Müller J, **Hollnagel JO**, Lippmann K, Friedman A, Heinemann U (2016). Synaptic plasticity in area CA1 of rat hippocampal slices following intraventricular application of albumin. Neurobiol Dis 91: 155-165.
Impact Factor (2014/2015)**: 5.078**

Klaft Z, **Hollnagel JO**, Salar S, Çalışkan G, Schulz S, Schneider UC, Horn P, Koch A, Holtkamp M, Gabriel S, Gerevich Z, Heinemann U (2016). Adenosine A_1 receptor-mediated suppression of carbamazepine-resistant seizure-like events in human neocortical slices. Epilepsia: 57(5):746-756.
Impact Factor (2014/2015)**: 4.571**

9.2 Submitted

ul Haq R*, **Hollnagel JO***, Behrens CJ, Grosser S, Liotta A, Maier N, Schmitz D, Heinemann U. Cholinergic regulation of hippocampal network oscillations. Submitted to Cerebral Cortex in February 2016

(*) equally contributing authors

10 Acknowledgements

This work would not have been possible without my supervisor Prof. Dr. Uwe Heinemann to whom I want to express my sincere gratitude. His immense knowledge, excellent supervision and enthusiasm inspired me and built the basis for my passion to science that I developed throughout my PhD studies. His support and generosity provided that special (almost legendary) environment that let me and my colleagues work as one while becoming friends. I will never forget having pizza at the night sessions when recording the human tissue.

I am grateful for having had the opportunity to spend some time abroad as a visiting scientist in Brazil. With Prof. Dr. Esper Cavalheiro I found another lovely and inspiring person whose kindness and generosity made my stay in São Paulo an outstanding experience. This trip was made possible by Dr. Sigrun Gabriel and her husband Dr. Hans-Jürgen Gabriel to whom I want to express my special thanks. I am additionally grateful for having had many fruitful discussions with both of them not only regarding technical issues.

I would like to particularly thank my colleagues I collaborated with and who contributed to my PhD work: Gürsel Çalışkan, Agustín Liotta, Anna Maslarova, Rizwan ul Haq, Anton Rösler, Prof. Istvan Mody, and my PostDoc Christoph Behrens. They all inspired me in their own ways to become what one could call a scientist.

Regarding organizational issues I received great support from Sonja Frosinski, Dr. Katrin Schulze, and Andrea Schütz as well as from Tanja Specowius.

I would like to add some of my colleagues who are not yet mentioned but contributed to the special atmosphere in the lab: Seda Salar, Zin Klaft, Julia Nichtweiß, Kristina Lippmann, Sabine Grosser, David Gruber, Marlene Anderson, Karl Schoknecht and from the extended scientific network in Berlin: Tuğba Özdogan and Ana Ferreira. I appreciate that my new colleagues from Heidelberg were patient at times and motivating at others while I was finalizing the thesis.

I finish with my friends and family who provided me with additional superpowers to keep (and sometimes not to keep) the track. I am happy that you are with me.

Funding

I am grateful for the financial support that provided the funding not only for conducting my experiments but also for my trip to Brazil which belongs to the best experiences I made in science. I received financial support from: GRK 1123 (Bernstein Focus Learning: “Cellular Mechanisms of Learning and Memory Consolidation”), DFG grant He 1128/17-1, DFG grant He 1128/17-1, DFG He 1128/18-1, and the excellence cluster NeuroCure EXC 257.